Integrated model of sulphur dioxide absorption into limestone slurry in an agitated vessel

D Mchabe

orcid.org/0000-0002-9422-6750

Thesis accepted in fulfilment of the requirements for the degree *Doctor of Philosophy in Chemical Engineering* at the North-West University

Promoter:	Prof RC Everson
Co-promoter:	Prof HWJP Neomagus
Co-promoter:	Prof PA Ramachandran (Washington University in St. Louis)

Graduation: May 2020

Student number: 21484007

Dedicated to my late father, Mr James Mkhachane Mchabe and the entire Manghove Royal Family.

Declaration

I, Dursman Mchabe, hereby declare that this thesis entitled: **Integrated model of sulphur dioxide absorption into limestone slurry in an agitated vessel**, submitted in fulfilment of the requirements for the degree Ph.D. in Chemical Engineering is my own work and has not previously been submitted to any other institution in whole or in part.

Signed at Potchefstroom on the **31st** day of **May 2019**.

Dursman Mchabe

Acknowledgements

The author would like to acknowledge, with gratitude, the support received from all those who aided in making this research a success. Special thanks to the following:

- Almighty God, for strength and health to do all things I have done so far.
- North-West University School of Chemical and Minerals Engineering for the opportunity.
- Eskom for financial support.
- Professors R. C. Everson, H. W. J. P. Neomagus and P. A. Ramachandran for supercalifragilisticexpialidocious supervision.
- Eskom Power Plant Engineering Institute (EPPEI) (Dr Z.T. Mathe),for support.
- Eskom Research and Innovation Centre (Mr. N. Haripersad, Dr. C. van Alphen and Mr. P. Swart), for analyses, guidance and support.
- Eskom Group Technology Boiler Engineering (Ms. C. L. Stephen, Ms. P. R. Godana, Mr J. Bore and Mr. Y. Singh), for guidance and support.
- Vaal University of Technology, Department of Chemical Engineering (Professor H. L. Rutto, Ms. L. Lerotholi and Mr. L Koech) for analysis, guidance and support.
- Phambile Trust for Tertiary Education (Mr H .J. Naumann), for undying support.
- Colleagues and friends (Dr Z. Phiri, Pofessor L.J. Legoabe and Mr. A. M. Kalushi), for their undying support.
- RCOLFAN (Dr N.E Tshikwatamba), for prayers and support.

- My family (Nhluvuko Blessing Mchabe, Johannah Zondheka Valoyi, Mangalani David Michavi, Giyani Kenneth Michavi, Dories Nkhensani Mchabe, Wiseman Vongani Mchabe, Winners Ntsako Mchabe, Happiness Tsakani Mchabe and Praise Valoyi) for their undying love and support.
- Ni nkhensa rirhandzu na nseketelo swo huma eka xiluva xa mbilu na moya wa mina, Livy Ntimani Mchabe.

Abstract

An investigation was undertaken to develop and validate an integrated model for absorption of sulphur dioxide involving a gas-slurry system consisting of limestone in order to contribute to the understanding and modelling of sulphur dioxide absorption in the absorber section of industrial Wet Flue gas desulphurisation processes. The experimentation was executed in a laboratory scale agitated reactor with a very dilute mixture of sulphur dioxide (2000 to 3000 ppm) with direct on-line measurement of important parameters and on-line sampling for subsequent measurements as a function of time. The research programme consisted of three parts involving separate experimentation and modelling respectively, with the first two parts confined to the validation of sub-models and the generation of parameters required for the final integrated modelling.For the third part of the investigation, an integrated model was developed consisting of sulphur dioxide absorption and dissolution, limestone dissolution, calcium sulphite crystallization and carbon dioxide liberation.

The modelling results were compared with experimental results for absorption in aqueous solutions and limestone slurries respectively. The model developed here comprises of seven differential equations with two equations for the concentrations of SO_2 and CO_2 in the exit gas, three equations for the total concentration of sulphur, carbon and calcium in the liquid and two more equations for the solids concentrations of calcium carbonate and calcium sulphite in the slurry phase.

The model parameters were fitted to the experimental results and the sensitivity to various phenomena (gas side mass transfer, liquid film transfer, dissolution rate and precipitation rate) were investigated. The estimated parameters were found to agree with results obtained for dissolution of the limestone determined separately (Part 1) and the mass transfer co-efficients determined with aqueous solutions without limestone with different initial pH values (Part 2).The agreement of the model with experimental results were found to be satisfactory. An analysis of the occurrence of different mass transfer reaction regimes (gas and liquid mass transfer and dissolution of limestone) during the experimental period with varying pH is also reported.

Conference Proceedings

List of Conference Presentations

1. Dursman Mchabe, Raymond Everson, Hein Neomagus, Characterisation of South African limestone and absorption of sulphur dioxide into its slurry in a stirred tank reactor, Fossil Fuel Foundation annual conference: Conference on Research in Coal Science and Technology: Latest Research and Development at Universities and Industry. Parys, South Africa, 13-14 November 2013

2. RC. Everson, D. Mchabe, D.J. Branken, H.W.J.P. Neomagus, An integrated diffusion-reaction model for the wet desulphurization with limestone sorberts: Absorption, reaction, leaching and precipitation. The seventh international conference on clean coal technologies (CCT2015), 17 - 21 May 2015, Kraków, Poland.

3. D. Mchabe, RC. Everson, D.J. Branken & H.W.J.P. Neomagus A reaction-rate model for desulphurisation of flue gases. The 20th South African conference (Fossil Fuel Foundation/North-West University) on Research in Coal Science and Technology: Latest Research at Universities and R&D Organisations. Potchefstroom. November 2015.

4. Mchabe D , Everson R.C , Ramachandran P. A. and Neomagus H.W.J.P. The modelling of the unsteady state absorption of sulphur dioxide in an aqueous limestone slurry with precipitation of calcium sulphite. The IEA Clean Coal Centre's 9th International Conference on Clean Coal Technologies. Houston. US. 3 - 7 June 2019.

Table of Contents

List of Figures

List of Tables

Nomenclature

Symbols

Symbol	Description	Units
BET_{CaCO_3}	BET specific surface area of $CaCO_3$	(m^2/g)
BET_{CaSO_3}	BET specific surface area of $CaSO_3$	(m^2/g)
C_{bulk}	concentration in the bulk	(mol/m^3)
$c^{eq}_{H^+}$	concentration at equilibrium	(mol/m^3)
$c^{i}_{H^+}$	concentrations at the interface	(mol/m^3)
c_s	concentration of solids	(mol/m^3)
$C_{SO_{2,in}}$	inlet flue gas SO_2 concentration	(mol/m^3)
C_{H^+}	H^+ bulk concentration	(mol/m^3)
$C^i_{H^+}$	H^+ solid-liquid interface	(mol/m^3)
D	impeller diameter	(m)
D_i	diffusivity of species i	(m^2/s)
d_p	particle size	(m)
E	enhancement factor	(-)
F	flue gas inlet flow rate	(m^3/s)
g	gravitational constant	(m/s)
H_{CO_2}	CO_2 Henry's law constant	(m^3Pa/mol)
H_{SO_2}	SO_2 Henry's law constant	(m^3Pa/mol)
K_{ad}	adsorption constant	(L/mol)
k_{L,CO_2}	CO_2 liquid-side mass coefficient	(mol/m^3)
k_ga	product of gas-side mass coefficient and interfacial surface area	(1/s)
$K_{HCO_3^-}$	HCO_3^- dissociation equilibrium constant	(mol/m^3)
$K_{HSO_3^-}$	HSO_3^- dissociation equilibrium constant	(mol/m^3)
k_{tot}	total dissolution rate constant	(L/$m^2 s$)
k_La	product of liquid-side mass coefficient and interfacial surface area	(1/s)
k_r	chemical reaction constant	(m/s)

Symbol	Description	Units
K_{SO_2}	SO_2 dissociation equilibrium constant	(mol/m^3)
$K_{SP,CaSO_3}$	solubility product of $CaSO_3$	(mol^2/m^6)
K_{CO_2}	CO_2 first dissociation equilibrium constant	(mol/kg)
$K_{HCO_3^-}$	second dissociation equilibrium constant	(mol/kg)
K_W	water dissociation equilibrium constant	(mol/m^3)
MW_{CaCO_3}	molecular weight of $CaCO_3$	(g/mol)
MW_{CaSO_3}	molecular weight of $CaSO_30.5H_2O$	(g/mol)
N	stirring speed	(rpm)
N_{js}	critical impeller speed	(1/s)
Np	power number	(-)
R	universal gas constant	(J/mol.K)
Re	Reynolds number	(-)
Sc	Schmidt number	(-)
Sh	Sherwood number	(-)
SSA_{BET}	specific surface area measured by physisorption	(m^2/g)
SA	surface area per volume	(m^2/m^3)
T	reactor temperature	(K)
V_{slurry}	volume of the slurry	(m^3)
$V_{Headspace}$	volume of the headspace	(m^3)

Greek Symbols

Symbol	Description	Units
α	first empirical parameters for evaluating diffusivity	(cm^2/s)
β	second empirical parameters for evaluating diffusivity	(cm^2/s.$^\circ$C)
ρ	density	(kg/m^3)
γ	stoichiometry	(-)
ρ_{CaCO_3}	density of limestone	(kg/m^3)
ρ_{CaSO_3}	density of $CaSO_30.5H_2O$	(kg/m^3)
δ	liquid film thickness	(m)
ϵ	mean dissipated energy	(W/kg)
λ	reaction plane position	(m)
ν	kinematic viscosity	(m^2/s)

Abbreviations

Abbreviation	Description
Afrox	African Oxygen
BET	Brunauer-Emmett-Teller
CCT	clean coal technologies
CFB	Circulating Fluidized Bed
CFD	Computational Fluid Dynamics
DR	Dubinin-Redushkevich
DSI	Dry Sorbent Injection
EPPEI	Eskom Power Plant Engineering Institute
ESKOM	South African electricity public utility (Elektrisiteits Voorsienings (Supply) Kommissie)
ESP	Electrostatic Precipitator
FF	Fabric filter
FGD	Flue Gas Desulphurisation
HK	Horvath-Kawazoe
ICP-OES	Inductively Coupled Plasma Optical Emission spectrometer
IEA	International Energy Agency
LIFAC	Limestone Injection into the Furnace and Activation of Calcium
LOI	Loss on Ignition
LTB	lithium tetraborate
MCM	Mercury Control Methods
MMD	mass median diameter
NAAQAS	National Ambient Air Quality Act Standard
OAT	one-factor-at-a-time
ODE	Ordinary Differential Equations
ODEs	ordinary differential equations
PSD	Particle Size Distributions
QEMSCAN	Quantitative Evaluation of Materials by Scanning Electron Microscopy
SA	sensitivity analysis
SCR	Selective Catalytic Reduction
SDA	Spray Dry Absorber
SSE	sum of square errors
US EPA	US Environmental Protection Agency
WFGD	Wet Flue Gas Desulphurisation
XRD	X-ray Diffraction
XRF	X-ray Fluorescence

Chapter 1 General Introduction

Introduction

An overview of the study undertaken towards the development of an integrated model of sulphur dioxide absorption into limestone slurry in an agitated vessel is given in this chapter. Background and motivation of the investigation are presented in Sections 1.1 and 1.2. The project statement is given in Section 1.3. The overall aim of the project and specific objectives are presented in Sections 1.4 and 1.5. The scope of this study is summarized in Section 1.6.

1.1 Background

1.1.1 Industrial perspective of coal-fired power stations and the emissions

In 2012, the global electric power production was about 21.6 T-kWh and it is expected to go up to 25.8 T-kWh in 2020 and a further hike to 36.5 T-kWh is expected for 2040, thus the worldwide net electricity generation will increase by 69 % in 2040 (Baig & Yousaf 2017, EIA 2017).

In 2007, working coal fired power stations were around 50,000, the number is expected to increase world wide. Coal is considered to be the most abundant power provenance globally, however, coal combustion contribute towards environmental pollution leading to problems such as acid rain, global warming, air pollution related diseases and so forth (Baig & Yousaf 2017). Coal fired power stations based on modern technologies emit less pollutants due to the interventions of technologies in cleaning the effluents, before emission; however pollutants are still being emitted to date.

Regulatory bodies all over the world place stringent environmental regulations

on coal-fired power plants. Various technologies are commonly used to mitigate particular emissions, e.g. electrostatic precipitator/fabric filter for particulates, selective catalytic reduction for NOx, flue gas desulphurization for SOx and others.Alternative ways of abating emissions include retiring coal fired power generating plants and/or co-generation by coal and natural gas e.g. until 2016, USA had been reported to have retired 175 coal fired power plants and France retired 7. USA had also been reported to have reduced coal consumption and carbon dioxide emissions by employing mixed fuel power generation (Baig & Yousaf 2017).

1.1.2 SO_2 emissions and regulations

The sulphur content in fossil fuels used in power plants may reach significant amounts and their combustion produce gaseous sulphur dioxide leading to problems such as acid rains, particulate matter, diseases and so forth. The degree of sulphur dioxide emission is dependent on numerous factors e.g. the quantity and type of inherent sulphur in the fossil fuel, the abating technology employed, equipment operation and so forth. The use of fossil fuel in electricity generation accounts for the highest percentage of SO_2 emission in many parts of the world e.g. United States of America (Srivastava & Jozewicz 2001), India (Garg et al. 2002), China (Yan & Wu 2017), Europe (Smith et al. 2011),South Africa (Pretorius et al. 2015) and so forth.

Various regulatory bodies across the world are putting stringent SO_x regulations in their areas of jurisdiction e.g. the United States Environmental Protection Agency (USEPA) is responsible for the United States of America, European Environmental Agency responsible for Europe and so forth. This study focus on South Africa, where the National Environment Management Air Quality Act (Act No 39 of 2004) governs the SO_x emissions. Certain parts of South Africa have exceeded the ambient air quality standards of National Ambient Air Quality Act Standard (NAAQAS)'s Section 18(1), e.g. Highveld, Vaal Triangle and Waterberg. This can be attributed to that electricity generating power stations are located in those areas and these areas are declared as National Priority Areas (Ross 2012).

The South African electricity public utility (ESKOM) had been conducting ambient air quality since in the late 1970's. On using the Atmospheric Dispersion modelling, the utility reported high concentrations in the Vaal Triagle Priority, despite meeting the NAAQS requirements.

The Waterberg Environmental Impact Assessment reported low concentrations. The model projected that the introduction of the WFGD technologies on newly built coal-fired plants will reduce the growing air pollution trends in the Highveld and Waterberg priority areas (Stephen et al. 2014).

1.1.3 Processes for SO_2 removal

Most SO_2 removal processes are based on the contact and/or reaction of SO_2-containing flue gas with alkaline matter in order to absorb SO_2 and other acid gases (e.g. HCl, HF) thereby producing sulphates and/or sulphites and by-products. Depending on the fate of the sorbent, flue gas desulphurization can be categorized into two main categories, namely, regenerative and non-regenerative processes. For regenerative processes, the spent sorbent is recovered thermal or chemical treatments and concentrated SO_2 is also generated and further processed to desired products e.g. elemental sulphur, H_2SO_4 and so forth. On the other hand, for non-regenerative processes, the sorbents are not recycled (Lisnic & Jinga 2018, Srivastava & Jozewicz 2001).

Classification of FGD processes depends on the aggregation state of the sorbent, namely, wet processes (solution or suspension), semi-dry processes (sorbent with controlled humidity) and dry processes (zero humidification). Figure 1.1 provides classification of FGD processes based on the commonly used technologies on industrial scale.

For dry process (sorbent injection,SI),sorbent particles are injected into the gas flow or gas flow passes the particles. Commonly used sorbents are limestone and dolomites, that are calcined at the burning point, and the produced CaO further react with SO_2 to produce either $CaSO_3$ or $CaSO_4$, which are collected at the ESP/FF. Semi-dry processes are similar to the dry processes, with the exception that both the sorbent and the flue gas are humidified. The commonly used semi-dry technologies are circulating dry scrubber (CDS) also known as circulating fluidized bed (CFB) and spray dry absorber (SDA) (Lisnic & Jinga 2018).

From all the processes presented in Figure 1.1, the most commonly used technology is the non-regenerative, wet process that employs either limestone or lime in counter-current spray towers. This can be attributed to low operation cost and high desulphurization performance (Córdoba 2015). The variants of limestone wet FGD are limestone inhibited oxidation and limestone forced oxidation, with the later being the most preferred, due to its ability to avoid scaling and the oxidation $CaSO_3$ to saleable gypsum (Srivastava & Jozewicz 2001).

1.1.4 Status of WFGD technology

The current status of the available WFGD processes is that there is a need to ameliorate the poor performing installations to achieve a desulphurization efficiency of up to 99.9 % and to retrofit the 99.9 %-technologies on plants without WFGD. There is also a need to use poor quality limestones and to reduce water usage, especially in

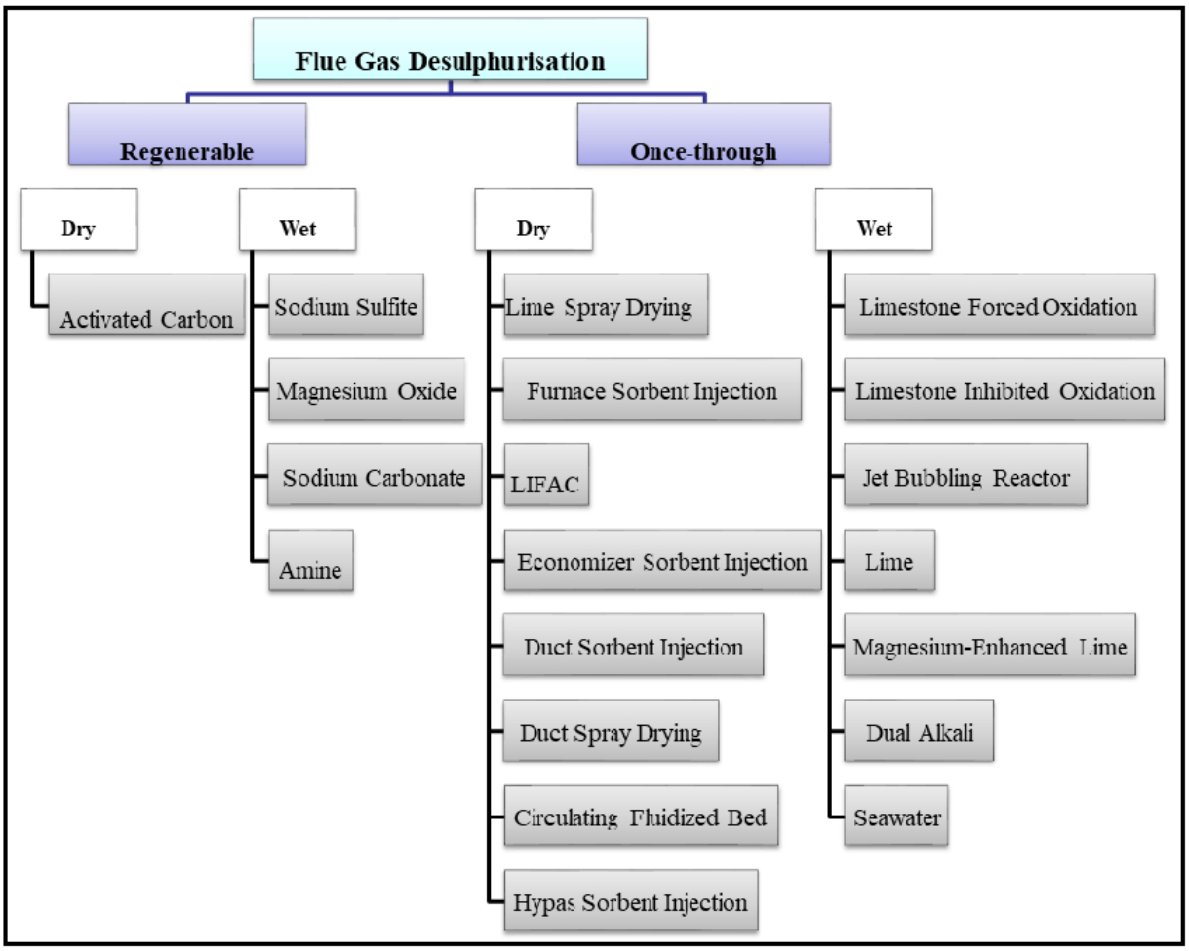

Figure 1.1: Classification of FGD processes (Adapted from Lisnic & Jinga (2018)).

water scare countries. The other current focus area is the reuse and/or recovery of the by-products.

Various strategies can be used to achieve 99.9% desulphurization, namely, installation of secondary absorbers, the use of modern nozzles and so forth. Lisnic & Jinga (2018) postulated that future installations will have stringent requirements, namely, low water consumption, high desulphurization efficiency, heavy metals abatement capacity, low investment, operating and maintenance costs, high reliability, saleable/re-usable by-products and so forth. Furthermore, regarding the limestone for the forced oxidation process, efforts will be directed at employing smaller installations in efforts to reduce investment costs (in addition to upgrading and optimization) (Lisnic & Jinga 2018).

The designing, installation and operation of the WFGD will require detailed understanding of control parameters, mass transfer and chemical reactions involved.

The commonly investigated control parameters includes pH, limestone reactivity, SO_2 concentration, PM concentration, water re-circulation, particles entrainment and so forth (Córdoba 2015).

1.2 Motivation

Various modelling methods had been used to develop mathematical models for the design and operation of industrial-, pilot- and laboratory scale plants for wet gas desulphurization process and the results have been extensively published by Agarwal & Rochelle (1993), Brogren & Karlsson (1997*c*), Eden & Luckas (1998), Kiil et al. (1998), Neveux et al. (2014), Olausson et al. (1993), Ortiz (2010). Comprehensive models for the description and integration of the hydrodynamics and the associated absorption/reaction kinetics respectively have been examined using very powerful computational fluid dynamic (CFD modelling codes) (Arif 2016, Gómez et al. 2007, Marocco 2010, Tseng & Li 2018, Xiao et al. 2014).

The validation of these comprehensive models with experimental results (Kallinikos et al. 2010, Ortiz 2010) have also been reported for a variety of process configuration and capacities including laboratory scale experimental studies designed to simulate and provide information for large scale operation (Kallinikos et al. 2010, Ortiz 2010).

Hydrodynamics modelling for the gas and liquid phases and resulting interaction between the phases appears to have been well established, whereas the detailed understanding of the coupled absorption and chemical reactions involving sulphur dioxide, limestone and calcium sulphite/sulphate in the slurry phase needs to be addressed in greater detail. In the case of the spray absorption column the modelling of the synchronous absorption and dissociation of SO_2 and CO_2 and the dissolution of limestone in the slurry droplets as a function of a varying pH throughout the absorber can affect the overall process.

The modelling of the latter would involve evaluating the different mechanism for mass transfer, the reaction kinetics for dissociating and precipitating species and the associated chemical and physical parameters (Bravo et al. 2002, Pasiuk-Bronikowska & Rudziński 1991).

To achieve success with this complex system with many associated coupled subprocess (diffusion-reaction-precipitation) it is essential to perform experiments that include measurement of that many variables. Thus, this project was undertaken to address the need for a meticulous integrated model for the mass transfer-reaction component of the overall model for the absorption of SO_2 in a WFGD process.

1.3 Project Statement

The project will involve the development of a comprehensive diffusion-reaction-precipitation mathematical model with experimental validation for the desulphurization of a flue gas using a wet process. Experimentation will be accomplished with a gas-slurry laboratory-scale stirred reactor with limestone operating as a semi-batch process. The research programme will include a systematic procedure involving the evaluation of the required sub-models consisting of mass transfer and dissociation of sulphur dioxide and carbon dioxide, dissociation of limestone and precipitation of calcium sulphite.

1.4 Aim of the project

The aim of this investigation is to contribute to the understanding and modelling of wet flue gas desulphurization confined exclusively to the unsteady absorption of sulphur dioxide and the behaviour of chemical reactions in the limestone slurry phase. The research programme will consist essentially of four main tasks involving laboratory scale experimentation and modelling in order to generate information required for developing the final integrated model.

1.5 Specific Objectives

To achieve the above mentioned aim, the following research programme comprising four specific objectives, each with the following distinct tasks, will be undertaken.

- To determine the physicochemical properties of the selected limestone and the corresponding properties of the sulphated product following the dissolution, sulphation and precipitation. This will be done to provide results for evaluating the integrated model and for comparison with limestones used by other researchers.
- To develop and validate the dissolution rate of limestone only using appropriate reaction conditions without sulphation. Reaction rate parameters will be determined for a specific limestone.
- To assess the mass transfer mechanism and the quantification of the transfer of SO_2 from the gas to the slurry phase involving an appropriate compounded model. This will involve experimentation without dissolution of limestone. Mass transfer coefficients for sulphur dioxide and derivatives will be determined.

- To develop and evaluate an integrated model for the overall process involving, adsorption and mass transfer of SO_2, dissolution of limestone, liberation and mass transfer of CO_2 and precipitation of calcium sulphite. The results from above-mentioned tasks and appropriate results from the literature will be used for this simulation. The results will be compared to experimental results obtained from an experimental programme involving all the mechanisms, namely absorption, mass transfer, dissolution and precipitation.

1.6 Scope of the Study

The study was conducted to contribute towards the understanding and modelling of wet flue gas desulphurization, specifically absorption of SO_2 and the role of chemical reactions in the limestone slurry phase. The scope of the study involves limestone characterization, laboratory scale experimentation and modelling in order to generate information required for developing the final integrated model, and is summarized in Figure 1.2. The literature survey conducted is presented in Chapter 2.

The model requires knowledge of physical and chemical properties of limestone used. Chapter 3 is dedicated towards characterization of the limestone used as well as comparing the properties with other limestones published in literature. Limestone dissolution is considered to also limit the WFGD process. Chapter 4 addresses the modelling (and validation) of the dissolution kinetics of the limestone. Furthermore, the solid-liquid mass transfer coefficient and the adsorption constant, which are the requirements for the integrated model, are assessed.

The integrated model also requires the knowledge of gas-liquid mass transfer coefficients. Chapter 5 is dedicated towards the evaluation of gas-side and liquid-side mass transfer coefficients. The same chapter also employs Two-film theory to model the absorption of SO_2 into water, thereby revealing the difference in SO_2 absorption into water and into limestone slurry (Chapter 6) as well as the role of chemical reactions involved.

In Chapter 6, an integrated model is developed, involving a set of ODEs and algebraic equations, that describes the mechanisms involved in the wet flue gas desulphurization confined exclusively to the unsteady absorption of sulphur dioxide and the behaviour of many chemical reactions in the limestone slurry phase. Matlab software (version 2018b) was used to solve these equations. The model was validated by experimental results generated using a laboratory scale stirred tank reactor. Conclusions drawn and recommendations made are given in Chapter 7.

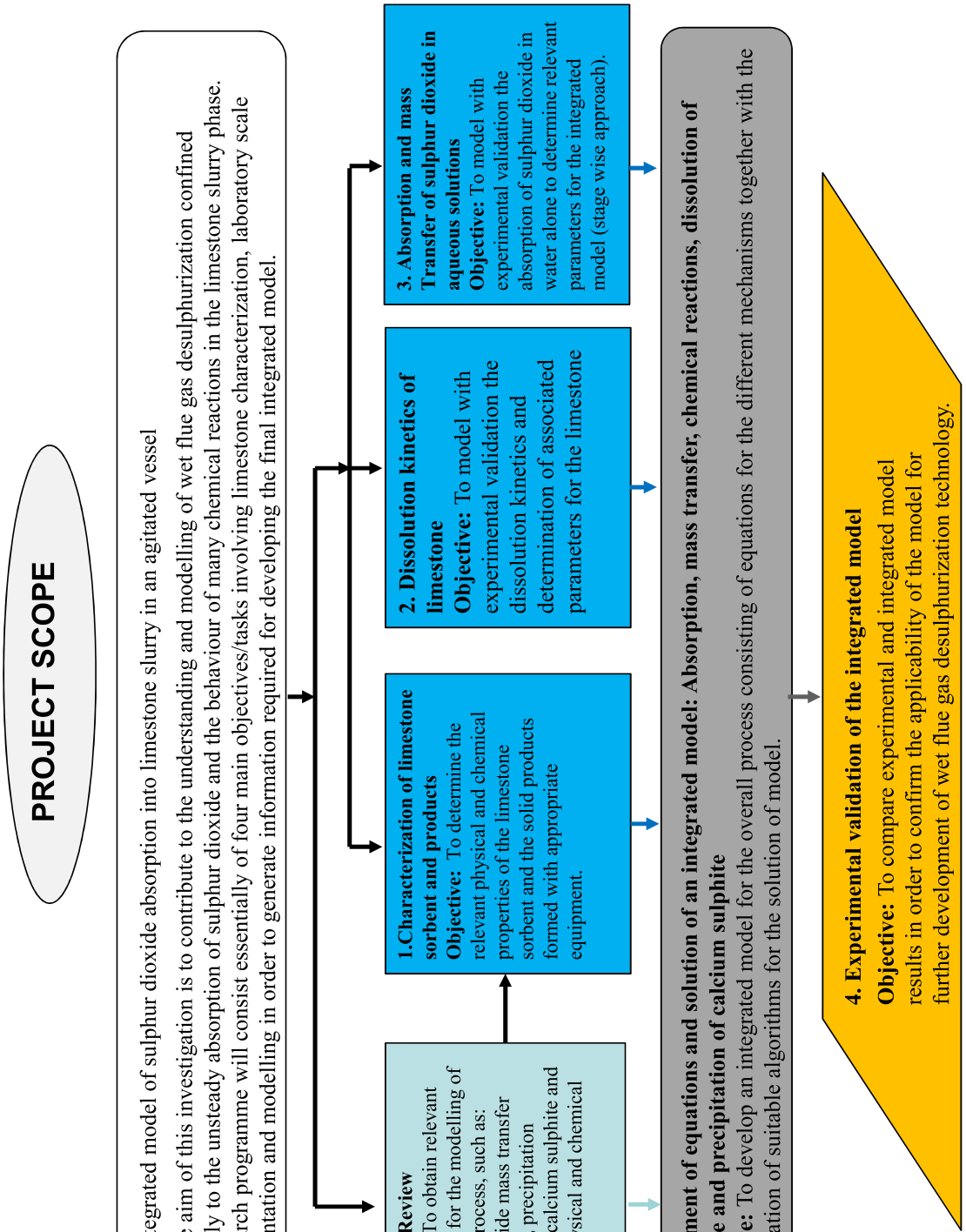

Figure 1.2: A flowchart illustrating project scope.

Chapter

2 Literature Review

Introduction

A review of work done by others towards understanding FGD processes is given in this chapter. The overview of FGD processes is presented in Section 2.1. The fundamentals of limestone wet flue gas desulphurisation are delineated in Section 2.2 with specific interest on the rate limiting steps. Section 2.3 provides the review of models commonly used for limestone WFGD processes on different operational scales.

2.1 Overview of FGD processes

There are more than 200 flue gas desulfurization technologies (Jamil et al. 2013), however, the phrase 'FGD-system' has been commonly used synonymous to WFGD for the removal of SO_2 from power production utilities (Córdoba 2015). Depending on the desulphurizing agent used, the common processes include calcium-based, ammonia-based , magnesium-based and others. Depending on the final co-product, FGD processes are divided into those whose co-product is disposed on landfill, and those with a commercially useful co-product.

The USEPA categorizes FGD systems according to non-regenerable and regenerable processes. The classification is based on the fate of the sulphur compounds, i.e. whether they are throwaway along with by-products or not (Córdoba 2015). Clarke & Sloss (1992) also designate them according to regenerable and non-regenerable, and furthermore, they subdivide the non-regenerable category into wet scrubber and spray dry systems.

Clarke & Sloss (1992), Soud (2000) and Nygaard et al. (2004) proposed the four classes, namely, wet/spray-dry scrubbers, SI and regenerable processes. Furthermore, main classes are sundered into several subclasses on the basis of chemical re-

actions and dispersion conditions. Specialised literature (Aunela-Tapola et al. 1998, Clarke 1993, Soud 2000) concurs that the limestone WFGD system is supereminent (87%). This can be attributed to its applaudable desulphurisation capacity and low-cost running (Córdoba 2015, Kiil et al. 1998).

2.2 Limestone WFGD: Description and Fundamentals

2.2.1 Description

2.2.1.1 The process: tank and absorber

Non-generable limestone WFGD can be classified into forced or natural oxidation, depending on whether air/oxygen is sparged or not. Chemical reactions are considered to take place both in the absorber and reaction tank sections. A typical wet FGD equipment is shown in Figure 2.1.

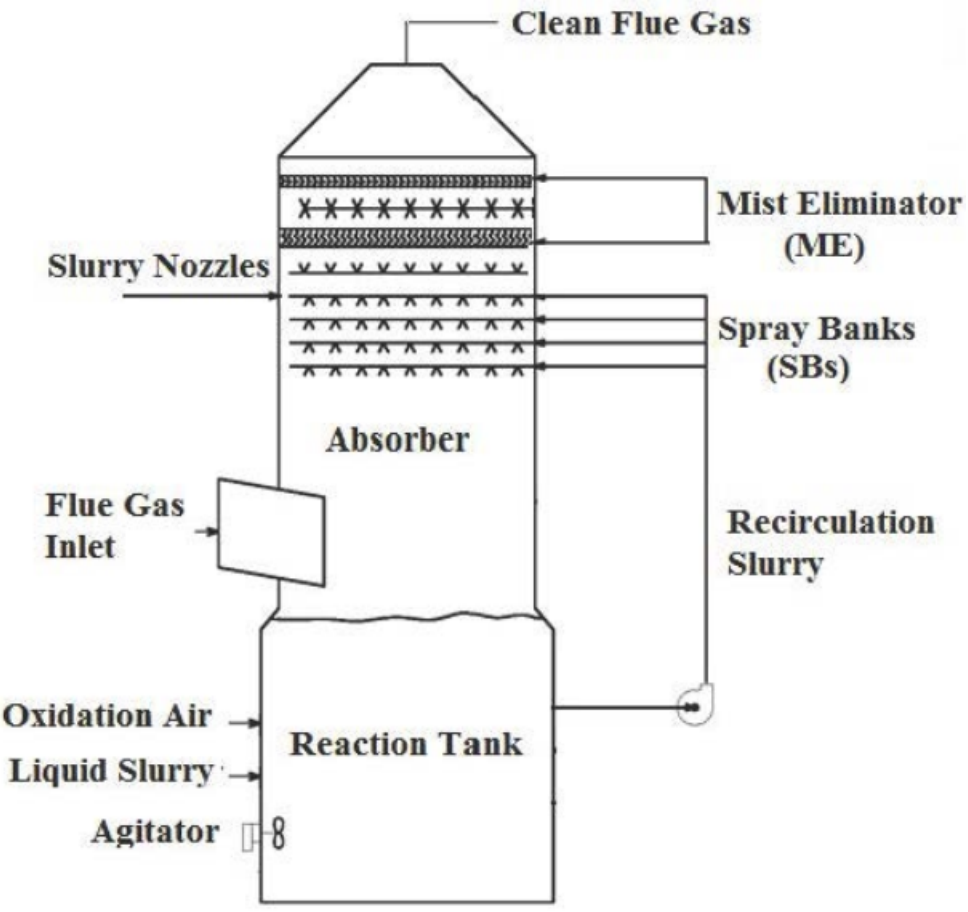

Figure 2.1: Typical WFGD equipment (Arif 2016).

2.2.1.2 Limestone sorbents

The factors that made lime/limestone/dolomite wet FGD processes to be favourable includes that:

- low-cost of both limestone and dolomitic-limestones, owing it to their copiousness.
- the specific properties of the aqueous slurries obtained by the partial dissolution of suspended limestone particles.
- the solid by-product of the process (gypsum), is saleable and can offset the costs of the lime/limestone/dolomite WFGD process.

Figure 2.2 shows the deposits and occurrences of limestone/dolomite in South Africa.The abundant calcareous minerals resources in South Africa had been

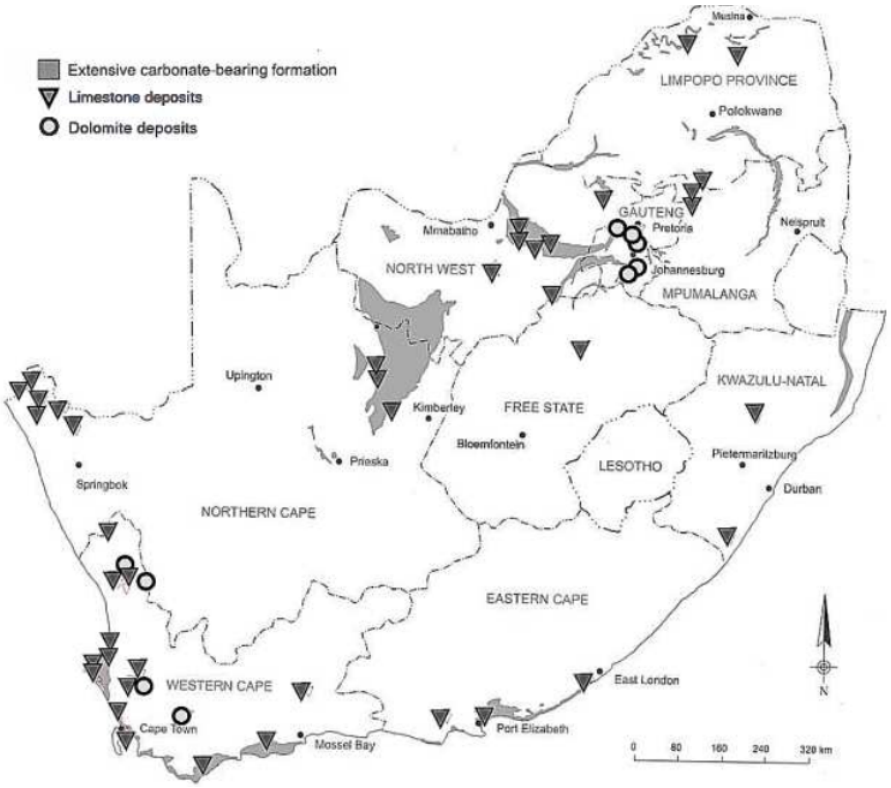

Figure 2.2: Deposits and occurrences of limestone/dolomite in South Africa (Agnello 2005)

reported to be comprised of a greater proportion of dolomite than limestone (Haripersad & Swart 2014). There are however greater reserves of limestone than there is dolomite due the existing market drivers favouring the application of limestone primarily in the cement industry. Assessment of the performance of limestone

WFGD involves the quantification of limestone utilization, SO_2 removal efficiency and gypsum quality, which in turn, is dependent on the physico-chemical properties of limestone/dolomite. This necessitate the studies towards characterization of limestone/dolomite deposit(s) (that are found near WFGD plants), as is done in Chapter 3.

2.2.1.3 Chemistry and reaction rates

The overview of chemical reactions in the spray tower is shown in Figure 2.3.

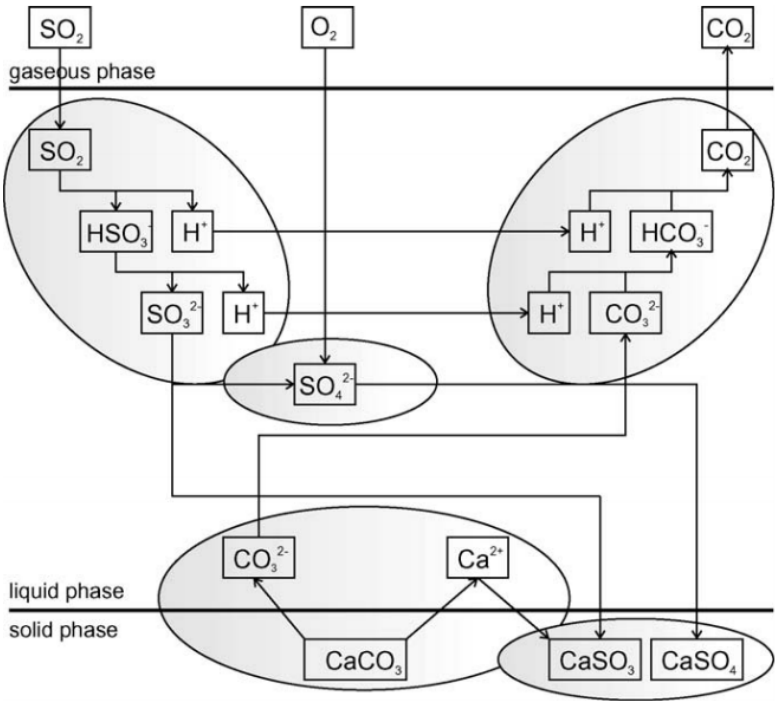

Figure 2.3: overview of chemical reactions in the spray tower (Desch et al. 2006)

The chemical reactions that are considered to take place in the absorber zone (pH 5 to 6) are presented below (Córdoba 2015):

SO_2 diffusion
SO_2 hydration:

$$SO_2\,(g) \leftrightharpoons SO_2\,(aq) \tag{R2.1}$$

SO_2 reaction:

$$SO_2\,(aq) + H_2O\,(l) \leftrightharpoons H_2SO_3\,(aq) \tag{R2.2}$$

H_2SO_3 dissociation:

$$H_2SO_3(aq) \rightleftharpoons H^+ + HSO_3^- \quad \text{(R2.3)}$$

HSO_3^- dissociation:

$$HSO_3^- \rightleftharpoons H^+ + SO_3^{2-} \quad \text{(R2.4)}$$

Limestone hydration:

$$CaCO_3(s) \longrightarrow CaCO_3(aq) \quad \text{(R2.5)}$$

$CaCO_3$(aq) dissociation:

$$CaCO_3(aq) \rightleftharpoons Ca^{2+} + CO_3^{2-} \quad \text{(R2.6)}$$

CO_3^{2-} protonation:

$$H^+ + CO_3^{2-}(aq) \rightleftharpoons HCO_3^- \quad \text{(R2.7)}$$

HCO_3^- protonation:

$$H^+ + HCO_3^- \rightleftharpoons H_2CO_3(aq) \quad \text{(R2.8)}$$

CO_2(g) desorption

$$H_2CO_3(aq) \rightleftharpoons CO_2(g) + H_2O(l) \quad \text{(R2.9)}$$

The overall reaction (R2.10) is given below:

$$CaCO_3(s) + SO_2(g) \longrightarrow CaSO_3 0.5\,H_2O(s) + CO_2(g) \quad \text{(R2.10)}$$

Chemical reactions that did not reach completion (in the absorber) are considered to proceed to completion in the reaction tank, owing it to longer residence period.The oxidation of the SO_3^{2-} to SO_4^{2-} takes place according to R2.11 in the reaction tank zone.

$$CaSO_3 0.5\,H_2O(s) + 0.5\,O_2(g) \longrightarrow CaSO_4 2\,H_2O(s) \quad \text{(R2.11)}$$

Different chemical reaction mechanism is expected at a lower pH range (4.5–5.5),

where the main product is $Ca(HSO_3)_2$ as shown in R2.12. Córdoba (2015) reported that at pH of 4.5 to 5.5, the favoured overall chemical reaction will be given by R2.12 and corresponding oxidation be given by R2.13

$$CaCO_3(s) + SO_2(g) + H_2O \leftrightharpoons Ca(HSO_3)_2(aq) + CO_2(aq) \quad \text{(R2.12)}$$

$$Ca(HSO_3)_2(aq) + O_2(g) + 2\,H_2O \longrightarrow CaSO_4{\cdot}2\,H_2O(s) + H_2SO_4(aq) \quad \text{(R2.13)}$$

As a way of regulating the pH of the slurry in the reaction tank (to a desired predetermined value e.g 5.5), predetermined amount of fresh limestone slurry is added for neutralization according R2.14.

$$CaCO_3(s) + H_2SO_4(aq) + H_2O \longrightarrow CaSO_4{\cdot}2\,H_2O(s) + O_2(g) \quad \text{(R2.14)}$$

Córdoba (2015) also reported that it is advantageous to operate the WFGD in the forced-oxidation mode, so as to optimize the production of gypsum, which will also depend on other operating conditions/parameters e.g. excess-air, slurry pH and so forth.

2.2.2 Modelling of rate determining mechanisms

Chemical-absorption of SO_2 into limestone slurry had been reported to be limited by numerous sub-processes (Figure 2.3), namely, limestone dissolution, SO_2 absorption, CO_2 desorption, $CaSO_3{\cdot}0.5H_2O$ crystallization, SO_3^{2-} oxidation,$CaSO_3{\cdot}0.5H_2O$ oxidation, $CaSO_4{\cdot}2H_2O$ crystallization (Brogren & Karlsson 1997*c*, Kiil et al. 1998, Olausson et al. 1993) and so forth. Various models have been employed to delineate these sub-processes in full scale and pilot scale plants and laboratory set-ups, by various researchers. This section presents some of the models used by some of the researchers.

2.2.2.1 Dissolution of limestone

Neveux & Le Moullec (2011) modelled limestone dissolution in the full-scale spray tower reaction tank using an empirical expression from the work of Desch et al. (2006).Brogren & Karlsson (1997*a*) employed the film theory, in a plot scale plant.

Most limestone dissolution studies were conducted in a laboratory scale set-ups using the rotating disc method and particles suspension, i.e. either the pH-Stat method or free-drift method, where either sulphuric acid (Brogren & Karlsson 1997*b*, Fusi et al. 2015, Huminicki & Rimstidt 2008) or hydrochloric acid (Alkattan et al. 1998, Carlett et al. 2015a, Carletti et al. 2012, 2015b, Chan & Rochelle 1982,

Gage & Rochelle 1992, Lund et al. 1973, Pepe 2001, Sjöberg & Rickard 1984*a*,*b*, 1985, 1983, Toprac & Rochelle 1982, Ukawa et al. 1993, Wallin & Bjerle 1989*a*,*b*, 1990) is used to emulate the acidic conditions in the wet FGD. The later is favoured because it prevents the production of solid products, making it possible to measure the concentration of calcium ions and the transient PSD of limestone.

The commonly used models for laboratory scale limestone dissolution studies are film theory based models (Gage & Rochelle 1992, Lancia et al. 1991, 1994*a*, Souza et al. 2010), basic mass transfer models (Brogren & Karlsson 1997*a*, Chan & Rochelle 1982) and semi-empirical model (Koech et al. 2014).

Following on from the work done by other researchers on limestone dissolution that pertains to WFGD (Blasio et al. 2018, Brogren & Karlsson 1997*a*,*b*, Carlett et al. 2015a, Carletti et al. 2012, 2015b, Fellner & Khandl 1999, Gage & Rochelle 1992, Koech et al. 2014, Lancia et al. 1991, 1994*a*, Souza et al. 2010, Toprac & Rochelle 1982, Ukawa et al. 1993), Chapter 4 of this study will address the mass transfer and reaction kinetics of limestone dissolution.

2.2.2.2 Interface mass transfer and dissociation of SO_2

Mass transfer of SO_2 into aqueous solutions/limestone slurry is determined by both diffusion and reaction processes. When chemical reaction enhances the absorption, the mass transfer is termed chemical-absorption (Lancia et al. 1994*b*). Most studies (plant and laboratory scales) on chemical-absorption of SO_2 into limestone slurry involved modelling of the rate of SO_2 mass transfer, with the commonly used models The two-film (Whitman 1924), the surface-renewal (Danckwerts 1955) and the penetration (Higbie 1935) theories.

Gerbec et al. (1995), Gómez et al. (2007), Kallinikos et al. (2010), Neveux & Le Moullec (2011), Olausson et al. (1993), Zhong et al. (2008) and others. employed Two-film theory on SO_2 mass transfer in full scale WFGD, the same was used by Kiil et al. (1998) on pilot scale plant. The two-film-based modelling on laboratory scale (SO_2-limestone slurry system) includes the work of Bravo et al. (2002), Dou et al. (2009), Lancia et al. (1997), Uchida et al. (1978) and so forth.

Ramachandran & Sharma (1969) were the first to propose models based on the significance and insignificance of solid dissolution in the liquid film. In case of the dissolution of solid being trifling, the processes (absorption and dissolution) are considered to take place in series, thus the reciprocal of the overall resistance is the sum of the reciprocal of the respective individual resistances. The same authors derived a rate equation for the case when solid dissolution is germane.

Their models were amended by Uchida et al. (1975, 1978), Uchida & Wen (1977) on basis of their experimental observation that solid dissolution aggrandize gas ab-

sorption. Further modifications were done by Sada et al. (1979) and (Sada et al. 1982). The same authors considered separate dissolution coefficients in the film and liquid bulk, respectively.

Studies by Lancia et al. (1994*b*), Sada, Kumazawa, Sawada & Hashizume (1981), Takashina et al. (2001), Uchida & Ariga (1985) and others, focused on the liquid film and the chemical reactions in the reaction planes within the film. Brogren & Karlsson (1997*c*) formulated a model (based on the penetration theory) to compute the dynamic absorption rate of SO_2 into limestone slurry droplets. Uchida et al. (1981) developed a penetration model for gas absorption into a slurry containing solid particles with an instantaneous irreversible chemical reaction.

The surface-renewal-based model developed by Chang & Rochelle (1982*a*) was used by the same authors to assess the impact of organic acids on SO_2 removal under WFGD conditions. (Gerard et al. 1996) reported that the surface-renewal model is more pragmatic and pedantic, however it is mathematically extortionate. Consequently, in Chapter 5 of this study, the two-film theory is used.

2.2.2.3 Desorption of CO_2

The effluence of CO_2 desorption on chemical-absorption of SO_2 into limestone slurry had been considered by researchers such as Bravo et al. (2002), Dragan & Ozunu (2012), Kallinikos et al. (2010) and others. The latter, employed a two-film theory based model to model the rate of CO_2 desorption. Furthermore, they considered CO_2 to be only affected by the liquid film resistances.

Bravo et al. (2002) proposed the use of a variable Y for the ratio of desorbed CO_2 moles to dissolved $CaCO_3$ moles. The same authors employed a non-linear regression fitting technique to generate the correlation for Y, on the basis that Y is dependent on temperature and time.

The contribution of the desorption of CO_2, into the developed integrated model, is addressed in Chapter 6 of this study, .

2.2.2.4 Crystallization of calcium sulphide hemihydrate

The work done by researchers such as Gao et al. (2008), Kallinikos et al. (2010), Olausson et al. (1993), Zhong et al. (2008) and so forth, considered the role calcium sulphite hemihydrate on the overall rate of SO_2 chemical absorption.The commonly used expression is given in terms of relative saturation,e.g, in the work of Kallinikos et al. (2010), Olausson et al. (1993), Tseng & Rochelle (1986*a*) and others.

In Chapter 6 of this study, the effect of calcium sulphite hemihydrate crystallization on the overall SO_2 absorption process is addressed.

2.2.2.5 Oxidation of calcium sulphite hemihydrate

Sulphite oxidation is an intricate process that is of rudimentary grandness in WFGD (Brogren & Karlsson 1997*c*). Sulphite oxidation rate is influenced by numerous factors, namely, chemical reactions, catalysts, mass transfer mechanisms and so forth.

A superlative compendium of sulphite oxidation has been provided by Stromberg (1992). pH is considered to be cardinal to sulphite oxidation rate, since the chemical equilibria of the slurry strongly rely on it. A wide range of values are reported in literature of reaction with respect to hydrogen, sulphite and oxygen concentrations (Brogren & Karlsson 1997*c*) . Sulphite oxidation has been reported to involve radicals that cause chain reactions (Bäckström 1927), susceptible to both catalyst and inhibitors.

In this study, oxygen or air was not introduced into the reactor, consequently, gypsum crystallization is ignored. This can be attributed to the fact that this study aims to contribute to the understanding and modelling of wet flue gas desulphurization confined exclusively to the unsteady absorption of sulphur dioxide and the of chemical reactions in the limestone slurry phase in the absorber zone, since 85% (or more) absorption takes place in the absorber zone (Kiil et al. 1998). The oxidation chemical reactions (on freshly fed limestone slurry) in the absorber zone are considered to be negligible, consequently, the SO_3^{2-} and $CaSO_3$ oxidation sub-models are also neglected.

2.2.2.6 Crystallization of calcium sulphate

Gypsum crystallization is dependent on the relative supersaturation RS_{CaSO_4} (Olausson et al. 1993, Warych & Szymanowski 2001). The determination of the crystallization rate constant has been reported to be difficult to carry out, and the results reported by different researchers are not in agreement (Warych & Szymanowski 2001).

According to Warych & Szymanowski (2001), there is scarcity of models that describe the gypsum crystal size distribution and, furthermore, the laboratory-scale results are not apposite to be used to delineate crystallization in full scale plants. Gypsum crystallization and crystal size distribution are influenced by numerous factors, e.g., operating temperature, mixing and so forth.

It is epochal for gypsum crystal to be relatively large, so that it could be used as a building material (Kiil et al. 1998). RS_{CaSO_4} requires to be maintained below 1.4 through implementing longer residence times, as crystallization will now occur on crystal surfaces (Warych & Szymanowski 2001).

2.3 Flue Gas Desulphurisation: Integrated Models and Validation

Wet FGD processes had been amply modelled since in the 1980s through different approaches, namely, statistical approach (Perales et al. 2008, Zhao et al. 2007) and ontological approach (Brogren & Karlsson 1997*c*, Kallinikos et al. 2010, Neveux & Le Moullec 2011) and so forth. Most models cynosures on limestone wet FGD processes, as it is the most commonly used technology.

There is a gap in the understanding of chemical reactions and the detailed modelling of sulphur dioxide absorption in the sprayer zone of typical WFGD tower (where SO_3^{2-} and calcium sulphite oxidation and gypsum crystallization are normally assumed to be minimal). Studies that considers limestone dissolution and calcium sulphite crystallization (in the sprayer zone of typical WFGD tower) are meagre. Investigations that provide models that integrate the rate limiting steps of the absorption of SO_2 into limestone in stirred tank reactors (semi-batch and batch processes) are also scarce in literature.

2.3.1 Models compared with laboratory-scale stirred tank reactor results

Various models had been developed by different researchers based laboratory scale experiments. The same laboratory equipment are also used to evaluate some of the parameters required for modelling. Such models focused on providing information for specific aspects of the WFGD processes. For example, the reaction plane model, which is based on the film model,was developed and used by investigators such as Sada et al. (1983), Sada, Kumazawa, Sawada & Hashizume (1981), Takashina et al. (2001), Uchida & Ariga (1985) and so forth, to explain the aspects SO_2 absorption and the chemical reactions and mass transfers that take place in the liquid film.

A model based on two-film theory, that does not consider the dissolution of limestone, had been used by workers such as Lancia et al. (1997), Uchida et al. (1978) and so forth to evaluate the rate of SO_2 absorption, while coupling the mass transfer and the chemical reactions in the stagnant film, using an enhancement factor. Mass transfer coefficients (gas-side and liquid-side) are also commonly evaluated using the same stirred reactor tanks, by changing solutions.

2.3.2 Models compared with pilot plants results

The models developed for and validated by pilot plant experimental experiments had been observed to entail further aspects (Dou et al. 2009, Eden & Luckas 1998, Kiil

et al. 1998). Kiil et al. (1998) developed a model appertaining to a packed tower. Their model integrate all rate-limiting step, namely, SO_2 absorption, HSO_3^- oxidation, limestone dissolution and calcium sulphate crystallization and also takes into account the population balance of particles. Kiil et al. (2002) expounded the model of Kiil et al. (1998) in order to include the effect of HCl absorption on the SO_2 absorption and the concentration of residual $CaCO_3$ in the gypsum produced. The same model was also extended by Frandsen et al. (2001) to subsume the impact of buffer additives and chloride ions.

Dou et al. (2009) formulated a model to estimate mass-transfer taking into account the chemical enhancement factor and sulphite concentration in the liquid phase. The model was used to evaluate the efficiency of SO_2 absorption, despite the dependence of the model on a wide range of variables.For pilot plants, state-of-the-art models had been reported to predict desulphurisation with deviation of ± 3 % (Neveux & Le Moullec 2011).

The use of computational fluid dynamics (CFD) for modelling earo- and hydrodynamic (with minimal chemistry) had gained popularity (Gao et al. 2008, Tseng & Li 2018, Xiao et al. 2014). Tseng & Li (2018) employed a CFD simulation based on the Eulerian-Eulerian model, and considered both flow structure and chemical reactions. Wet FGD nozzle efficiency parameters were modelled by Brown et al. (2010) employing Lagrangian particle tracking method.

2.3.3 Models compared with industrial-scale results

A lot of work had been done towards the development of models that were compared with industrial data (Kallinikos et al. 2010, Neveux & Le Moullec 2011, Nygaard et al. 2004, Warych & Szymanowski 2001, Zhong et al. 2008). Different investigations focused on different issues, e.g. work by Kaesemann & Fahlenkamp (2002), Michalski (1997) explored the aero and hydrodynamics in order to relate the rate of desulphurisation to parameters such as droplet coalescence, pressure drop, gas distribution and so forth. As in Section, 2.3.2, results of CFD modelling (aerodynamic, hydrodynamic and chemistry) were compared with industrial data (Gómez et al. 2007, Marocco 2010, Marocco & Inzoli 2009). The model used by Gómez et al. (2007) employed Eulerian-Eulerian approach and considered mass-transfer mechanisms of gases. Marocco & Inzoli (2009) and Marocco (2010) used the Euler-Lagrange approach to simulate the aero and hydrodynamics inside a WFGD tower.

Brogren & Karlsson (1997*c*) developed and used a model premised on penetration theory. The model was employed to evaluate the dynamic rate of SO_2 absorption into droplets inside the spray tower whilst considering both instantaneous and finite rate chemical reactions(CO_2 hydrolysis, sulphite oxidation, limestone dissolution and

calcium sulphate crystallization).

A process model that calculate indispensable parameters for approximating limestone WFDG costs (capital,operation,existing and so forth), had been developed by Warych & Szymanowski (2001). Their model and the one developed by Neveux & Le Moullec (2011) takes into account, the rate-limiting steps of WFGD process, namely, SO_2 absorption, SO_3^{2-} oxidation, $CaCO_3$ dissolution and $CaSO_4 \cdot 2H_2O$ crystallization.

Chapter

3 Characterization

Introduction

The physico-chemical characteristics of limestone plays a major role on the performance of limestone during wet FGD, since they determine its dissolution, which (in turn) is the rate-limiting step of desulphurisation. The aim of characterisation study is in two folds, first to evaluate the limestone physico-chemical properties that are essential for the integrated model, second, to compare such properties with those of previously studied limestones. The techniques applied and results of characterisation of limestone and hannebachite before and after dissolution and SO_2 absorption are presented in this chapter. Materials were characterized with regard to mineral analysis (QEMSCAN), chemical analysis (XRF) and physical structural analysis (SSA, pore size distribution, PSD and helium skeletal density). Sections 3.1 and 3.2 present the details of the methodology and discussion of the generated results, respectively.

3.1 Methodology

3.1.1 Origin of materials

Limestone sample was supplied by PPC (Northern Cape Province, South Africa). The limestone was selected based on its relevance to the South African market, i.e. the high probability that it would be used in the local electricity supplier's (ESKOM) WFGD operations. The sample was ground to —45 μm (D90 = $\pm$23 μm). Two simulated flue gases ((2000 ppm SO_2, balance N_2) and (3000 ppm SO_2, 8.0 v/v % CO_2, 8.0 v/v%)), were supplied by African Oxygen, South Africa (Afrox). Hydrochloric acid (HCl, 36.5%) was supplied by Sigma-Aldrich (Pty) Ltd.

3.1.2 QEMSCAN

QEMSCAN analyses were conducted at the Eskom Research and Innovation Centre (South Africa,Gauteng province). The QEMSCAN equipment is commonly used to analyse coal, ashes, clinkers, fouling deposits etc. The equipment acquire 450 000 points per hour. A 1000 count energy dispersive spectrum was used to identify minerals (Van Alphen 2009*a*,*b*).

The limestone sample is first mixed with molten carnauba wax or with epoxy resin, thereby forming moulds of 30 mm thickness. The molten wax is left to set, whilst the epoxy resin is left to cure. The cross sections of individual particles were exposed by polishing the solid wax and cured epoxy resin to a 1μm final finish. The scanning electron microscope electron beam strikes the prepared sample at a predefined points.

A 7 millisecond 1000 count X—ray spectrum is acquired at each point.At each point, the elemental proportions are used to determine the mineral/amorphous phase (Van Alphen 2009*a*,*b*). The standard used for classification of mineral phases is the Eskom/VAC fly ash mineral/phase standard (Van Alphen 2009*a*,*b*).

3.1.3 X-ray diffraction

Back loading preparation method was employed for XRD analyses. X'Pert Highscore plus software was employed to identify the phases. Rietveld method (Autoquan program) was used for the quantification of relative phase amounts (in wt%). Crystalline structure of minerals on X-rays was the basis for the measurements.

3.1.4 X-ray fluorescence spectroscopy

XRF analysis for major and minor elemental compositions was conducted according to ASTM 3682 standards. Micronized samples (-75μm) were used for this analysis for acceptable results. Samples were initially dried at a temperature of 110 °C to a constant weight. The dried samples were then calcined in air at a temperature of 500 °C for 60 min and at 815 °C for 4 h, in order to remove water (as well as all organic components and to determine the loss on ignition value on coals). The calcined sample was converted into a solid solution by fusion with lithium tetraborate (Li2B4O7), LTB (one gram of the calcined ash to nine grams of LTB). The prepared solid solution and standard SARM—2, an international syenite certified reference material from MINTEK were placed in the sample holders and put in the sample compartment of the XRF spectrometer.

3.1.5 Surface area and pore volume

A Micromeritics ASAP 2010 instrument was used to determine both the specific surface area and pore volume (ASAP: Accelerated Surface Area and Porosimetry System). It has an accuracy of 0.15% for the pressure and ± 0.02 °C for temperature. The degas system has a deviation of less than ± 10 °C from the desired set-point (Micromeritics 2010).

Limestone sample mass of 0.2 g was used for the carbon dioxide adsorption experiments, the sample was first degassed and evacuated to 10 μmHg at a temperature of 380 °C. The analysis of the evacuated limestone sample was conducted at 0 °C (ice bath). For the nitrogen adsorption/desorption experiments, a samples were analysed at -195.8 °C (liquid nitrogen bath).

3.1.6 Density

Measurements of the skeletal density were conducted using a manual Quantachrome Helium Pycnometer (Quantachrome, Florida, USA). The accuracy of the equipment is 0.2% when appropriately set; when thermally equilibrated; and when the sample fills $>$ 75% of the nominal sample cell volume (Quantachrome 2009).Density is calculated from the ratio of the mass of discrete solid particles (and inaccessible pores) to the volume of discrete solid particles (and inaccessible pores). The volume of the discrete solid particles and their inaccessible pores are measured by pycnometer. A limestone sample weighing ± 7 grams was used in the small cell with a volume of 20 cm^3. Due to its small molecular volume and its ability to penetrate easily, helium was the gas medium used. The second motivation for using helium was its van der Waals forces that are weak enough that the adsorption of helium on the limestone surface can be neglected (Saha et al. 2007). Limestone sample was pressurized to 117.211 kPa during the analysis. (Quantachrome 2009, Webb 2001).

3.1.7 Particle size distribution

Malvern Mastersizer 3000 (supplied by Micron), was used to measure particle size distributions. Particle size distribution was performed using laser diffraction by applying the Mie theory. The PSD measurements were taken before and after the dissolution and desulphurization experiment. The particle volume was first determined, that was followed by the computing of the diameter of a sphere with the equivalent volume.

3.2 Results and Discussion

3.2.1 QEMSCAN results

The integrated model developed in Chapter 6 requires the knowledge of concentration of $CaCO_3$ in limestone. This necessitated the need to conduct mineral analysis (QEMSCAN) and chemical analysis (XRF). The later was conduct in order to provide additional information. A summary of QEMSCAN analysis is given in Table 3.1. The sample contains both crystalline and amorphous phases, with crystalline phases being dolomite and calcite. Dolomite (3.68 wt%) and calcite (95.31 wt%) are considered to be the source of calcium ions that reacts with sulphite ions to form calcium sulphite during SO_2 absorption. The source of calcium ions in limestone was distributed as calcite (78.8 wt%) and dolomite (0.4 wt%).

Literature on QEMSCAN analysis of limestone is scarce, the results from this study were compared with two South African limestones and one Polish limestone from the study conducted by Schutte (2018).

It is important to state that infinitesimal traces were normalized to 0 in this study. The QEMSCAN analysis results obtained in this study compared fairly well with those for Limestone A of Schutte (2018). Results of the Polish limestone were also fairly comparable.

3.2.2 X-ray Fluorescence (XRF) Spectroscopy Results

Results of XRF analysis limestones are tabulated in Table 3.2. It is clearly evident that CaO dominates (98.45 wt %). The intensity of an element during quantitative analysis by X-ray fluorescence is considered to be proportional to its percent composition, whilst, for complex matrix (e.g. ashes and limestones), the intensity of an element may not be directly proportional to the concentration due to result of an additional element within the sample.

Table 3.2: XRF analysis results.

	Composition (wt, %)									
Analyte	CaO	MgO	SiO_2	Al_2O_3	TiO_2	Fe_2O_3	MnO	Na_2O	K_2O	SO_3
This study	94.85	1.73	1.24	0.35	0.024	0.34	1.18	0.046	0.12	0.12
Carletti et al. (2015b) Finland	54.4	0.60	N/A	N/A	N/A	N/A	N/A	N/A	N/A	N/A
Carletti et al. (2015b) Polish	55.1	0.32	N/A	N/A	N/A	N/A	N/A	N/A	N/A	N/A

The reason given in Sub-section 3.2.1 regarding the comparison of results obtained by Schutte (2018) and those in this study, is also valid in this sub-section.

Table 3.1: QEMSCAN analysis results.

	Composition (wt %)												
Analyte	Calcite	Calcite-Siliceous	Dolomite	Dolomite-Siliceous	Kaolite	Ankerite	Gypsum	Feldspar	Quartz	Clay	Mica	Pyrite	Andalusite (Al-Sil)
This study	95.31	0.0	3.68	0.0	0.12	0.0	0.0	0.0	0.89	0.0	0.0	0.0	0.0
Schutte (2018) Limestone A	92.2	2.6	4.1	0.1	0.0	0.0	0.0	0.1	0.5	0.0	0.2	0.1	0.0
Schutte (2018) Limestone K	40.7	33.6	15.9	2.7	0.0	0.7	0.0	1.3	4.5	0.1	0.2	0.0	0.0
Schutte (2018) Poland	97.1	1.6	0.1	0.0	0.0	0.0	0.1	0.1	0.9	0.0	0.1	0.0	0.0

3.2.3 Structural analysis results

The integrated model developed in Chapter 6 requires a limestone dissolution model (presented in Chapter 4) as one of its input sub-models, which in turn requires the knowledge of the structural characteristics,namely, surface area and density. These requirements necessitated the determination of such parameters in this sub-section. Additional parameters that were not required in the model are considered to be additional information that could be useful in interpreting trends and other results.

Textural characteristics and the pore size distribution of limestones was investigated by fitting the data of CO_2 adsorption to several well-known adsorption models, namely, BET model, Langmuir model and DR model. One of the limiting steps of wet flue gas desulfurization has been reported to be limestone dissolution, which is in turn influenced by the particle size alongside other properties.

The summary of structural analysis results is tabulated in Table 3.3

Table 3.3: Summary of structural analysis results.

	Parameter							
	L-N_2-BET (m^2/g)	L-CO_2-DR (m^2/g)	L-PSD-SSA (m^2/g)	HK-Pore (cm^3/g)	L-PSD (μm)	L-Density (kg/m^3)	H-PSD-SSA (m^2/g)	H-PSD (μm)
This study	12.54	12.73	0.18	2.43	36.4	2440	0.83	34.45
Carletti et al. (2015b) Finland	0.05 - 0.1	N/A	0.01 - 0.021	N/A	74 - 250	2720	N/A	N/A
Carletti et al. (2015b) Polish	0.55-0.65	N/A	0.008 - 0.027	N/A	74 - 250	2703	N/A	N/A

Notes:

L-N_2-BET : Limestone specific surface area using Brunauer–Emmett–Teller theory and N_2 as adsorbate

L-CO_2-DR : Limestone specific surface area using Dubinin-Radushkevich equation and CO_2 as adsorbate

L-PSD-SSA : Limestone specific surface area using by the laser diffraction technique

HK-Pore : Limestone pore volume using the Horvath-Kawazoe approach

L-PSD : Limestone particle size distribution using the laser diffraction technique

L-Density : Limestone skeletal density using the gas pycnometry technique

H-PSD-SSA : Hannebachite specific surface area using by the laser diffraction technique

H-PSD :Limestone particle size distribution using the laser diffraction technique

N/A : Not available

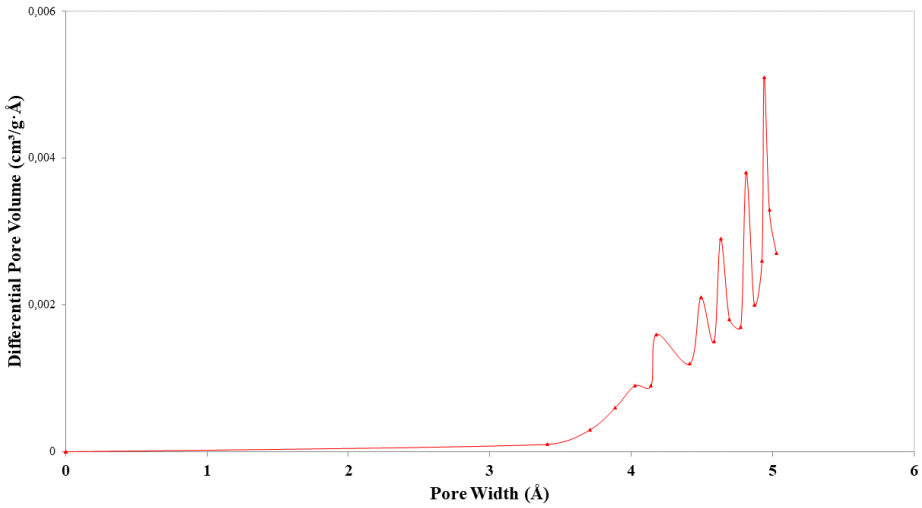

Figure 3.1: Limestone pore volume analysis.

The standard percentile diameters values were observed to decrease as expected. The Particles with diameters in the region of 1 to 3 μm are completely consumed. The dissolution of limestone under wet flue gas conditions had been reported to be a function of BET specific surface area and adsorption properties of ions on the surface of the particles (Carletti et al. 2015b).

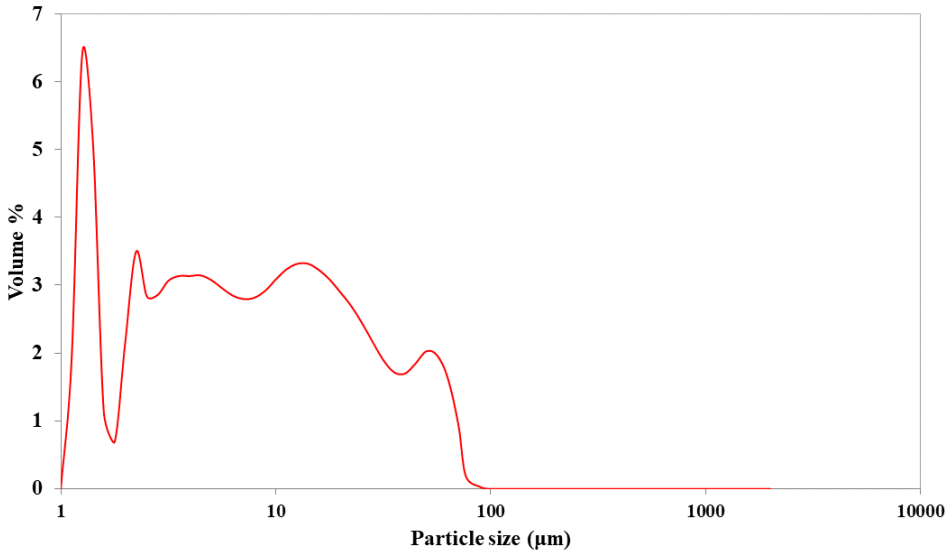

Figure 3.2: Particle size distribution of limestone.

The limestone used in this study is considered to be predominantly a mixture of minerals, and are thus expected to have pore sizes $> 2 < 50$ nm (predominantly

micropores). The properties are summarized in Table 3.3, there, the DR model had a satisfactory correlation coefficient.

The HK model is designed to describe the slit-shape pores and is primarily used to determine the pore sizes of predominantly microporous materials (Horváth & Kawazoe 1983). The differential pore volume distributions are presented in Figure 3.1,showing the differential pore volume values within the micro-porous range (1.5 to 5 nm).

Smaller particles are expected to dissolve more readily and thus they have a higher sulphur dioxide absorption rate. The PSD of raw limestone is presented in Figure 3.2. Table 3.3 provides a summary of average diameters of particles with cumulative fractions of 10, 50 and 90% (D(v, 0.1), D(v, 0.5), D(v, 0.9)); the average diameter of weighted volume D[4,3]; specific surface area and the average diameter of weighed surface.

3.3 Summary

- The techniques and results of characterisation of limestone are presented in this chapter.
- A South African limestone sample (from the Northern Cape province) was prepared through milling and sieving. Hydrochloric acid was supplied by Sigma-Aldrich (Pty) Ltd.
- The mineral analysis in this study were conducted using QEMSCAN technique, and the results thereof are presented in this chapter.
- The technique used for the analysis of major and minor elemental compositions (XRF) and the results thereof are presented in this chapter.
- The methods used to measure/determine the physical structural properties (SSA, pore size distribution, PSD and helium skeletal density) and the results thereof, are given in this chapter.
- The physico-chemical properties from this chapter were used in the later chapters for various purposes. This because, the physico-chemical properties of a limestone affects the dissolution of limestone, which in turn, is one of the rate-limiting steps of wet FGD desulphurisation.
- The examples characterisation results usage are:

i. Concentration of $CaCO_3$ used in modelling limestone dissolution (chapter 4) was determined using QEMSCAN.

ii. Concentration of both $CaCO_3$ and $CaSO_3 \cdot 2H_2O$ used to validate the limestone dissolution and hannebachite sub-models of the integrated model (chapter 6) were determined using XRD. The XRF results confirmed the distributions.

iii. The BET_{CaCO_3} surface area and pore volume used for limestone dissolution (in chapters 4 and 6) were evaluated using the results from the Micromeritic ASAP 2010 presented in 3.1.5

iv. The limestone density used during the determination of limestone dissolution mass transfer coefficient (chapter 4) was measured using the Quantachrome Helium Pycnometer.

v. The limestone particle size used during the determination of limestone dissolution mass transfer coefficient (chapter 4) was measured using the Malvern Mastersizer 3000.

Chapter 4 Dissolution kinetics of limestone: Experimentation and reaction rate modelling

The integrated model that was later developed (in Chapter 6) requires the knowledge of the total dissolution constant (k_{tot}). The aim of this chapter involves determining k_{tot} (from the evaluated k_l and k_r) of a South African limestone. k_l was evaluated using the Frössling-type correlation of Sherwood number, and was found to be reliant on the experimental operating conditions (solution pH, temperature and agitation speed) whereas the k_r was estimated from the gradient of the linear plot of $\ln C_{H^+}$ vs t on dissolution conducted at stirring rates greater than triple the critical impeller speed($N>3N_{js}$). The total dissolution constant (k_{tot}) was estimated by the reciprocal addition of $1/(k_l)$ and $1/(k_r)$.The obtained k_{tot} is comparable with the k_{tot} regressed from the model fitting. The activation energy of limestone dissolution in the present study is comparable to those published in literature. Section 4.1 presents a review of work done by other workers. Experimentation is given in Section 4.2. The mass transfer-reaction model is given in Section 4.3 and the results thereof are discussed in Sections 4.4 and 4.8.

4.1 Introduction

SO_2 emissions, mainly from fossil fuel combustion, poses a threat to the environment and are a health risk. This led to stringent regulations being set by regulatory bodies across the world. One of the most commonly used SO_2 abating technology is limestone WFGD due to their relatively low cost and greater efficiency.Limestone dissolution is one of the rate-limiting steps in the limestone WFGD process as it directly affects the chemical reaction equilibria, thereby influencing SO_2 absorption, $CaCO_3$ utilization,scaling and other relevant sub-processes. As a result, the understanding

and modelling of limestone dissolution for WFGD processes is crucial.

Besides its applicability to WFGD studies, limestone dissolution is applicable to many other technological processes e.g. acid water neutralization (Barton & Vatanatham 1976, Santoro et al. 1987), waste water bio-mediation (Gibert et al. 2003), carbonate geological behaviour (Buhmann & Dreybrodt 1985, Busenberg & Plummer 1986, Morse 1974, Morse & Arvidson 2002) and calcium carbonate equilibrium in oil wells (Coto et al. 2012). Studies of limestone dissolution for WFGD processes had been conducted by authors like Carlett et al. (2015a), Carletti et al. (2012, 2015b), De-Blasio et al. (2012), Fellner & Khandl (1999), Gage (1989), Gage & Rochelle (1992), Lancia et al. (1991), Santoro L. & G. (1973), Shih et al. (2000), Toprac & Rochelle (1982).

Earlier studies on limestone dissolution focused on various aspects, the most common being controlling mechanisms (mass transfer or reaction kinetics or a combination of both), effect of pH on the apparent activation energy, effect of inhibitors on dissolution, effect of CO_2 (desorption/absorption/reaction), PSD, effect of agitation and other properties. Several authors (Barton & Vatanatham 1976, Berner & Morse 1974, Plummer & Wigley 1976, Sjöberg & Rickard 1984*a*) reported that limestone dissolution at low pH is mass transfer-controlled and is reaction kinetics-controlled at high pH. Low apparent activation energy (< 20 kJ/mol) had been reported by various investigators (Chan & Rochelle 1982, Plummer et al. 1978) for experiments at low pH (< 5), the inverse is true for experiments at high pH (> 5.5) (Lund et al. 1973, Sjöberg & Rickard 1984*b*). The reaction of CO_2 was reported not to be important under WFGD conditions (Jarvis et al. 1988), it is only at high CO_2 pressure, that the hydrolysis of CO_2 can enhance limestone dissolution Chan & Rochelle (1982). The same authors reported that the partial pressure of CO_2 can vary from near zero to 0.1 atm. The effect of inhibitor (e.g. sulphite ions, phosphate ions, aluminium ions, copper ions, fluorite ions, scandium ions, manganese ions etc.) was investigated by several researchers. (Gage & Rochelle 1992, Jarvis et al. 1988, Morse 1974). The effect of agitation had been studied by various authors (Fusi et al. 2012, Pepe 2001, Plummer et al. 1978, Sjöberg & Rickard 1983). Plummer & Busenberg (1982), and it was reported that the role of agitation is more pronounced with an increase in limestone particle size. Studies on the role of PSD were conducted by investigators such as Tress et al. (1985), Ukawa et al. (1993)

Particle size plays an important role during limestone dissolution, e.g., for larger particles, k_l is proportional to 0.5 power of agitation rate. For finer particles, the mass transfer coefficient is inversely proportional to particle size (Harriott 1962).

For surface reaction controlled dissolution, the mass transfer and chemical reaction resistances are considered to be in series, and their reciprocal sum can be

used to describe the dissolution rate (Lund et al. 1975). For low pH (pH less than 3.5) and low activation energy (8.4 kJ/mol), the diffusion of H_3O^+ ions (designated as H^+ in the equations) limits the dissolution. The activity of H_3O^+ ions is also directly proportion to the dissolution rate (Plummer et al. 1978). For high pH (pH greater than 3.5) and high apparent activation energies, the same authors suggested that the role played by surface reaction is more conspicuous with accretionary pH. The conclusions drawn by Sjöberg & Rickard (1984*b*) concerning the k_l and k_r are similar to the ones presented by Plummer et al. (1978).

Various limestone dissolution models based on either experiments, theory or both, had been presented in literature Amrhein et al. (1985), Bjerle & Rochelle (1984), Brogren & Karlsson (1997*b*), Buhmann & Dreybrodt (1985), Carletti et al. (2012), Chan & Rochelle (1982), Koech et al. (2014), Sjöberg & Rickard (1984*a*,*b*), Wallin & Bjerle (1989*a*,*b*, 1990), namely, semi-empirical, shrinking-core, film theory, penetration theory etc. The limestone dissolution studies that are inclined on WFGD includes the work of Blasio et al. (2018), Brogren & Karlsson (1997*a*,*b*), Carlett et al. (2015a), Carletti et al. (2012, 2015b), Fellner & Khandl (1999), Gage & Rochelle (1992), Koech et al. (2014), Lancia et al. (1991, 1994*a*), Souza et al. (2010), Toprac & Rochelle (1982), Ukawa et al. (1993). The models developed by Gage & Rochelle (1992), Lancia et al. (1991, 1994*a*), Souza et al. (2010) were based on film theory, and were reported to be dependent on the properties of limestone (structural and physico-chemical properties) and experimental conditions (solution pH,inhibitors,hydrodynamics etc). Models based on mass transfer theory were developed by authors such as Brogren & Karlsson (1997*b*)) and Chan & Rochelle (1982). They considered the role of CO_2 hydrolysis to be negligible under WFGD conditions (i.e low concentration of CO_2 in the presence of sulphite species). The semi-empirical model was developed and used by Koech et al. (2014).

The important conclusions that can be drawn from this review includes that, at low pH (<5.5), and low activation energy (< 20 kJ/mol), limestone dissolution is mass transfer-controlled. The inverse in true for chemical reaction-controlled. The influence of CO_2 chemical reactions and desorption is not significant at low partial pressures of CO_2.The aim of this part of the study is to evaluate the total dissolution constant (k_{tot}) of a South African limestone. This involves the determination of solid-liquid mass transfer coefficient (k_l) and chemical reaction constant (k_r). The study also aims to evaluate the activation energy of the of limestone dissolution process as well as to fit a model to the experimental results.

4.2 Experimental

4.2.1 Materials

Details of the limestone (origin, motivation for selection and preparation) used are in Chapter 3, Sub-section 3.1.1. Hydrochloric acid (HCl, 36.5%) was supplied by Sigma-Aldrich (Pty) Ltd.

4.2.2 Apparatus and methods

Limestone dissolution experiments were conducted using a thermostatted reactor. A stirrer with two sets of blades (eight blades per set) is placed in the centre of the reactor. The Eight baffles are installed along the inner circumference of the reactor at equidistant positions.

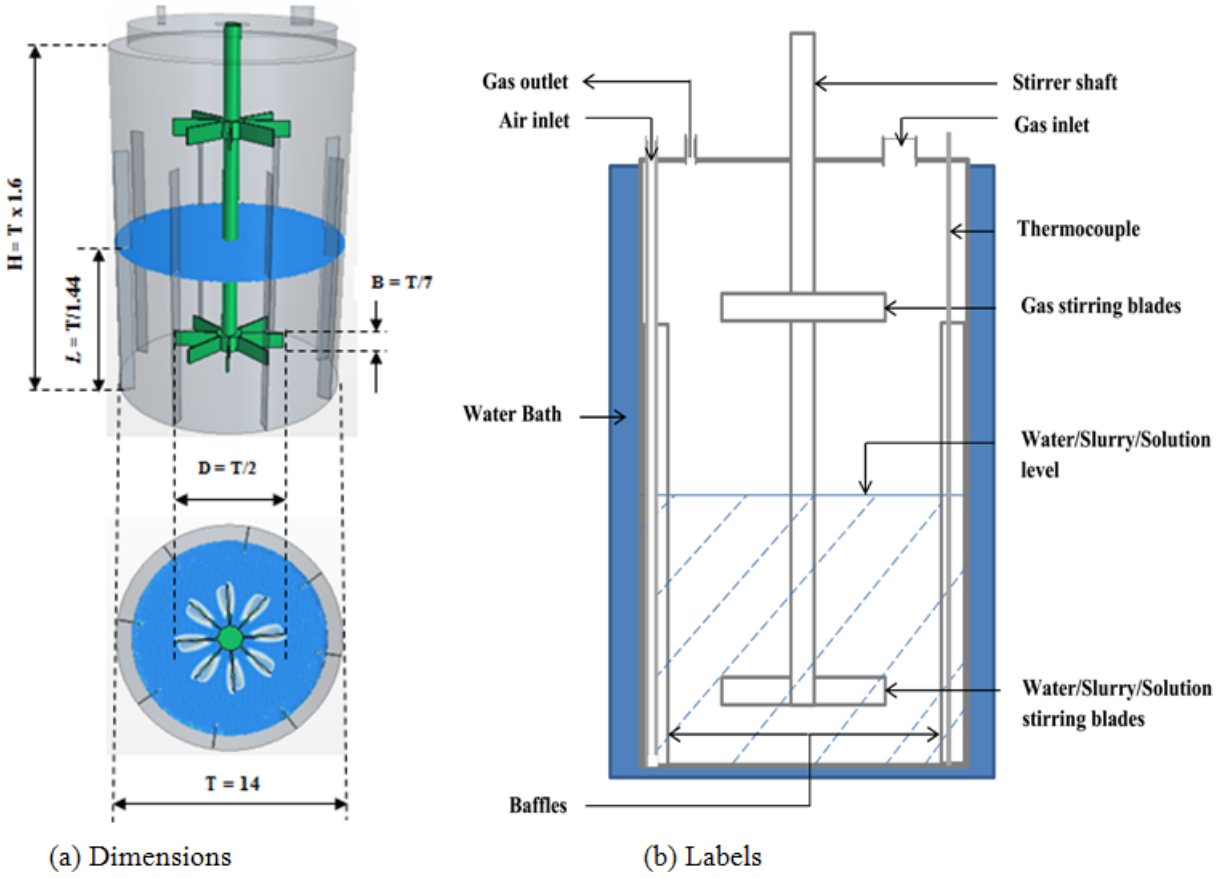

Figure 4.1: Stirred tank reactor (T in cm).

Metrohm 691 pH meter and a unitrode with Pt 1000 (Metrohm, South Africa) were employed for pH measurement per 2 seconds. A Memmert water-bath, with a 1 Pt100 sensor class A in 4-wire-circuit (supplied by Lasec) was used to keep the

temperature of the reactor at a set value. A K-type thermocouple (WIKA) was employed to measure the temperature inside the reactor. The Metww-05-L watt-meter (supplied by Schneider Electric South Africa (Pty) Ltd) was used to measure the power consumption.

Table 4.1: Summary of operating conditions.

Condition	Range/Value	Units
Sample mass	1 - 5	g
Slurry volume	5 x 10^{-4} – 1.5 x 10^{-3}	m^3
HCl concentration	0.05 - 0.4	M
Temperature	293.15 – 343.15	K
Stirring rate	1-6	s^{-1}

Details of limestone characterization methods are given in Chapter 3,Section 3.1, with the corresponding results in Section 3.2. Dissolution experiments were conducted by free drift method, in which the pH is allowed to freely increase from the initial value to a higher desired value (e.g. equilibrium pH) as result of limestone dissolution. The operating conditions are summarized in Table 4.1. Slurry pH was recorded as a function of time. On some experiments, slurry samples were collected and sieved. The aliquot was analysed using the using the inductively coupled plasma optical emission spectrometer (ICP Expert II, Agilent Technologies 720 ICP-OES).

4.3 Mass Transfer - Reaction Model

The mass transfer-reaction model requires the knowledge of the overall dissolution rate constant, k_{tot}, which in turn requires both the k_l and k_r. Sub-section (4.3.1) present the method used to evaluate the k_l whereas Sub-section (4.3.2) present approach used to delineate the chemical reaction constant. The determination of the overall dissolution constant and the development of the overall mass transfer-reaction model are presented in Sub-sections 4.3.3 and 4.3.4.

4.3.1 Determination of mass transfer coefficient

k_l in agitated solid-liquid systems are usually computed using a Frössling-type correlation. In this study, the k_l was calculated using Sh. Equation 4.1 gives the correlation for spherical particles

$$Sh = a + b \cdot Re^{\frac{1}{2}} \cdot Sc^{\frac{1}{2}} \tag{4.1}$$

where Re and Sc are the Reynolds (for particle) and Schmidt numbers, respectively, a and b are dimensionless coefficients. Sh can be outlined as per Equation 4.2

$$Sh = \frac{k_l d_p}{D_i} \tag{4.2}$$

where d_p is the diameter of the particle and D_i is the diffusion coefficient of the species i, defined by the equation given by Boudreau (1997)

$$D_i = \alpha + \beta \cdot T \tag{4.3}$$

where α and β are the empirical parameters specific for every species.

The Reynolds number for particles can be defined as

$$Re = (\frac{\varepsilon d_p^4}{\nu^3})^{\frac{1}{3}} \tag{4.4}$$

where ν is the kinematic viscosity of the liquid and ε is the mean dissipated energy, defined as

$$\varepsilon = \frac{N_p \rho N^3 D^5}{V} \tag{4.5}$$

where N_p, ρ, N, D and V are the power number, density of the liquid, stirring rate,impeller diameter and volume of the liquid. The Schmidt number is given by

$$Sc = \frac{\nu}{D_i} \tag{4.6}$$

The definition of the Sh can be rearranged to give k_l as per Equation 4.7

$$k_l = \frac{D_i}{d_p}(\frac{\varepsilon d_p^4}{\nu^3})^{\frac{1}{6}}(\frac{\nu}{D_i})^{\frac{1}{3}} \tag{4.7}$$

4.3.2 Determination of Chemical Reaction Constant

Two approaches of determining k_r were considered in this study, namely, regression and higher stirring rate approach. The second approach was arbitrarily favoured in this study. In this approach, dissolution of limestone in HCl solution is conducted at different stirring rates,where above a particular stirring rate, dissolution is no longer affected by stirring. Carletti et al. (2015b) reported that stirring rate to be three times the minimum critical impeller speed (defined as the speed at which no solids remained stationary on the base of vessel for longer than 2 seconds (Zwietering 1958))

Under this condition, the change in hydronium ions concentration in the bulk can be given by Equation 4.8

$$-V\frac{dC_{H^+,slurry}}{dt} = k_r \cdot SSA \cdot (C_{H^+,interphase} - C_{H^+,equilibrium})^n \tag{4.8}$$

where V, is the volume of the slurry and $C_{H^+,slurry}$, $C_{H^+,interphase}$ and $C_{H^+,equilibrium}$, are hydronium concentration in the slurry bulk, liquid-solid interphase and at equilibrium. SSA_{BET} is the product of the BET surface area and the mass off solid limestone and n is the order of the chemical reaction.

At low pH values (pH≤4.5), the effect of equilibrium hydronium concentration and CO_2 are considered to be negligible. First order overall reaction is also assumable, i.e. n equals 1. Moreover, under these high stirring rates, the hydronium ions concentration at the interphase can be estimated by the concentration in the bulk slurry,consequently, Equation 4.8 can be abridged to Equation 4.9

$$-V\frac{dC_{H^+,slurry}}{dt} = k_r \cdot SSA \cdot C_{H^+,slurry} \tag{4.9}$$

Equation 4.9 can be integrated to give

$$lnC_{H^+,slurry} = lnC^o_{H^+,slurry} - \frac{k_r \cdot SSA}{V_{slurry}}t \tag{4.10}$$

where $C^o_{H^+,slurry}$ is the initial concentration of H_3O^+ ions in the bulk slurry. k_r, can thus be estimated from the gradient of the linear plot of Equation 4.10, i.e. $\ln c_{H^+}$ vs t. It is imported to reiterate that this approach is only applicable under cases in which $k_l \gg k_r$, and thus controlled by reaction resistance ($1/k_r$).

The effect of temperature on the chemical reaction constant can be given by the Arrhenius equation (Equation 4.11),

$$k_r = k_1 \cdot e^{\frac{-E_a}{RT}} \tag{4.11}$$

where k_1 is the pre-exponential factor, E_a, is the apparent activation energy, R is the universal gas constant and T is the temperature in the reactor.

4.3.3 Determination of Overall Rate Constant

The relative significance of mass transfer and chemical reactions during limestone dissolution in HCl solutions depends on the magnitudes of k_l and k_r and the level of disequilibrium in the system (Murphy et al. 1989).

The total dissolution constant (k_{tot}) was estimated by the reciprocal addition of $1/(k_l)$ and $1/(k_r)$ according to Equation 4.12, (MacInnis & Brantley 1992)

$$\frac{1}{k_{tot}} = \frac{1}{k_l} + \frac{1}{k_r} \tag{4.12}$$

Before it was used in the mass transfer-reaction model, k_{tot} was first modified to account for the concentration of hydronium ions on the surface of the limestone particles, rather than in the bulk slurry.

4.3.4 Mass Transfer-Reaction Model development

The chemical reactions considered during the dissolution of limestone can be represented by this mechanism:

$$CaCO_3(s) \longrightarrow CaCO_3(aq) \tag{R4.1}$$

$CaCO_3$(aq) dissociation:

$$CaCO_3(aq) \leftrightharpoons Ca^{2+}(aq) + CO_3^{2-}(aq) \tag{R4.2}$$

HCO_3^- dissociation:

$$H^+(aq) + CO_3^{2-}(aq) \leftrightharpoons HCO_3^-(aq) \tag{R4.3}$$

HCO_3^- dissociation:

$$H^+(aq) + HCO_3^-(aq) \leftrightharpoons CO_2(aq) + H_2O(l) \tag{R4.4}$$

CO_2(g) desorption

$$CO_2(aq) \leftrightharpoons CO_2(g) \tag{R4.5}$$

The above mechanism can be simplified into one overall reaction consisting of a forward and backward reactions (R4.6 and R4.7),(Brantley et al. 2008, Carletti et al. 2015b). This had been termed 'two-step' mechanism, in literature. Where the first step (R4.6) is rate determining, and the second step (R4.7) is assumed to be quasi-equilibrium Carletti et al. (2015b).

A two steps mechanism proposed by Carletti et al. (2015b) can be given R4.6 and R4.7, which lead to the overall reaction (R4.8)

$$CaCO_3(s) + H^+(aq) \rightleftharpoons Ca^{2+}(aq) + HCO_3^-(aq) \quad \text{(R4.6)}$$

$$HCO_3^-(aq) + H^+(aq) \rightleftharpoons H_2O(l) + CO_2(aq) \quad \text{(R4.7)}$$

The overall dissolution reaction (Carletti et al. 2015b, Morse 1974) presented as

$$CaCO_3(s) + 2\,H^+(aq) \rightleftharpoons Ca^{2+}(aq) + CO_2(g) + H_2O(l) \quad \text{(R4.8)}$$

Chemical reaction R4.8 yields a stoichiometric ratio of 1:2 (i.e for Ca:H_3O^+). Stoichiometry has been used by other researchers (Chan & Rochelle 1982, Plummer & Busenberg 1982, Shih et al. 2000, Siagi & Mbarawa 2009, Toprac & Rochelle 1982) to estimate Ca^{2+} ions in the bulk liquid whilst employing pH-Stat method. Since partial pressure of CO_2 is minimal, the effect of CO_2 reactions and desorption (on limestone dissolution) is considered to be insignificant in this study.

The schematic diagram of mass transfer and chemical Reaction during limestone dissolution is proposed by Gunn (2003) had been modified to suite the transport and reaction mechanism above, and is given in Figure 4.2. Ca^{2+} and CO_3^{2-} ions released from the surface of the mineral are transported away into the bulk of the solution by mass transfer. On the other hand, CO_2, H_2CO_3, and H_3O^+ are also transported from the bulk slurry to the surface. In Figure 4.2, the dashed lines represent mass transfer, and solid lines symbolises chemical reactions. Due to mass transfer, concentration gradients build up such that the concentrations in the bulk are different from those on the solid surface Gunn (2003).

The model developed by Carletti et al. (2015b) was employed in this study. The model comprises of both the mass transfer step in the liquid phase and the chemical reaction step at the solid-liquid interface. The thickness of the diffusion layer is assumed to be negligible when the mass transport is sufficiently enhanced. Hydronium ions mass transfer from the bulk liquid to the solid-liquid interface can be given by Equation 4.13

$$R_{H^+,slurry} = k_l \cdot SA \cdot (C_{H^+,slurry} - C_{H^+}, interphase) \quad (4.13)$$

where $C_{H^+,slurry}$ and $C_{H^+}, interphase$, are concentrations of hydronium ions in bulk slurry and in the solid-liquid interface, respectively.SA, is the solid-liquid interface surface area, R_{H^+} is the rate of dissolution.

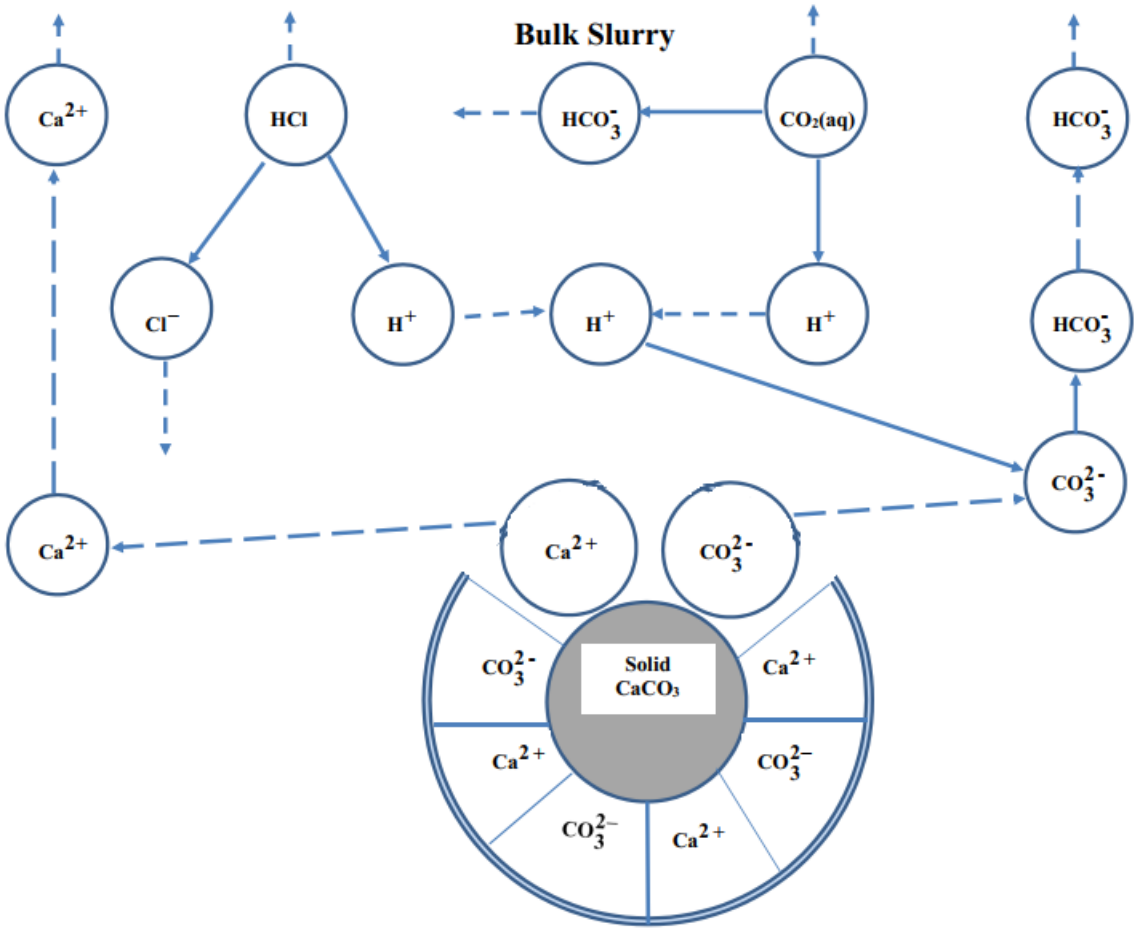

Figure 4.2: Schematic Diagram of Mass Transfer and Chemical Reaction during dissolution.

The dissolution rate due to chemical reaction at the solid-liquid interface can be given by Equation 4.14

$$R_{H^+,slurry} = k_r \cdot SA \cdot (C_{H^+}, interphase - C_{H^+}, equilibrium) \tag{4.14}$$

where $C_{H^+,equilibrium}$ and k_r are the concentration at equilibrium and the chemical reaction constant,respectively.

SA is evaluated by multiplying SSA_{BET} by the molecular weight (MW_{CaCO_3}) and the concentration (C_{CaCO_3}) of solids according to Equation 4.15

$$SA = SSA_{BET} \cdot MW_{CaCO_3} \cdot C_{CaCO_3} \tag{4.15}$$

The total rate can be given by the reciprocal addition of resistances of according to Equation 4.12, and thus, the overall rate of dissolution can be given by Equation 4.16

$$R_{H^+,slurry} = k_{tot} \cdot SA \cdot (C_{H^+,slurry} - C_{H^+,equilibrium}) \tag{4.16}$$

when $C_{H^+,slurry} \gg C_{H^+,equilibrium}$, Equation 4.16 can be simplified to Equation 4.17 (Ahlbeck et al. 1995). This assumption is not applicable to a typical limestone WFGD operated at a pH range of 5 to 6 (Córdoba 2015), however in this study, the pH was observed to drop below 2.5 in some instances (Chapter 6).

$$R_{H^+,slurry} = k_{tot} \cdot SA \cdot C_{H^+,slurry} \tag{4.17}$$

For dissolution to take place, hydronium ions should come into contact with the limestone particles, considering that the limestone sample in this study had been reported to have a Horvath-Kawazoe pore volume of 2.43 cm^3/g in Table 3.3. Equation 4.17 can be re-written in terms of surface concentration (θ_{H^+}) rather than bulk concentration (c_{H^+}):

$$R_{H^+,slurry} = k_{tot} \cdot SA \cdot \theta_{H^+} \tag{4.18}$$

The coverage of H_3O^+ ions on the solid surface (θ_{H^+}) can be estimated using the Langmuir adsorption isotherm:

$$\theta_{H^+} = \frac{K_{ad} \cdot C_{H^+}, slurry}{1 + K_{ad} \cdot C_{H^+,slurry}} \tag{4.19}$$

Where K_{ad} is the adsorption. On introducing the Langmuir adsorption isotherm, Equation 4.18 gives

$$R_{H^+,slurry} = k'_{tot} \cdot SA \cdot \frac{K_{ad} \cdot C_{H^+}, slurry}{1 + K_{ad} \cdot C_{H^+,slurry}} \tag{4.20}$$

The constant on the numerator,K_{ad}, and k'_{tot}, can be lumped according to Equation 4.20

$$k_{tot} = k'_{tot} \cdot K_{ad} \tag{4.21}$$

When the coverage of limestone surface is considered to be $1 - \theta_{H^+}$, the rate of change of concentration of species can be given by an ODEs tied by stoichiometric

constraints. The rate of change in concentrations of C_{CaCO_3} and $C_{H^+,slurry}$ can be given by Equations 4.22 and 4.23, respectively

$$\frac{dC_{CaCO_3}}{dt} = -k_{tot} \cdot SA \cdot C_{H^+,slurry} \cdot (1 - \frac{K_{ad} \cdot C_{H^+}, slurry}{1 + K_{ad} \cdot C_{H^+}, slurry}) \tag{4.22}$$

$$\frac{dC_{H^+,slurry}}{dt} = -\gamma \cdot k_{tot} \cdot SA \cdot C_{H^+,slurry} \cdot (1 - \frac{K_{ad} \cdot C_{H^+}, slurry}{1 + K_{ad} \cdot C_{H^+}, slurry}) \tag{4.23}$$

where γ is the dissolution stoichiometric coefficient. The change in concentration of calcium ions and bicarbonate ions can be given by Equations 4.24 and 4.25, respectively, when the stoichiometric coefficient is assumed to be 1.

$$\frac{dC_{Ca^{2+}}, slurry}{dt} = k_{tot} \cdot SA \cdot C_{H^+,slurry} \cdot (1 - \frac{K_{ad} \cdot C_{H^+}, slurry}{1 + K_{ad} \cdot C_{H^+}, slurry}) \tag{4.24}$$

$$\frac{dC_{HCO_3^-}, slurry}{dt} = k_{tot} \cdot SA \cdot C_{H^+,slurry} \cdot (1 - \frac{K_{ad} \cdot C_{H^+}, slurry}{1 + K_{ad} \cdot C_{H^+}, slurry}) \tag{4.25}$$

When surface inhibition is negligible (e.g. when $SO_3^{2-} \geq 1$ M and Al^{3+} and F^{1-} are traces), dissolution of limestone in the WFGD process had been reported to be controlled by mass transfer of species to and from the surface of the suspended limestone particles (Gage & Rochelle 1992, Jarvis et al. 1988, Weng 2016). The mass transfer limitations are overcame through operating the reactor under conditions in which the kinetics is slower than mass transfer,namely, operating the reactor at a stirring rate that is greater than thrice the critical impeller speed ($N > 3 \cdot N_{js}$) and air flow greater than 9500 cm^3/min (Carletti et al. 2015b).

4.3.5 ODEs Numerical Methods

A system of ODEs that describes the dissolution of limestone (Equations 4.22 through 4.25) was solved numerically employing a software package MATLAB (MATLAB 2018). The nature of the equations, the range of parameters and variables involved, permitted the use of MATLAB's standard solver for ODEs, that is, the ODE45 and ODE15s functions.

The most commonly used ODE solver for ordinary differential problems is ODE45, owing it to its versatility. However, it is not recommendable for stiff problems and those requiring high accuracy, suitable solvers are ODE15s, ODE23 and so forth (MATLAB 2018).

The mathematical method used by ODE45 is Runge-Kutta whilst employing variable time step for expeditious computing. Ordinary differential equations of the form $y' = f(t, y)$ are integrated from t0 to tf when the initial condition is taken to be y0, i.e., the problem is considered to be specified when the vector of $f(t, x)$ is set and both $y0$ and $t0$ are specified (MATLAB 2018).

4.3.6 Parameters estimation

The goodness of the numerical simulation is reliant on the correctness of the input parameters and initial conditions. Both input parameters and initial conditions, in turn, depends on the validity of assumptions made and experimental errors that were made. Under circumstances where the assumptions are not valid and/or the experimental errors are more pronounced, parameters are checked by fitting. Error analysis for the measurements done in Chapters 4 to 6 is given in Appendix A.

The parameters estimated in this present study includes chemical reaction constant (k_r), stoichiometric coefficient (γ), diffusivity constants (D_i), adsorption constant (K_{ad}) and enthalpy of adsorption (ΔH^0_{ad}). Ordinary differential equations 4.22 through 4.25 were used in the regress K_{ad}. The initial concentrations of Ca^{2+} and HCO_3^- are considered to be zero. Matlab R2018b software was employed, as it was the case in Sub-Section 4.3.5.

The commonly used approach is the use of sum of square errors and the corresponding root mean square. Let x_i be the experimental value approximated by numerical solution $x(t)$ at time t_i. Define $\{y_i, z_i\}$ similarly. The sum of square errors can be given by Equation 4.26

$$SSE = \sum_{i=1}^{n}((x(t_i) - x_i)^2 + (y(t_i) - y_i)^2 + (z(t_i) - z_i)^2) \tag{4.26}$$

and the root mean square error is given by Equation 4.27

$$RMSE = \sqrt{SSE/3n} \tag{4.27}$$

The Nelder-Mead Simplex Method algorithm (Nelder & Mead 1965) has been reported to be efficient by Wright (2012), and is implemented by $lsqcurvefit$ optimization tool in MATLAB.

4.4 Results and Discussion: Experimental Results

The dissolution of finely ground limestone ($\leq$ 45 μm) were conducted employing the equipment and following the free-drift method given in Section 4.2.

Limestone dissolution was determined from the transient pH mensuration in the bulk slurry, considering that the change in H_3O^+ concentration is stoichiometric to $CaCO_3$ dissolution. A better delineation of limestone is considered to be the plotting of transient H_3O^+ ions concentration against time. The same approach was employed by Carletti et al. (2015b), and is espoused this study.

The effects of stirring rate, HCl concentration, temperature and solid-to-liquid ratio were investigated. Except for the case of the effect of HCl concentration, two distinct steps were observed, namely, a very fast dissolution step (leading to a quick decrease in H_3O^+ ions), and a slow dissolution step (leading to a slow steady decrease in H_3O^+ ions). This observation is consistent with that of Pepe (2001), and the second step can be attributed to the CO_2 gas - liquid mass transfer and the solid-liquid hydrodynamics. The same authors reported that under their experimental conditions used, a fraction of a second (0.4 second) is sufficient for dissolution to take place and to ameliorate pH to a value above 7. Under the conditions of the current study, presented in Section 4.2, a period of 30 seconds was considered.

4.4.1 Effect of experimental parameters

Figure 4.3 spectacle the effect of reaction temperature on limestone dissolution rate. It is evident that the dissolution rate is directly proportional to temperature over the first 4 seconds.The deviation at 40 °C can be ascribed to experimental error.

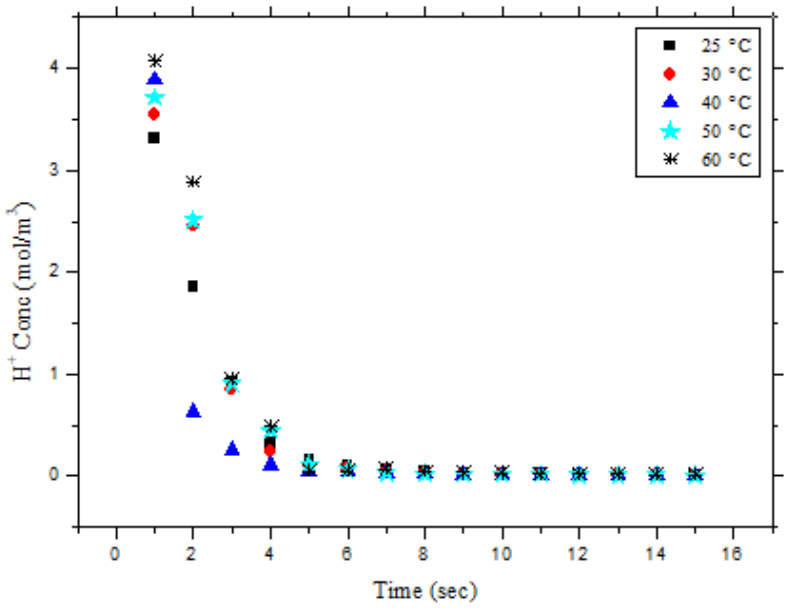

Figure 4.3: Effect of temperature on dissolution of limestone.

It has been reported in literature (Aydoğan et al. 2007, Xiang et al. 2009) that chemical reaction controlled processes are reliant in temperature, whereas diffusion controlled processes are meagerly dependent. Accordingly, temperature plays a pivotal role in this study.

The results presented in Figure 4.4 shows that limestone dissolution is dependent on agitation rate until adequately vigorous turbulence is attained ($\geq$ 424 rpm). The enhancement of species transfer can be ascribed to stirring. This observation is in agreement with work reported of other researchers who studied effect of stirring on mass transfer between liquid and suspended solid particles (e.g. limestone) (Carletti et al. 2017, Fusi et al. 2012). Carlett et al. (2015a) reported that at a stirring rate greater than three times the minimum critical impeller speed, agitation does not affect limestone dissolution.

The dissolution experiments in this investigation were conducted under stirring rate that does not allow mass transfer to be limiting i.e. under agitation where the speed of the impeller is greater than twice the critical impeller speed (Carlett et al. 2015a, Carletti et al. 2015b). For the reactive surfaces of particles to be perpetually exposed to the tempestuousness, particles need to be kept suspended. In this investigation, the critical impeller speed was estimated using the Zwietering method and correlation Zwietering (1958).

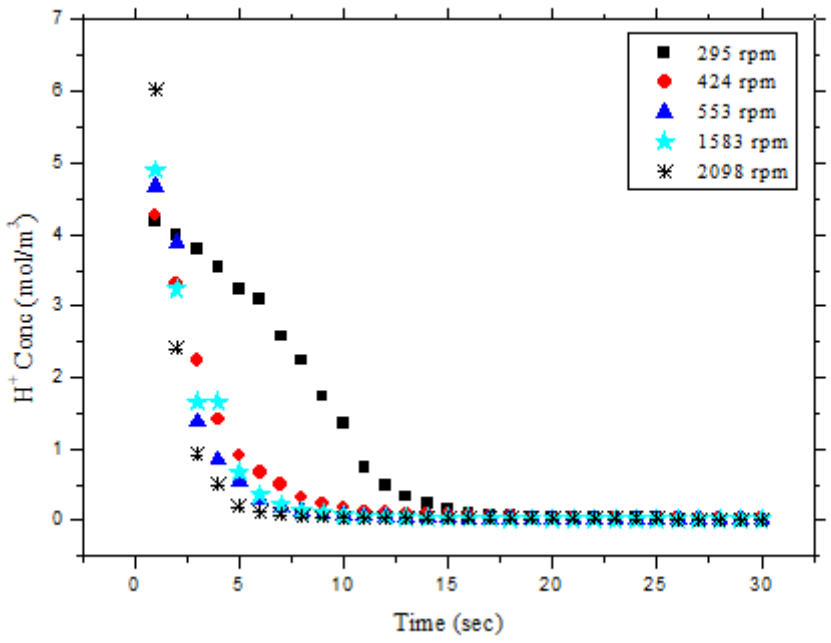

Figure 4.4: Effect of stirring rate on dissolution of limestone.

In this investigation, the critical impeller speed was at 150 rpm. Carlett et al. (2015a) reported that for an agitated vessel operated at impeller speed greater or equal to three-folds the critical impeller speed ($N \geq 3N_{js}$), stirring does not affect dissolution of limestone.

The stirring rate of 553 rpm was employed in this study, to ensure that mechanical energy dissipated does not control the mass transfer of species. A stirring rate higher than 2098 rpm was avoided due the shaking of the experimental set-up.

Convective transportation of species between suspended limestone and liquid is deemed to be augmented by agitation. Figure 4.5 shows influence of initial HCl concentration on limestone dissolution rate. When the driving force for limestone dissolution is gradient of the concentration of H_3O^+ ions between the limestone particle surface and the bulk liquid, then low pH (initial HCl concentration) will enhance the dissolution process.

At low pH (< 4), the concentration of hydronium ions in the bulk liquid is considered to be much greater than that on the surface of suspended limestone particles, such that the concentration on the particles surfaces is assumed to be negligible. This observation and assumption is in concurs with those of Carletti et al. (2015b) and Ahlbeck et al. (1995).

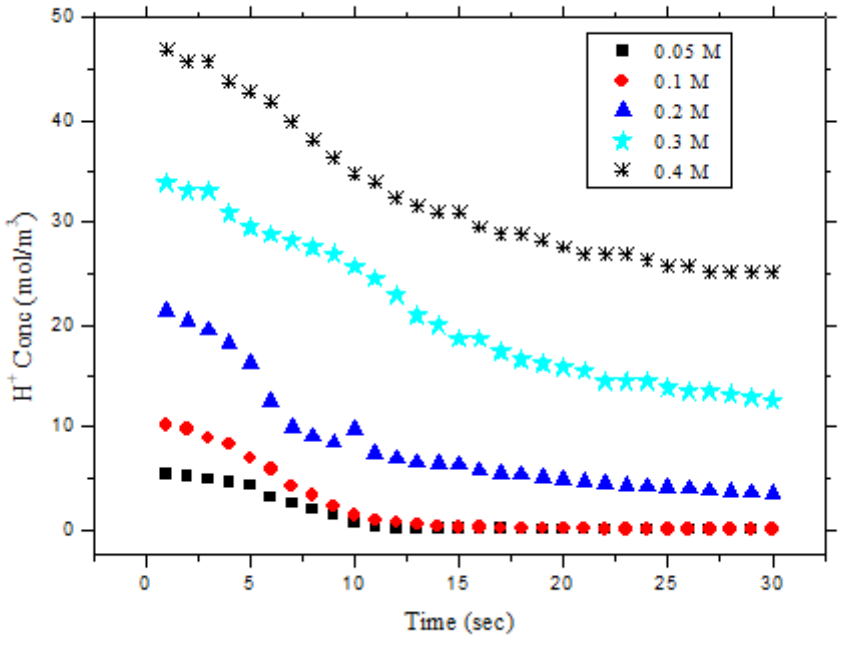

Figure 4.5: Effect of initial HCl concentration on dissolution of limestone.

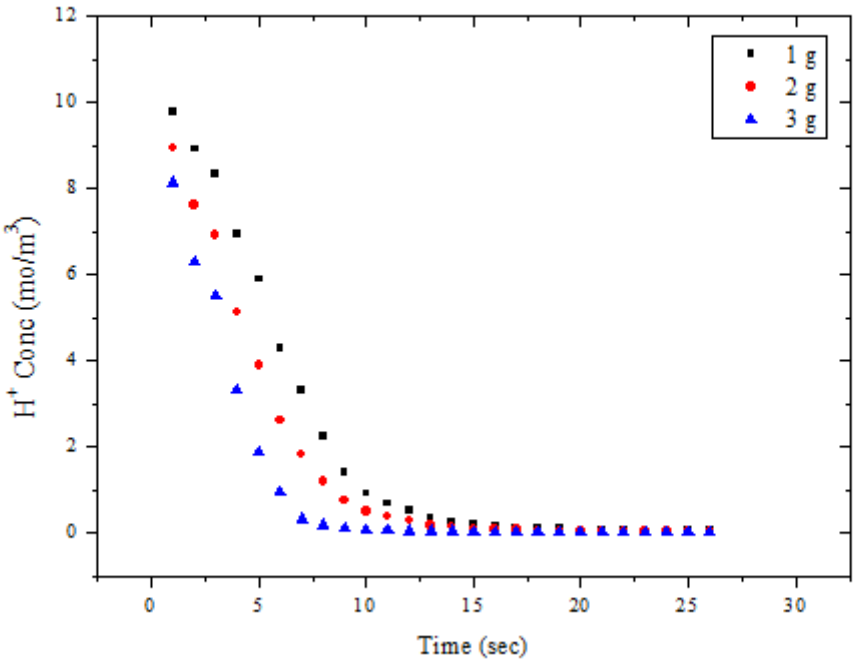

Figure 4.6: Effect of solid-to-liquid ratio on dissolution.

Figure 4.6 shows the experimental results of the concentration of H_3O^+ ions during the dissolution of 1, 2 and 3 g_limestone/1.5 $\times$ $10^{-6}m^3\_HClsolution$ of limestone. Dissolution was observed to increase as the solid-to-liquid ratio increase.

4.5 Particle size distribution

PSD had been reported to be one of the characteristics that influences limestone dissolution rate (Carletti et al. 2012). In this study PSD analysis were done before and after dissolution experiments as shown in Figure 4.7.

Raw limestone is observed to have a sharp peak for 1.13 μm fines, and a bimodal distribution with maxima at 3.55 and 12.62 μm particles. After dissolution, all particles that were $\leq$ 1.5 μm were consumed, whereas other larger particles were reduced. The depletion of particles less than 1.13 μm can be attributed to effect particle size on limestone dissolution.

The particles remaining were all less than 71 μm, implying that the standard percentile diameter values decreased during the dissolution. The reduction (in size) of larger particles led to the increase a population of particles of 12.62 μm. The PSD presented in Figure 4.7 shows that the shift is towards the smaller diameters.

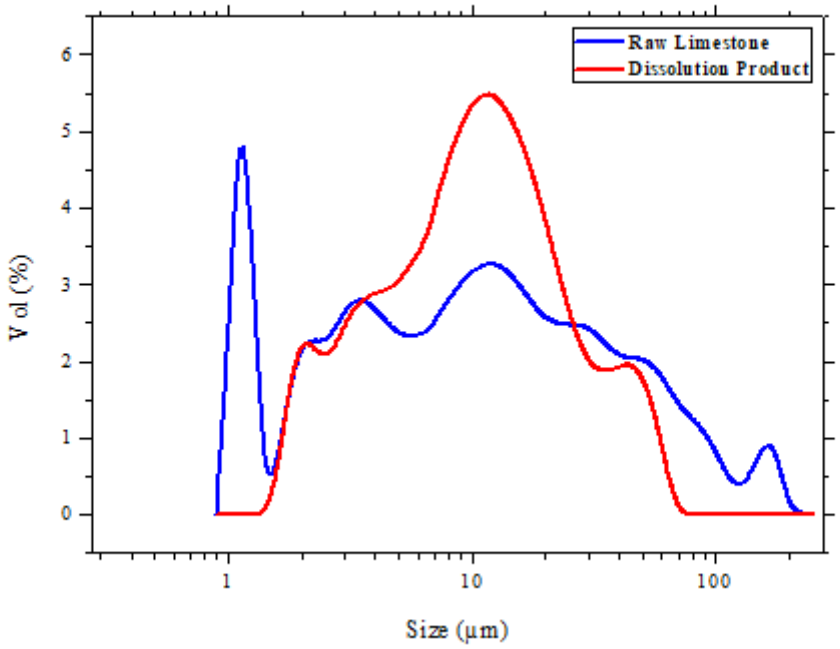

Figure 4.7: Limestone PSD before and after dissolution.

This observation concurs with the results promulgated by Carletti et al. (2015b), under similar experimental conditions.

4.6 Calcium concentration

ICP-OES was employed to quantify the concentration of Ca^{2+} ions, as discussed in Section 4.2, the results are given in Figure 4.8. As discussed in Sub-section 4.3.4, chemical reaction R4.8 give a stoichiometric ratio of 1:2 for Ca^{2+}:H_3O^+, and similarly to Plummer & Busenberg (1982), Shih et al. (2000), Siagi & Mbarawa (2009), Toprac & Rochelle (1982) and Chan & Rochelle (1982), stoichiometry had been used to estimate the concentration of Ca^{2+} in this investigation. A stoichiometric coefficient of 2.85 was obtained in this study (Figure 4.8), designating a two-stepped reaction mechanism. The method sum of least squares regression was employed.

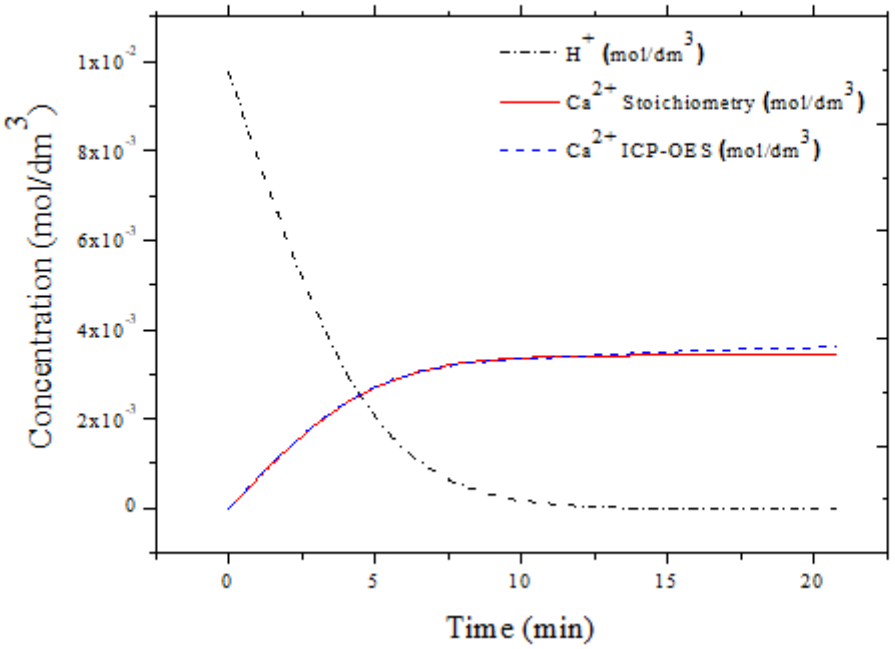

Figure 4.8: Calcium ICP-OES measurements.

4.7 Results and Discussion: Mass Transfer Coefficients and Chemical Reaction Constants

4.7.1 Mass Transfer Coefficients

The mass transfer coefficient (k_l) was estimated following the method presented in Sub-section (4.3.1). Figure 4.9 presents the k_l obtained under varied temperatures. k_l in Equation 4.7 is directly proportional to the diffusivity of species, that is in turn, a function of temperature (Equation 4.3). Thus k_l can be expected to increase with temperature in Figure 4.9. The observation in this study concurs with that of Carletti et al. (2015b).

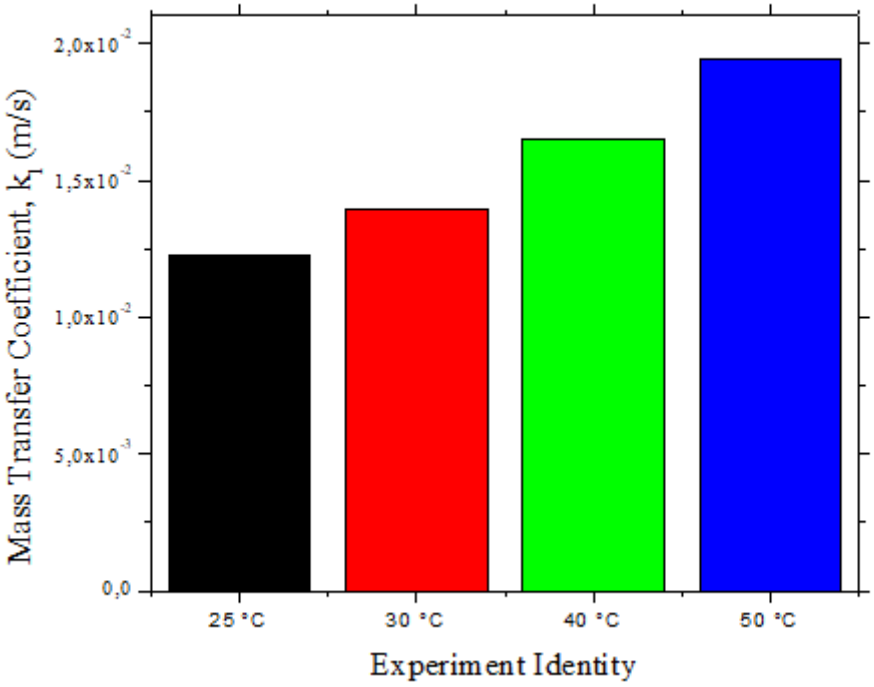

Figure 4.9: Chemical reaction constants and mass transfer coefficients: Effect of temperature.

4.7.2 Chemical Reaction Rate Constant

The chemical reaction constant (k_r) was estimated by following to the technique presented in Sub-section (4.3.2). Figure 4.10 presents the obtained k_r results under varied temperatures. This implies that k_r can be expected to increase with temperature in Figure 4.10. The order of k_l is 100 times bigger than that of k_r, indicating that dissolution was controlled by mass transfer in this study. The observation in this study concurs with that of Carletti et al. (2015b).

The activation energy of limestone dissolution was estimated from the gradient of Arrhenius plot (Figure 4.11) using Equation 4.10, i.e. $\ln k_r$ vs 1/T, that was found from taking natural logarithmic on both sides of Equation 4.8.

$$lnk_r = lnk_1 - \frac{E_a}{RT} \tag{4.28}$$

where k_1 is the pre-exponential factor, E_a, is the apparent activation energy, R is the universal gas constant and T is the temperature in the reactor.

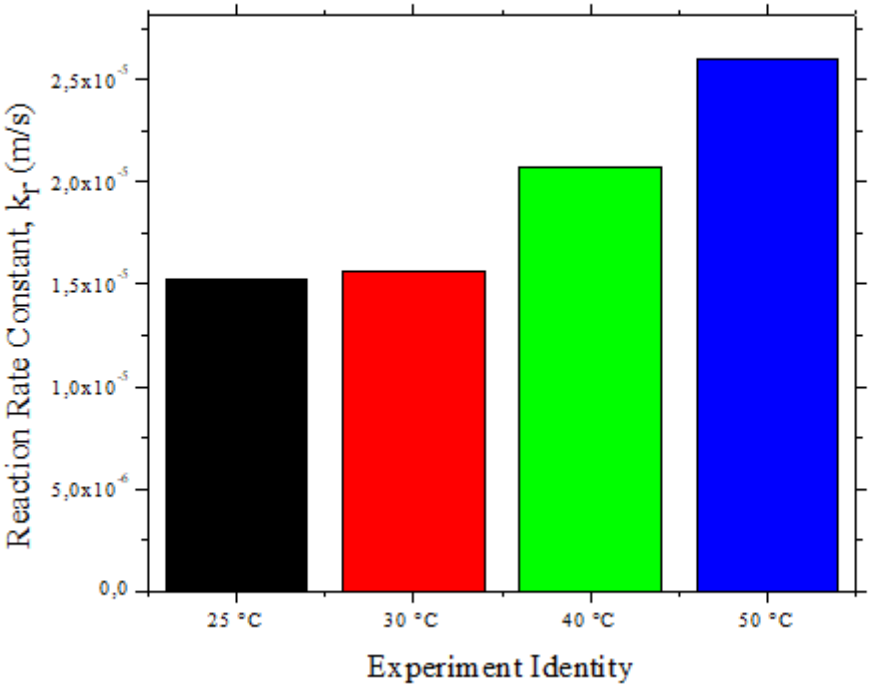

Figure 4.10: Chemical reaction constants : Effect of temperature.

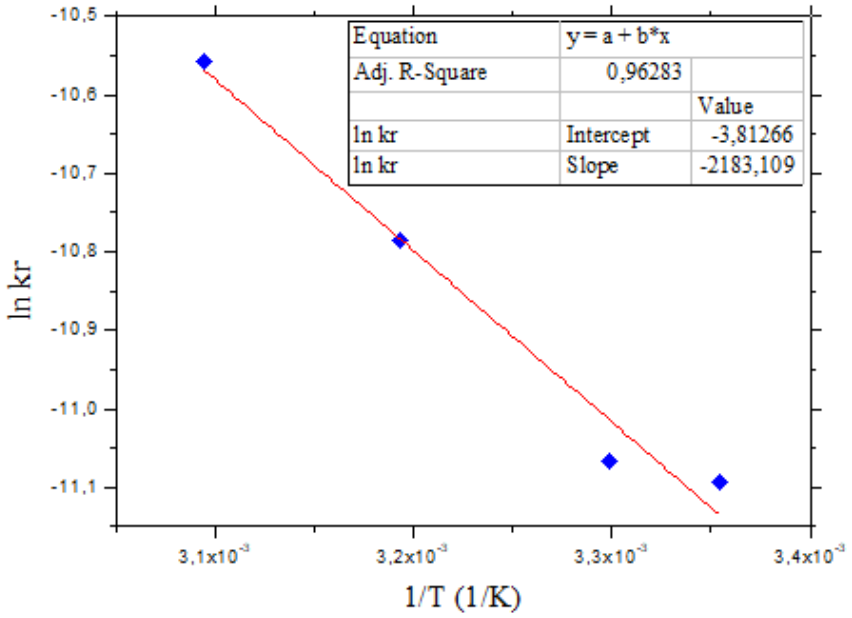

Figure 4.11: Arrhenius plot.

Table 4.2: Estimated kinetic parameters.

Parameter	k_r (m/s)	E_a (kJ/mol)	k_1 (m/s)	K_{ad} (m^3/mol)	T (°C)
This study	1.52 - 2.60 $\times 10^{-5}$	18.15	2.2×10^{-2}	0.12	25 - 50
Carletti et al. (2015b) (WSS)	1 - 2 $\times 10^{-4}$	21.27	1.16×10^{-4}	0.88	20 - 50
Carletti et al. (2015b) (PSS)	-	16.45	3.93×10^{-4}	0.35	25 - 50
Gledhill & Morse (2006)	2.73 - 10.54 $\times 10^{-2}$	21	-	-	25 - 82.5
Alkattan et al. (1998)	-	19	-	-	25 - 80

*Notes:
WSS - Walica Small Sample
PSS - Parainen Small Sample

Low activation energy was observed in this study (18.15 kJ/mol). This observation is an indicant of chemical reaction mechanism, i.e. mass transfer controlled. This postulation is in line with the report of Siagi & Mbarawa (2009) that chemical reactions with activation energies less than 20 kJ/mol are diffusion-controlled, whereas those between 40 and 80 kJ/mol are surface reaction-controlled.

A panoptic range of activation energies has been blazoned in literature, this can be attributed to variations in experimental conditions. The obtained apparent activation energy, in this study, concurs with the values published by other workers (Alkattan et al. 1998, Barton & Vatanatham 1976, Carletti et al. 2015b, Chan & Rochelle 1982, Gledhill & Morse 2006, Plummer et al. 1978).

4.7.3 Overall Rate Constant

The total dissolution constant (k_{tot}) was estimated by the reciprocal addition of $1/(k_l)$ and $1/(k_r)$ according to Equation 4.12, as presented in Section 4.3.3. Table 4.3 present the comparison of k_{tot} obtained through methods presented in Subsections 4.3.1 and 4.3.2 with the model-regressed k_{tot} (Section 4.8). The obtained results were also compared with those published by Carletti et al. (2015b) on one of their samples.

The calculated values of k_{tot} are comparable with those regressed through the model. Likewise, the obtained results are commensurate with those of Carletti et al. (2015b) on one of their sample as shown in Table 4.3. The samples of matlab codes and regressed fitting plots are given in the Appendices (Appendix B). It is important to realize that during regression, k_{tot} can be enunciated in terms of k_l and k_r (as per Equation 4.12) in the model equations, in case there is a need to regress k_l and k_r individually. Likewise, k_r, can be expressed according to Equation 4.11 if there is a need to regress k_1 and Ea directly.

Table 4.3: Overall Rate Constants.

Experiment Identity	Calculated k_l $\times 10^{-2}$ (m/s)	Calculated k_r $\times 10^{-5}$ (m/s)	Fitted k_r $\times 10^{-4}$ (m/s)	Calculated k_{tot} $\times 10^{-5}$ (m/s)	Fitted k_{tot} $\times 10^{-4}$ (m/s)
This study 25 °C	1.22	1.52	3.39	1.52	3.39
This study 30 °C	1.39	1.56	2.96	1.56	2.89
This study 40 °C	1.65	2.07	6.72	2.07	6.46
This study 50 °C	1.95	2.62	2.59	2.62	2.55
Carletti et al. (2015b) (WLS) 20 °C	0.09	-	1.26	1.24[a]	-
Carletti et al. (2015b) (WLS) 30 °C	0.105	-	0.13	1.25[a]	-
Carletti et al. (2015b) (WLS) 40 °C	0.120	-	0.13	1.25[a]	-
Carletti et al. (2015b) (WLS) 50 °C	0.135	-	0.25	2.45[a]	-

*Notes:
[a] - Estimated using Equation 4.12 from reported k_l and reported-fitted k_r.
WLS - Walica Large Sample

4.8 Results and Discussion: Modelling and Comparison with Experimental Results

One of the contributing factors on the challenges of modelling limestone dissolution is that, the equilibria, of the chemical reactions that takes place, is reliant on the reaction pH and temperature, and thus it keeps on changing (Carletti et al. 2015b).For commensurate assessment of the fitting of the model results (obtained through procedure given in Section 4.3) onto experimental results (obtained through experimental method given in Section 4.2) , the H_3O^+ concentrations computed through numerical models were juxtaposed with the experimental concentrations.

The model H_3O^+ concentration values were obtained using Equation 4.23, requiring the values of k_{tot}, SA and K_{ad}, that are evaluated according to the procedure given in Section 4.3.6. The comparison was done with interest on the effects of temperature, acid and calcium carbonate concentration on limestone dissolution. The discussions given in Sections 4.4 are applicable in this section.

For the influence of temperature on limestone dissolution, a comparison between the experimental and numerical modelling results is shown in Figure 4.12. Over the first 2 seconds, a deviation is observed between the experimental and model values. The model is observed to over-predict the dissolution rate over this period.

In Figure 4.13, the effect of initial HCl concentration on dissolution of limestone can be observed. It can be seen that the concentration has an important effect on limestone dissolution, with greater dissolution rates at higher concentration.

Figure 4.14 shows the comparison of model and experimental results for the dissolution of 1, 2 and 3 g_limestone/1.5 $\times$ $10^{-6}m^3\_HClsolution$. The model was observed to give good prediction for 2 and 3 g_limestone/1.5 $\times$ $10^{-6}m^3\_HClsolution$.

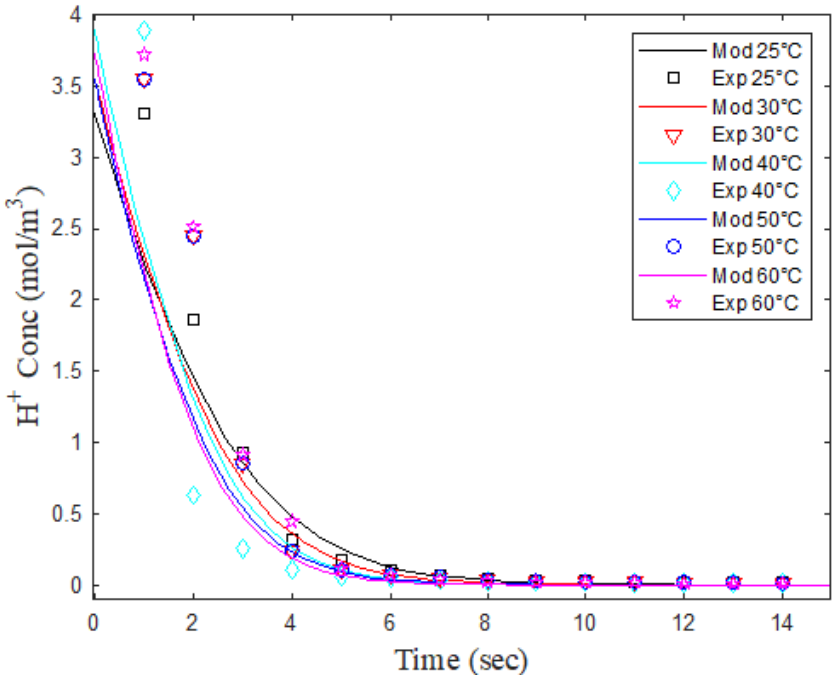

Figure 4.12: Comparison of model and experimental results: Effect of temperature on dissolution of limestone.

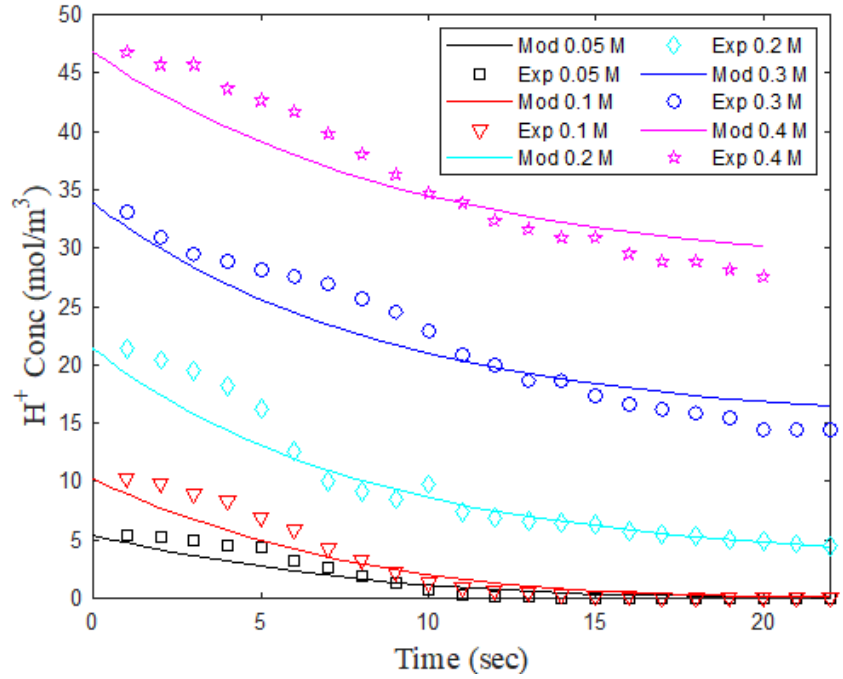

Figure 4.13: Comparison of model and experimental results: Effect of initial HCl concentration on dissolution of limestone.

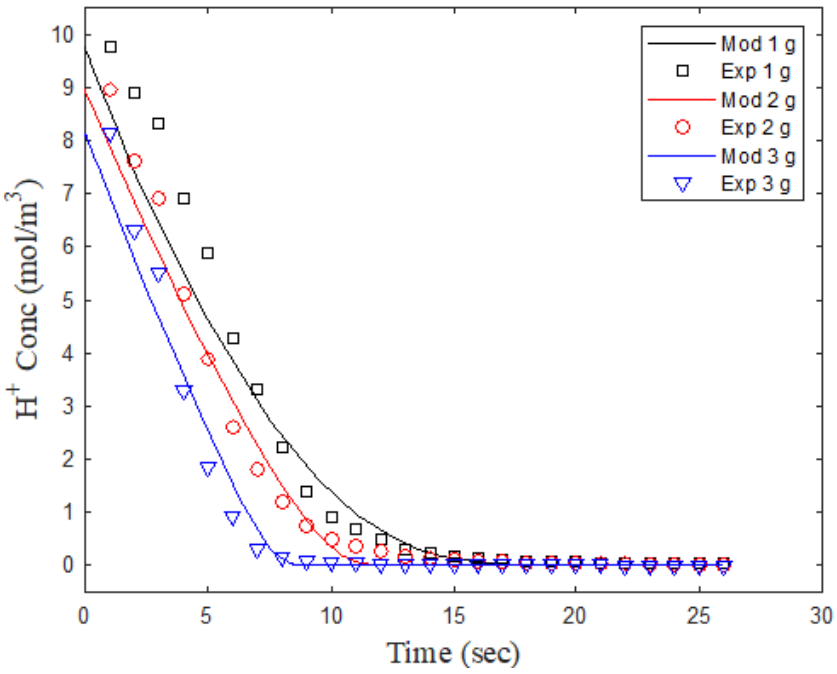

Figure 4.14: Comparison of model and experimental results: Effect of solid-to-liquid ratio on dissolution.

4.9 Summary

- The objectives of this chapter are:

  i. to examine the effect of operating conditions (temperature, agitation, acid and calcite concentrations) on the dissolution of limestone in the HCl acid solutions of varied concentrations.

  ii. to evaluate the solid-liquid mass transfer coefficient, chemical reaction constant and overall dissolution constant.

  iii. the study also seek to estimate the kinetic parameters of dissolution.

  iv. to compare the limestone dissolution experimental and modelling results.

- Experimentation that employs free-drift method was employed to measure the dissolution rate of limestone.

- Mass transfer-reaction model was employed to model the limestone dissolution rate.

Chapter 5 Mass transfer of SO_2 into aqueous solutions of varied pH

The integrated model developed (see Chapter 6) requires the knowledge of gas-liquid mass transfer coefficients, both gas-side and liquid-side. The aim of the work described in this chapter involved the determination of both gas-side and liquid-side mass transfer coefficients of SO_2 absorption from simulated flue gas in a agitated tank reactor whilst employing solutions of various pHs. A NaOH solution was used in the evaluation of the product of the gas-side mass transfer coefficient and the interfacial surface area and, a HCl solution was used in the evaluation of the product of the liquid-side mass transfer coefficient and the interfacial surface area. The absorption of SO_2 into water was found to be enhanced by chemical reactions. A mass balance model based on the two-film theory described the rate of SO_2 absorption satisfactorily.

5.1 Introduction

SO_2 emissions, mainly from fossil fuel combustion, poses a threat to the environment and are a health risk. This led to stringent regulations being set by regulatory bodies across the world. One of the most commonly used SO_2 abating technology is limestone wet FGD, due to its low costs and efficiency. SO_2 absorption is one of the rate-limiting steps in this process as it directly affects the chemical reaction equilibria. As a result, a good understanding and modelling of SO_2 absorption for wet FGD processes is crucial.

The absorption of SO_2 into limestone slurry is rather complicated due to the chemical reactions and species involved. A lot of work had been done by various researchers (Bravo et al. 2002, Lancia et al. 1997, 1994*b*, Olausson et al. 1993, Sada, Kumazawa & Hashizume 1981, Sada et al. 1983, Sada, Kumazawa, Sawada & Hashizume 1981, Takashina et al. 2001, Uchida & Ariga 1985, Uchida et al. 1978)

towards understanding the absorption of SO_2 into limestone slurries.

WFGD processes had been amply modelled, ever-since the 1980s, through different approaches, namely, statistical approach (Perales et al. 2008, Zhao et al. 2007) and ontological approach (Brogren & Karlsson 1997c, Kallinikos et al. 2010, Neveux & Le Moullec 2011) etc. Most models focus on limestone wet FGD processes,as it is the commonly used technology.

Various models had been developed by different researchers based laboratory scale experiments. The same laboratory equipment are also used to evaluate some of the parameters required for modelling. Such models focused on providing information for specific aspects and areas of the wet FGD e.g. the reaction plane model, which is based on the film model,was formulated and used by investigators such as Sada et al. (1983), Sada, Kumazawa, Sawada & Hashizume (1981), Takashina et al. (2001), Uchida & Ariga (1985) etc to explain the aspects SO_2 absorption and the chemical reactions and mass transfers that take place in the liquid film.

A model based on two-film theory, that does not consider the dissolution of limestone, had been used by workers such as Lancia et al. (1997), to evaluate the rate of SO_2 absorption, while coupling the mass transfer and the chemical reactions in the stagnant film, using the enhancement factor. Mass transfer coefficients (gas-side and liquid-side) are also commonly evaluated using the same stirred reactor tanks, simply by changing solutions.

Studies that evaluates the gas-side gas-liquid mass transfer coefficients employing the absorption of SO_2 gas into concentrated NaOH solution are abundant in literature (Bravo et al. 2002, Chu et al. 2003, Deshwal & Hyung Keun 2009, Lancia et al. 1997, Sada et al. 1979, Takashina et al. 2001, Uchida & Ariga 1985, Uchida et al. 1978), however, most of the workers use the slope of the plot of absorption rate vs the driving force. This approach does not allow the evaluation of the contribution of chemical reactions into the total mass transfer of SO_2.

There are only few studies that employ the absorption of SO_2 gas into HCl acid solution to evaluate the liquid-side gas-liquid mass transfer coefficients. Most workers employed the absorption of O_2 or CO_2 in water (Bravo et al. 2002, Deshwal & Hyung Keun 2009, Takashina et al. 2001, Uchida et al. 1978). Some workers e.g Dagaonkar et al. (2001), Sada et al. (1979) and others, N_2O-Water systems to evaluate the liquid-side gas-liquid mass transfer coefficients.

The objective of this part of the study is to evaluate the gas-side and liquid-side gas-liquid mass transfer employing the method that would allow the evaluation of the contribution of chemical reactions. Experiments were conducted using an agitated tank reactor employing SO_2/NaOH and SO_2/HCl systems for determining the respective coefficients.

5.2 Experimental

5.2.1 Materials

Sodium hydroxide (NaOH pellets) and hydrochloric acid (HCl, 36.5%) were supplied by Sigma-Aldrich (South Africa). Carbon dioxide and two simulated flue gases ((2000 ppm SO_2, balance N_2) and (3000 ppm SO_2, 8.0 v/v% CO_2, 8.0v/v% O_2 and 83.7 v/v% N_2)), were supplied by African Oxygen (Afrox, South Africa).

5.2.2 Apparatus

Details of the apparatus used can be seen in Chapter 4 (Sub-section 4.2.1), the main difference is how it is used and need for accessories such as gas mass flow controller and gas analyzer.

Table 5.1: Summary of operating conditions.

Parameter	Value/Range	Units
Temperature	298.15 - 323.15	K
Gas flow rate	1.67 x 10^{-5}	$m^3 s^{-1}$
Water/solution volume	2 x 10^{-4} – 1.5 x 10^{-3}	m^3
Stirring rate	1 - 6	s^{-1}

Brooks-5850 mass flow controller units were used to achieve desired flow-rates. Effluent SO_2 concentration was measured using the gas analyser (X-STREAM GP Compact 1/2 19" Rack-mount & Portable Gas Analyser), supplied by Rand Instruments (South Africa). The absorption experiments were continuous with respect to gas phase and batch solution/water. The operating conditions are similar to those reported in Chapter 4, with exception that Table 5.1 gives the gas flow rates.

5.3 Absorption and Reaction in Aqueous Solutions: Theory and Modelling

Assumptions

- Gas in the headspace is assumed to be well-mixed, such that the $C_{SO_2,headspace} \approx C_{SO_2,outlet}$.
- The rate of absorption of SO_2 is diffusion-controlled.

- H_3O^- transfer chemical reactions are instantaneous and they are rate-limiting.
- Convection transportation of species in the gas-side film is insignificant when compared to convection in the liquid bulk. Similarly, convection does not take place in the liquid-side film.
- Convection in the bulk gas and in the bulk liquid is fast, such that concentrations of species at respective compartments are the same in all points.
- The gas and liquid at the interphase between the gas and liquid films are in equilibrium.

5.3.1 Two-film theory model

Figure 5.1 gives a schematic representation of the two-film theory, where the gas and liquid films at the boundary are indicated to have a definite thickness, although in reality, the sharp demarcation does not exist.

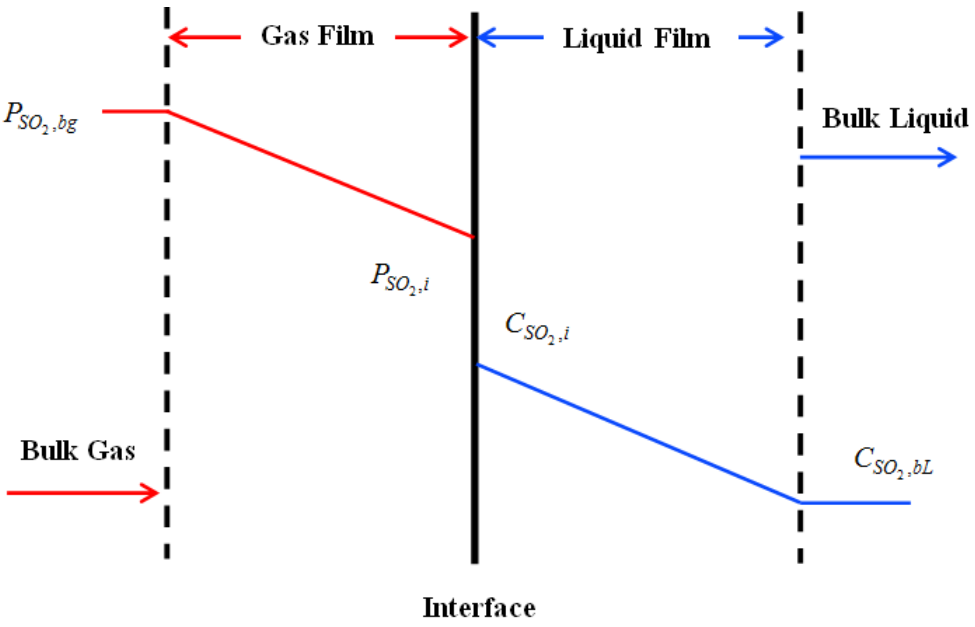

Figure 5.1: Two-film Theory.

The rate of absorption of SO_2 from simulated flue gas is proportional to the driving potential multiplied by a coefficient(s) that is/are subject to the construction and size of the apparatus and the operating conditions.

The rate of SO_2 transfer across the gas film is directly proportional to the difference of its partial pressures in the bulk gas and gas-liquid interphase (Equation 5.1)

$$N_{SO_2,gas-film} = k_g a(P_{bulkgas} - P_{interphase}) \tag{5.1}$$

Where k_g and a are the gas-side mass transfer coefficient (in mol/$m^2 \cdot Pa \cdot s$) and gas-liquid interfacial surface area (in m^2/m^3_{liquid}),respectively. When pure SO_2 is absorbed, $k_g a$ is non-existence.

The rate of transfer of species across the liquid film is directly proportional to the difference of their concentrations in the gas-liquid interphase and bulk liquid (Equation 5.2)

$$N_{SO_2,liquid-film} = k_L a(c_{interphase} - c_{liquid}) \tag{5.2}$$

where k_L is the liquid-side mass transfer coefficient (in m/s).

The quantities of the respective species contained in the films are insignificant when compared to those passing through. This due to the thinness of the films. The species that diffuses through the gas film can be assumed to also diffuse through the liquid film. The mass transfer resistances are considered to be in series, and the rate can be given by Equation 5.3

$$N_{SO_2,overall} = K_g a(P_{bulkgas} - P_{liquid}) = K_L a(c_{bulkgas} - c_{bulkliquid}) \tag{5.3}$$

where K_g and K_L are the overall coefficients, given by

$$K_g = \frac{H_{SO_2} k_L k_g}{H_{SO_2} k_L + k_g} \tag{5.4}$$

and

$$K_L = \frac{K_g}{H_{SO_2}} = \frac{k_L k_g}{H_{SO_2} k_L + k_g} \tag{5.5}$$

5.3.2 Evaluation of gas-liquid mass transfer coefficients: Effect of pH on SO_2 absorption

Case I: Evaluation of gas-side mass transfer coefficients (high pH, NaOH solution)

During SO_2 absorption into NaOH solution, the gas molecules diffuse from gas phase core to the gas-liquid interphase (according to R5.1) and the dissolution in the so-

lution is considered to take place according to R5.2, due to the equivalence of the chemical potentials in the phases (Schultes 1998, Wang et al. 2015). The simulated flue gas used in this study had low SO_2 concentration (in the order of ppm), and thus,the absorption process can be considered to obey the Henry's law.

Some of the dissolved SO_2 molecules would be dissociated according to reaction R5.3, and others react with OH^- ion directly, according to reactions R5.6 and R5.7. The above processes are affected by the dissociation of the water (according to reaction R5.4), NaOH (according to reaction R5.5), and the products (according to reactions R5.9 and R5.10) (Schultes 1998, Wang et al. 2015). NaOH solution is the strong alkaline with high ionization equilibrium constant (Pasiuk-Bronikowska & Rudziński 1991), because of reaction R5.5, which will render the excess of the hydroxide ion.

The main reaction steps are:

Diffusion of SO_2 through the gas film

SO_2 dissolution:

$$SO_2\,(g) \leftrightharpoons SO_2\,(aq) \tag{R5.1}$$

SO_2 dissociation:

$$SO_2\,(aq) + H_2O\,(l) \leftrightharpoons H_2SO_3\,(aq) \tag{R5.2}$$

H_2SO_3 dissociation:

$$H_2SO_3\,(aq) \leftrightharpoons H^+ + HSO_3^- \tag{R5.3}$$

H_2O dissociation:

$$H_2O \leftrightharpoons H^+ + OH^- \tag{R5.4}$$

NaOH dissociation:

$$NaOH \leftrightharpoons Na^+\,(aq) + OH^-\,(aq) \tag{R5.5}$$

$SO_2(aq)$ reaction with OH^-:

$$SO_2\,(aq) + OH^- \leftrightharpoons HSO_3^- \tag{R5.6}$$

SO_2(aq) reaction with OH^-:

$$SO_2\,(aq) + OH^- \leftrightharpoons H^+ + SO_3^{2-} \tag{R5.7}$$

Consecutive reaction:

$$HSO_3^- + OH^- \leftrightharpoons H_2O\,(l) + SO_3^{2-} \tag{R5.8}$$

Na_2SO_3(aq) dissociation:

$$Na_2SO_3 \leftrightharpoons 2\,Na^+ + SO_3^{2-} \tag{R5.9}$$

$NaHSO_3$(aq) dissociation:

$$Na_2SO_3 \leftrightharpoons Na^+ + HSO_3^- \tag{R5.10}$$

The overall reaction:

$$SO_2\,(aq) + 2\,OH^- \leftrightharpoons H_2O + SO_3^{2-} \tag{R5.11}$$

In line with the reports in literature (Chang & Rochelle 1985, Zidar 2000), the overall reaction (R5.11) is considered to be instantaneous and irreversible, owing it to chemical reactions R5.7 and R5.8. High rate constants ($> 10^9$ (mol^{-1} s^{-1} L)) render chemical reaction R5.7 to be fast. By virtue of being proton transfer, chemical reaction R5.8 is deemed to be instantaneous (Hikita et al. 1977).

The rates of mass transfer of SO_2 into NaOH solution is affected by both diffusion and chemical reactions (Schultes 1998). Chemical reactions are considered not to occur in the gas film, and the diffusion of SO_2 from the bulk gas to the gas-liquid interphase can be given by Equation 5.6 (Zidar 2000).

$$N_{SO_2} = k_g a(P_{bulkgas} - P_{interphase}) \tag{5.6}$$

where $P_{bulkgas}$ is the partial pressure of SO_2 in the bulk gas at the overhead-space (above the NaOH solution) in the reactor and $P_{interphase}$ is the partial pressure of SO_2 at the gas-liquid interphase.

At very high pH of NaOH solution, $SO_{2(aq)}$ is considered to be instantly spent at the gas-liquid interphase and therefore the liquid-side resistance can be ignored (Lancia et al. 1997), i.e $P_{interphase}$ approaches zero, and Equation 5.6 becomes Equation 5.7.

$$N_{SO_2} = k_g a(P_{bulkgas}) \tag{5.7}$$

The product between the gas-side mass-transfer coefficient and the interfacial area per unit volume ($k_g a$) had been estimated from the plot of N_{SO_2} vs $P_{bulkgas}$, as a slope. The results are given in Section 5.4.2, were also compared with the results of the work of Bravo et al. (2002), Deshwal & Hyung Keun (2009), Lancia et al. (1997), Takashina et al. (2001), Uchida & Ariga (1985), Uchida et al. (1978) and others, who followed a similar approach.

When the contribution of chemical reactions is considered, $k_g a$ can be regressed from fitting a model onto experimental results. In this study, the model based on film theory was fitted onto experimental results. The concentrations of Na^+, H_3O^+, OH^-, $SO_{2,aq}$, $SO_{2,bulkgas}$, HSO_3^-, and SO_3^{2-} are evaluated on basis of the equilibrium relationships for the $SO_{2,bulkgas} - SO_{2,aq} - HSO_3^- - SO_3^{2-} - H_2O$ system, the mass balance equation and the charge balance equation (Zidar 2000). The equilibrium relationships at the gas-liquid interphase can be given by Equations 5.7 through 5.11.

$$C_{OH^-,interphase} = \frac{K_W}{C_{H^+,interphase}} \tag{5.8}$$

$$C_{SO_2,interphase} = H_{SO_2} \cdot C_{SO_2,bulkgas} \cdot R \cdot T \tag{5.9}$$

$$C_{HSO_3^-,interphase} = \frac{K_{SO_2} \cdot H_{SO_2} \cdot C_{SO_2,bulkgas} \cdot R \cdot T}{C_{H^+,interphase}} \tag{5.10}$$

$$C_{SO_3^{2-},interphase} = \frac{K_{HSO_3^-} \cdot K_{SO_2} \cdot H_{SO_2} \cdot C_{SO_2,bulkgas} \cdot R \cdot T}{(C_{H^+,interphase})^2} \tag{5.11}$$

The equilibrium relationships in the bulk NaOH solution can be given by Equations 5.12 through 5.15. The equilibrium constants were adopted from Chang & Rochelle (1985), Pasiuk-Bronikowska & Rudziński (1991), Schultes (1998).

$$C_{OH^-,NaOHSolution} = \frac{K_W}{C_{H^+,NaOHSolution}} \tag{5.12}$$

$$C_{SO_2,NaOHSolution} = \frac{S_{total} \cdot C^2_{H^+,NaOHSolution}}{C^2_{H^+,NaOHSolution} + K_{SO_2} \cdot C_{H^+,NaOHSolution} + K_{SO_2} \cdot K_{HSO_3^-}} \tag{5.13}$$

$$C_{HSO_3^-,NaOHSolution} = \frac{S_{total} \cdot K_{SO_2} \cdot C_{H^+,NaOHSolution}}{C^2_{H^+,NaOHSolution} + K_{SO_2} \cdot C_{H^+,NaOHSolution} + K_{SO_2} \cdot K_{HSO_3^-}} \tag{5.14}$$

$$C_{SO_3^{2-},NaOHSolution} = \frac{S_{total} \cdot K_{SO_2} \cdot K_{HSO_3^-}}{C^2_{H^+,NaOHSolution} + K_{SO_2} \cdot C_{H^+,NaOHSolution} + K_{SO_2} \cdot K_{HSO_3^-}} \tag{5.15}$$

As the pH of the NaOH decreases, the quantity of SO_2 becomes significant, and SO_2 absorption rate can be given by Equation 5.16

$$N_{SO_2} = \frac{C_{SO_2,bulkgas} \cdot R \cdot T - H_{SO_2} \cdot C_{SO_2,NaOHSolution}}{\frac{1}{k_g a} + \frac{H_{SO_2}}{E \cdot k_L a}} \tag{5.16}$$

where H_{SO_2} is the Henry's constant and E is the enhancement factor for SO_2 absorption into NaOH solution, defined as the ratio between the absorption of SO_2 with and without chemical reaction, and is calculated using Equation 5.17 (Zidar 2000)

$$E = 1 + \frac{D_{HSO_3^-}}{D_{SO_2}} \frac{(C_{HSO_3^-,interphase} - C_{HSO_3^-,NaOHSolution})}{(C_{SO_2,interphase} - C_{SO_2,NaOHSolution})} + \frac{D_{SO_3^{2-}}}{D_{SO_2}} \frac{(C_{SO_3^{2-},interphase} - C_{SO_3^{2-},NaOHSolution})}{(C_{SO_2,interphase} - C_{SO_2,NaOHSolution})} \tag{5.17}$$

where D_{SO_2}, $D_{HSO_3^-}$ and $D_{SO_3^{2-}}$ are the diffusivities of SO_2, HSO_3^- and SO_3^{2-}, respectively. The temperature dependent diffusivities were adopted from Boudreau (1997).

The mass balance equations (Equations 5.18 through 5.22) that were developed based on chemical reactions R5.1 through R5.11, equilibrium constants, electroneutrality etc. For SO_2 in gas phase:

$$\frac{dC_{SO_2}}{dt} = \frac{1}{V_{Headspace}} \cdot (F \cdot C_{SO_2,inlet} - F \cdot C_{SO_2,bulkgas}) - \frac{V_{NaOHSolution}}{V_{Headspace}} \cdot N_{SO_2} \tag{5.18}$$

Total sulphur balance:

$$\frac{dC_{S_{total}}}{dt} = N_{SO_2} \tag{5.19}$$

Total Sodium balance:

$$\frac{dC_{Na^+_{total}}}{dt} = R_{NaOH} \tag{5.20}$$

Sodium hydroxide dissolution

$$\frac{dC_{NaOH}}{dt} = R_{NaOH} \tag{5.21}$$

Electroneutrality in the NaOH solution

$$C_{H^+,NaOHSolution} + C_{Na^+,NaOHSolution} = C_{HSO_3^-,NaOHSolution} + 2 \cdot C_{SO_3^{2-},NaOHSolution} + C_{OH^-,NaOHSolution} \tag{5.22}$$

Case II: Evaluation of liquid-side mass transfer coefficients (low pH HCl solution)

When SO_2 in a simulated flue gas is absorbed into a solution at low pH (< 2), dissociation of SO_2(aq) is insignificant. Consequently, SO_2 is considered to be physical, however, both gas-side and the liquid-side resistances are important Lancia et al. (1997). Equation 5.23 can be used

$$N_{SO_2} = \frac{P_{bulkgas} - H_{SO_2} C_{SO_2,HClsolution}}{\frac{1}{k_g a} + \frac{H_{SO_2}}{k_L a}} \tag{5.23}$$

When the small contribution of chemical reactions is considered (supposedly at the initial stages of SO_2 absorption into HCl solution), the mechanisms proposed by Krissmann et al. (1998, 1997), Zimmermann et al. (2009) can be followed. Reactions R5.1 through R5.4 are applicable in Case II, the additional chemical reactions are given below (reactions R5.12 and R5.13). The dissociation of HCl (a strong acid) is assumed to run to completion according to reaction (R5.12).

At the low pH in this study, the formation of SO_3^{2-} (from dissociation of HSO_3^-) and OH^- (from dissociation of H_2O) were neglected.In this study, the formation of a complex (SO_2Cl^-) in reaction R5.13 was proposed based the work of Khan et al. (1978), Krissmann et al. (1998), Salama et al. (1971), Wedzicha & Webb (1996), Zimmermann et al. (2009). The equilibrium relationships and other relationships are presented in Equations 5.24 to 5.33. The equilibrium constants for reactions R5.12

through R5.14 were adopted from Goldberg & Parker (1985) and that of reaction R5.13 was adopted from Krissmann et al. (1998).

HCl dissociation:

$$HCl\,(aq) \rightleftharpoons H^+\,(aq) + Cl^-\,(aq) \tag{R5.12}$$

Ion complex (SO_2Cl^-):

$$SO_2\,(aq) + Cl^-\,(aq) \rightleftharpoons SO_2Cl^-\,(aq) \tag{R5.13}$$

The equilibrium relationships at the gas-liquid interphase can be given by Equations 5.24 through 5.28.

$$C_{OH^-,interphase} = \frac{K_W}{C_{H^+,interphase}} \tag{5.24}$$

$$C_{SO_2,interphase} = H_{SO_2} \cdot C_{SO_2,bulkgas} \cdot R \cdot T \tag{5.25}$$

$$C_{HSO_3^-,interphase} = \frac{K_{SO_2} \cdot H_{SO_2} \cdot C_{SO_2,bulkgas} \cdot R \cdot T}{C_{H^+,interphase}} \tag{5.26}$$

$$C_{SO_3^{2-},interphase} = \frac{K_{HSO_3^-} \cdot K_{SO_2} \cdot H_{SO_2} \cdot C_{SO_2,bulkgas} \cdot R \cdot T}{(C_{H^+,interphase})^2} \tag{5.27}$$

Cl balance at the gas-liquid interphase can be given by Equation 5.28

$$C_{Cl,interphase} = C_{HClInitial,interphase} - C_{SO_2Cl^-,interphase} \tag{5.28}$$

The equilibrium relationships in the bulk HCl solution can be given by Equations 5.29 through 5.33.

$$C_{OH^-,HClSolution} = \frac{K_W}{C_{H^+,HClSolution}} \tag{5.29}$$

$$C_{SO_2,HClSolution} = \frac{S_{total} \cdot C^2_{H^+,HClSolution}}{C^2_{H^+,HClSolution} + K_{SO_2} \cdot C_{H^+,HClSolution} + K_{SO_2} \cdot K_{HSO_3^-}} \tag{5.30}$$

$$C_{HSO_3^-,HClSolution} = \frac{S_{total} \cdot K_{SO_2} \cdot C_{H^+,HClSolution}}{C^2_{H^+,HClSolution} + K_{SO_2} \cdot C_{H^+,HClSolution} + K_{SO_2} \cdot K_{HSO_3^-}} \tag{5.31}$$

$$C_{SO_3^{2-},HClSolution} = \frac{S_{total} \cdot K_{SO_2} \cdot K_{HSO_3^-}}{C^2_{H^+,HClSolution} + K_{SO_2} \cdot C_{H^+,HClSolution} + K_{SO_2} \cdot K_{HSO_3^-}} \tag{5.32}$$

Cl balance in the bulk HCl solution can be given by Equation 5.33

$$C_{Cl,HClSolution} = C_{HClInitial,HClSolution} - C_{SO_2Cl^-,HClSolution} \tag{5.33}$$

The mass balance equations (Equations 5.34 through 5.38) used to calculate SO_2(g), S_{total}, H^+, Cl^- and SO_2Cl^-, were developed in consideration of chemical reactions R5.12 through R5.13, equilibrium relationships, electroneutrality etc.

SO_2 in gas phase

$$\frac{dC_{SO_2}}{dt} = \frac{1}{V_{Headspace}} \cdot (F \cdot C_{SO_2,inlet} - F \cdot C_{SO_2,bulkgas}) - \frac{V_{HClSolution}}{V_{Headspace}} \cdot N_{SO_2} \tag{5.34}$$

Total sulphur balance

$$\frac{dC_{S_{total}}}{dt} = N_{SO_2} - R_{SO_2Cl^-,HClSolution} \tag{5.35}$$

Total chloride balance

$$\frac{dC_{Cl^-_{total}}}{dt} = R_{HCl} - R_{SO_2Cl^-,HClSolution} \tag{5.36}$$

Hydrochloric acid dissociation

$$\frac{dC_{HCl}}{dt} = R_{HCl} \tag{5.37}$$

Complex formation

$$\frac{dC_{SO_2Cl^-}}{dt} = R_{SO_2Cl^-,HClSolution} \tag{5.38}$$

Similarly to Case I in Subsection 5.3.2, the rates of reactions for species i (where i = HCl and SO_2Cl^-) were calculated employing Equations 5.37 and 5.38, where they are expressed in terms of the forward reaction constants and equilibrium constants according to Chen et al. (2009). The respective constants were adopted from literature (Chen et al. 2011, Goldberg & Parker 1985, Krissmann et al. 1998, Schwartz & Freiberg 1981, Tanaka 2010).

Case III: Intermediate pH (Deionised Water)

The absorption of SO_2 into water involves physical absorption and hydrolysis reactions (Eriksen 1969). The equilibrium at gas-liquid interphase can be described by Henry's law. When SO_2 from flue gas is absorbed into water, both the gas- and liquid-films are important.The rate of SO_2 absorption can be given by Equation 5.39

$$N_{SO_2} = \frac{P_{bulkgas} - H_{SO_2} C_{SO_2,water}}{\frac{1}{k_g a} + \frac{H_{SO_2}}{E k_L a}} \tag{5.39}$$

where E is the enhancement factor, and is given by Equation 5.40

$$E = \frac{D_{SO_2}(C_{SO_2,int} - C_{SO_2,water}) + D_{HSO_3^-}(C_{HSO_3^-,int} - C_{HSO_3^-,water} + D_{SO_3^{2-}}(C_{SO_3^{2-},int} - C_{SO_3^{2-},water})}{D_{SO_2}(C_{SO_2,int} - C_{SO_2,water})} \tag{5.40}$$

The mechanisms proposed by Chen et al. (2011), Falk & Giguère (1958), Hikita et al. (1978), Terraglio & Manganelli (1967) were followed in this study. Chemical reactions R5.1 through R5.4 are applicable in this study, with additional reactions being R5.17 and R5.18. Since SO_2 dissociates in water (reaction R5.2), Henry's law does not apply to the S_{total}, but rather to the concentration of SO_2(aq) in reaction R5.1.

HSO_3^- dissociation:

$$HSO_3^-(aq) \rightleftharpoons H^+(aq) + SO_3^{2-}(aq) \tag{R5.17}$$

Diffusion of dissolved chemical species in liquid film

Chemical reaction of diffused species:

$$SO_2(aq) + SO_3^{2-}(aq) + H_2O(l) \rightleftharpoons 2\,HSO_3^-(aq) \tag{R5.18}$$

Both the first and second dissociations had been reported to be fast processes by various workers (Carmichael & Peters 1979, Eriksen 1969, Hikita et al. 1978, Yates & Best 1976). At 20 °C, the forward and reverse rate constants of the first dissociation had been reported to be of the order of 10^6 s^{-1} and 10^8 L· $mol^{-1}s^{-1}$, respectively. Similarly,10^4 s^{-1} and 10^{11} L· $mol^{-1}s^{-1}$, for the second dissociation (Beilke & Lamb 1975). Therefore, on the time scale of the diffusion processes, the equilibrium can be treated as being instantaneously established (Lynn et al. 1955).

The equilibrium relationships at the gas-liquid interphase can be given by Equations 5.41 through 5.45.

$$C_{OH^-,interphase} = \frac{K_W}{C_{H^+,interphase}} \tag{5.41}$$

$$C_{SO_2,interphase} = H_{SO_2} \cdot C_{SO_2,bulkgas} \cdot R \cdot T \tag{5.42}$$

$$C_{HSO_3^-,interphase} = \frac{K_{SO_2} \cdot H_{SO_2} \cdot C_{SO_2,bulkgas} \cdot R \cdot T}{C_{H^+,interphase}} \tag{5.43}$$

$$C_{SO_3^{2-},interphase} = \frac{K_{HSO_3^-} \cdot K_{SO_2} \cdot H_{SO_2} \cdot C_{SO_2,bulkgas} \cdot R \cdot T}{(C_{H^+,interphase})^2} \tag{5.44}$$

Electroneutrality at the gas–liquid interphase can be given by Equation 5.45

$$C_{H^+,interphase} = C_{HSO_3^-,interphase} + 2 \cdot C_{SO_3^{2-},interphase} + C_{OH^-,interphase} \tag{5.45}$$

The equilibrium relationships in bulk water can be given by Equations 5.46 through 5.50.

$$C_{OH^-,water} = \frac{K_W}{C_{H^+,water}} \tag{5.46}$$

$$C_{SO_2,water} = \frac{S_{total} \cdot C_{H^+,water}^2}{C_{H^+,water}^2 + K_{SO_2} \cdot C_{H^+,water} + K_{SO_2} \cdot K_{HSO_3^-}} \tag{5.47}$$

$$C_{HSO_3^-,water} = \frac{S_{total} \cdot K_{SO_2} \cdot C_{H^+,water}}{C_{H^+,water}^2 + K_{SO_2} \cdot C_{H^+,water} + K_{SO_2} \cdot K_{HSO_3^-}} \tag{5.48}$$

$$C_{SO_3^{2-},water} = \frac{S_{total} \cdot K_{SO_2} \cdot K_{HSO_3^-}}{C_{H^+,water}^2 + K_{SO_2} \cdot C_{H^+,water} + K_{SO_2} \cdot K_{HSO_3^-}} \tag{5.49}$$

Electroneutrality in the bulk water can be given by Equation 5.50

$$C_{H^+,water} = C_{HSO_3^-,water} + 2C_{SO_3^{2-},water} + C_{OH^-,water} \tag{5.50}$$

The mass balance equations (Equations 5.51 and 5.52) used to calculate SO_2(g), S_{total}, H^+, Cl^- and SO_2Cl^-, were developed in consideration of chemical reactions R5.12 through R5.13, equilibrium relationships, electroneutrality etc.

SO_2 in gas phase:

$$\frac{dC_{SO_2}}{dt} = \frac{1}{V_{Headspace}} \cdot (F \cdot C_{SO_2,inlet} - F \cdot C_{SO_2bulkgas}) - \frac{V_{water}}{V_{Headspace}} \cdot N_{SO_2} \tag{5.51}$$

Total sulphur balance:

$$\frac{dC_{S_{total}}}{dt} = N_{SO_2} \tag{5.52}$$

5.4 Results and discussion

5.4.1 Absorption and reaction in aqueous solutions

The experiments for the absorption of SO_2 into aqueous solutions and limestone slurry were conducted using the material, apparatus, methods and operating conditions presented in Sections 5.2 respectively. Figures 5.2 through 5.4 presents the results of SO_2 absorption, obtained whilst varying solutions and operating conditions.

Figures 5.2 and 5.3 present the concentration of SO_2 in the effluent stream and the pH of respective solutions, respectively. The SO_2 were observed to increase steadily in the cases of solutions with low initial pH solution (1 M HCl solution, $pH_{Initial} \approx 0$, at 50 °C) and intermediate initial pH solution (deionized water, $pH_{Initial}$ = 7 at 50 °C). This can be attributed to poor dissociation of aqueous SO_2, indicating that the absorption is diffusion controlled. The concentration of SO_2 in the effluent stream has been observed to remain between 0.018 and 0.022 mol/m^3 over a period of 49.9 hours, in the case of high initial pH solution (0.1 M NaOH solution, $pH_{Initial}$ = 9.13). This can be attributed to high (initially instantaneous) dissociation rates of SO_2, as also reported by Schultes (1998), Wang et al. (2015) and Vázquez et al. (1988) .

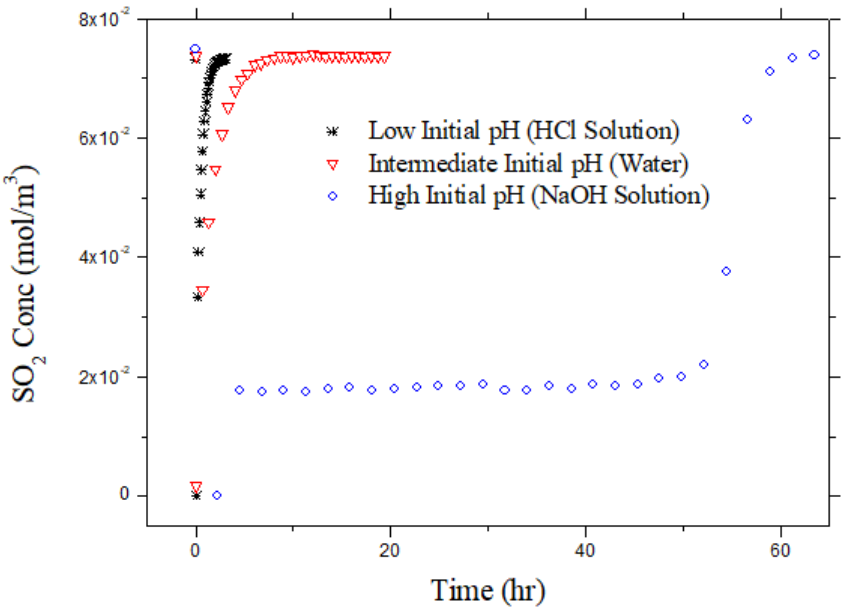

Figure 5.2: Concentration of effluent SO_2: Effect of initial pH.

No further increase in the concentration of SO_2 (in the effluent stream) was observed after 2.7 hours (in the case of HCl solution), 8.7 hours (in the case of deionized water) and 49.9 hours (in the case of NaOH solution), indicating that saturation or equilibrium condition had been reached. For water case, the results were in agreement to those reported by Terraglio & Manganelli (1967) and Al-Enezi et al. (2001) .

The pH during the absorption of SO_2 into HCl solution was observed to be negative, a similar observation was made by Zimmermann et al. (2009). The pH values of water were observed to decrease rapidly during the absorption SO_2 in the first 1.15 hours. Similar results were reported by Terraglio & Manganelli (1967) and Al-Enezi et al. (2001) . The pH of NaOH solution was observed to be greater than 12 for a period of 9.4 hours. Lee et al. (2001) reported a pH values of 13.41 – 13.51 for 0.33 – 0.4 NaOH solutions at 22 °C. The water pH results in Figure 5.3 are in agreement with those of Al-Enezi et al. (2001) and Sharma et al. (2012). The later reported a pH drop from 12.57 to 4.75 over a period of 75 minutes under their experimental conditions.

The transient effluent SO_2 concentration profiles for the water case at 25 °C and 50 °C are given in Figure 5.4. The absorption rate and quantity was observed to be higher at higher temperature (50 °C). This can be attributed to the higher average kinetic energy possessed by SO_2 gas molecules at higher temperatures, leading to higher diffusion.

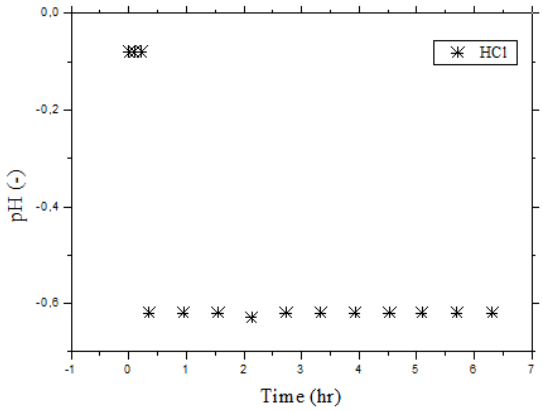

(a) HCl Solution

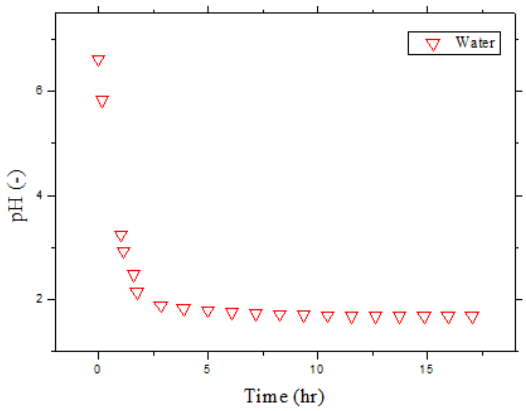

(b) Water

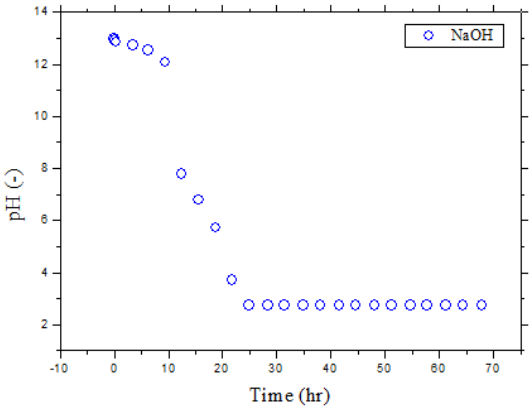

(c) NaOH Solution

Figure 5.3: Transient pH of aqueous solutions.

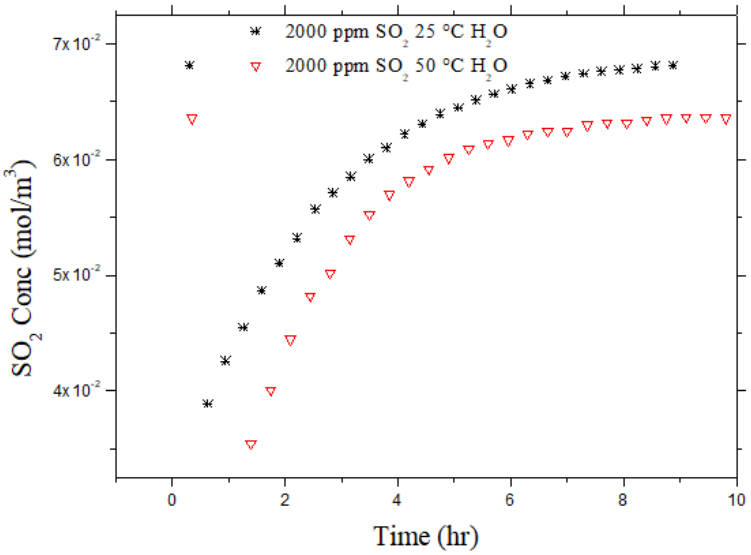

Figure 5.4: Concentration of effluent SO_2: Effect of temperature (Water Case).

This observation is consistent with the argument presented above, i.e. the absorption of SO_2 into water is diffusion-controlled, and concurs with the work reported by Terraglio & Manganelli (1967) and Al-Enezi et al. (2001).

SO_2 solubility function in water had been reported to have a second-order dependence on the temperature by Al-Enezi et al. (2001), who investigated the solubility of SO_2 in distilled water, sea water and blends over a temperature range of 10 – 40 °C under atmospheric pressure.

5.4.2 Absorption and reaction in aqueous solutions: Gas-Liquid Mass Transfer Constants

Case I Results and Discussion: Evaluation of gas-side mass transfer coefficients (High pH NaOH solution)

$k_g a$ was evaluated as per method given in Sub-section 5.3.2 i.e from the absorption of SO_2 from SO_2/N_2 mixture into high pH solution (0.1 kmol/m^3 NaOH solution).Since in relatively concentrated NaOH solution, the dissolved SO_2 reacted instantaneously and irreversibly with the liquid phase reactant at the gas-liquid interphase, consequently, the liquid phase mass transfer resistance is considered to be negligible.

Figure 5.5 presents the obtained results, the slopes are on insert tables in the respective sub-figures. The values of $k_g a$ were taken as the slope from the plot of rate of SO_2 absorption vs the driving force. Table 5.2 compares the gas-side mass transfer coefficient obtained in this study with those of other researchers. Takashina et al. (2001) and Uchida et al. (1978) evaluated the gas-liquid interfacial surface employing the absorption of CO_2 gas into NaOH solution, due to the nature of the chemical reaction involved, i.e. irreversible pseudo-first-order-reaction (Uchida et al. 1978, Yoshida & Miura 1963). The knowledge of interfacial area enabled the researchers to report the gas-side mass transfer coefficients separately. In this study, the product of the gas-liquid interfacial surface area and the gas-side mass transfer coefficient were reported, and for consistent comparison, the literature gas-side mass transfer coefficients were multiplied by their respective gas-liquid interfacial surface areas.

Researchers such as Deshwal & Hyung Keun (2009), Bravo et al. (2002), Takashina et al. (2001), Lancia et al. (1997),Uchida & Ariga (1985), Uchida et al. (1978), Sada et al. (1979), Uchida et al. (1978) etc. developed empirical correlations to calculate the gas-side mass transfer coefficients. The correlations are dependent on the stirring rates, indicating that the gas-side mass transfer coefficients is a function of the gas film thickness. Therefore, workers such as Bravo et al. (2002) and Takashina et al. (2001) evaluated the gas film thickness. Deshwal & Hyung Keun (2009) conducted experiments over a range of gas flow rates, the same authors developed an empirical

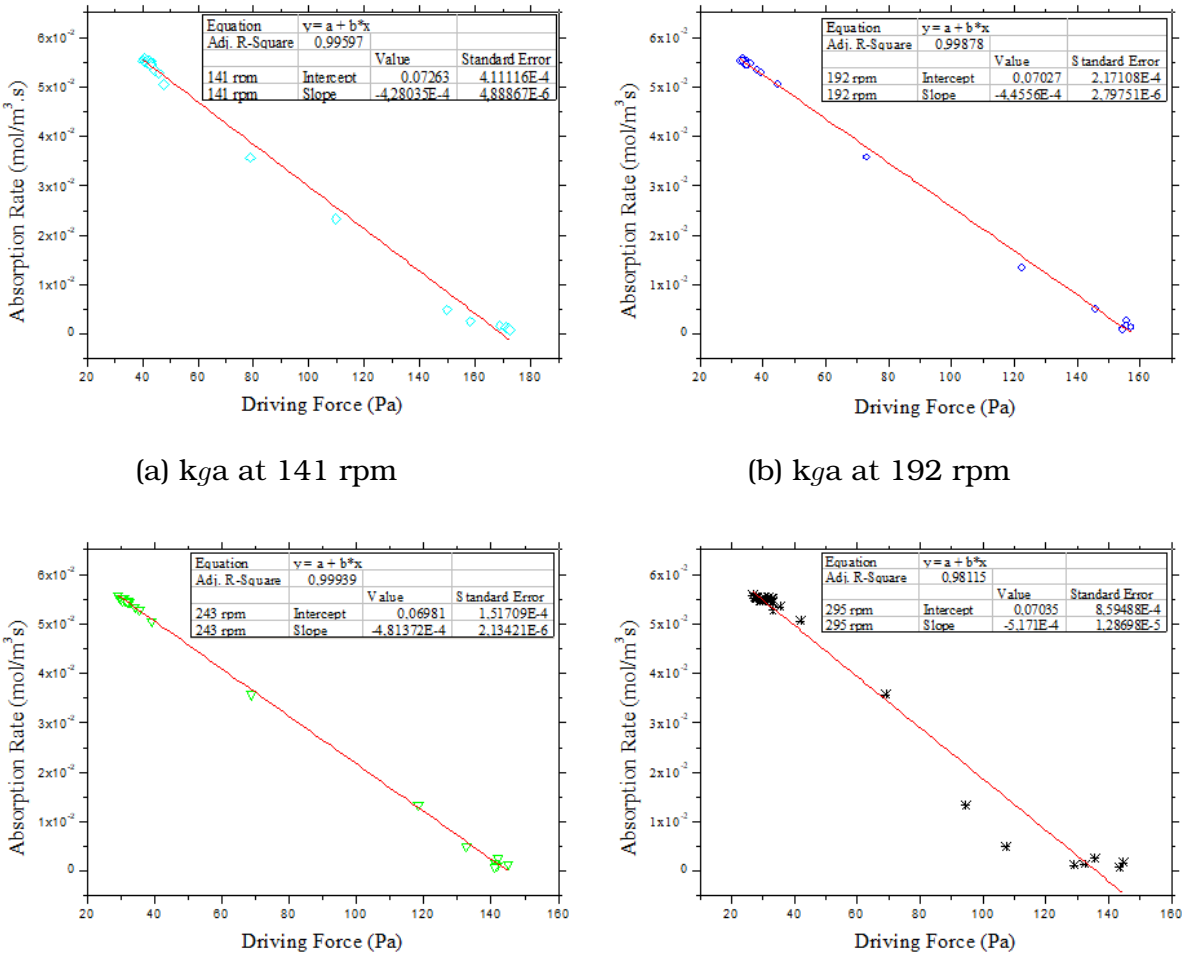

(a) k$_g$a at 141 rpm

(b) k$_g$a at 192 rpm

(c) k$_g$a at 243 rpm

(d) k$_g$a at 295 rpm

Figure 5.5: Determination of gas-side mass transfer coefficient (at 50 °C).

Table 5.2: Comparison of the product interfacial area and gas-side mass transfer coefficients with literature.

Study	Stirring rate (rpm)	Temperature (°C)	System	k$_g$a (mol/m^3·s·Pa)
This study	141 - 295	50	SO_2-NaOH solution	4,28 $\times 10^{-4}$ - 5.17 $\times 10^{-4}$
Bravo et al. (2002)	400	20 - 40	SO_2-NaOH solution	9,39 $\times 10^{-7}$ - 7,49 $\times 10^{-7}$
Takashina et al. (2001)	1000 - 1500	50	SO_2-NaOH solution	7.75 $\times 10^{-1}$ - 1.16
Lancia et al. (1997)	300 - 900	25	SO_2-NaOH solution	4,84 $\times 10^{-4}$ - 1.01 $\times 10^{-4}$
Uchida et al. (1978)	91 - 391	20	SO_2-NaOH solution	2,18 $\times 10^{-5}$ - 6.37 $\times 10^{-5}$

correlation that is dependent on both stirring speed and gas flow rate. The k$_g$a range in this study is comparable with that of Lancia et al. (1997) and Uchida et al. (1978), the difference with other researchers can be attributed to a experimental conditions. The results reported in this section are compared with the value obtained through

model fitting in Chapter 6, i.e. when considering the contribution of chemical reactions.

Case II Results and Discussion: Evaluation of liquid-side mass transfer coefficients (low pH HCl solution)

k_La was estimated as per method presented in Sub-section 5.3.2 , i.e. by absorbing SO_2 from SO_2/N_2 mixture into 1 kmol/m^3 HCl solution.

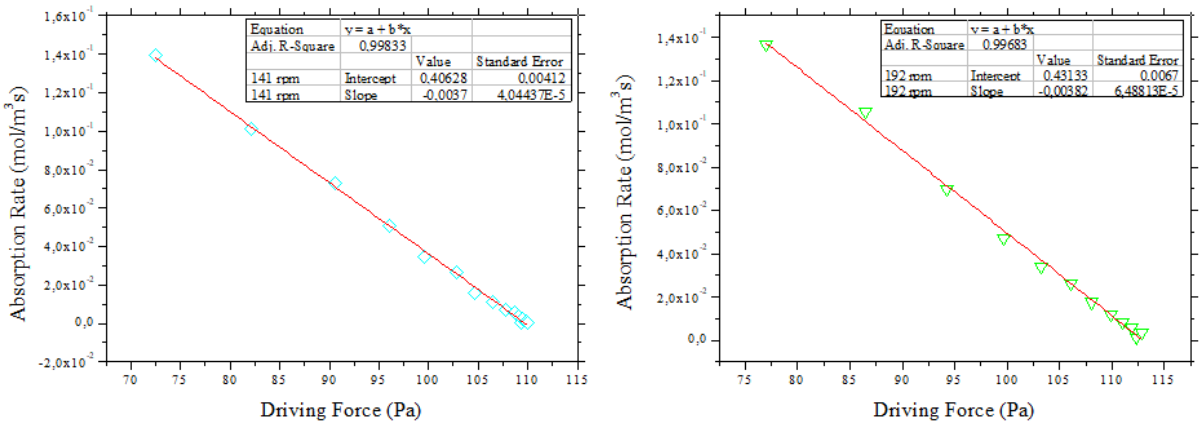

(a) k_La at 141 rpm

(b) k_La at 192 rpm

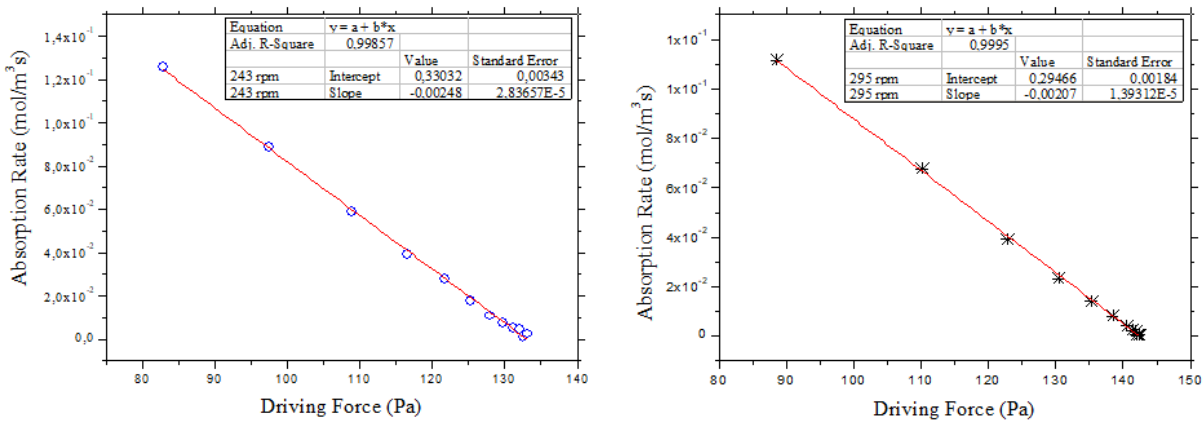

(c) k_La at 243 rpm

(d) k_La at 295 rpm

Figure 5.6: Determination of liquid-side mass transfer coefficient.

Figure 5.6 presents the obtained results, the slopes are on insert tables in the respective sub-figures. The values of k_La were evaluated from the slope from the plot of rate of SO_2 absorption vs the driving force, in conjunction with k_ga determined in Case I above, whilst employing Equation 5.23. Table 5.3 compares the liquid-side mass transfer coefficient obtained in this study with those of other researchers. It can be seen that the most commonly used systems are the O_2 systems. Under the

O_2-water system, the gas phase mass transfer resistance can be neglected because due to low solubility of O_2 in water and that O_2 concentration in atmospheric air is as high as 20 percentage by volume (Deshwal & Hyung Keun 2009).

Table 5.3: Comparison of liquid-side mass transfer coefficients product.

Study	Stirring rate (rpm)	Temperature (°C)	System	k_La (1/s)
This study	141 - 295	50	SO_2-HCl acid solution	$7{,}26 \times 10^{-2}$ - 1.04×10^{-1}
Bravo et al. (2002)	400	20 - 40	Calculated	2.95×10^{-5} - 3.62×10^{-5}
Takashina et al. (2001)	150 - 250	50	O_2-water	$1{,}25 \times 10^{-3}$ - 3.87×10^{-3}
Lancia et al. (1997)	300 - 900	25	SO_2-HCl acid solution	5.31×10^{-3} - 1.20×10^{-1}
Uchida & Ariga (1985)	153	20	O_2-water	$2{,}30 \times 10^{-1}$
Uchida et al. (1978)	91 - 391	20	O_2-water	$2{,}37 \times 10^{-1}$ - 1.06

Investigators such as Deshwal & Hyung Keun (2009) and Sada et al. (1979), developed empirical correlations to calculate the liquid-side mass transfer coefficients,which are dependent on the stirring rates, indicating that the liquid-side mass transfer coefficients is a function of the gas film thickness. On the same basis as given in Case I above, Deshwal & Hyung Keun (2009) developed an empirical correlation to calculate k_La, which is dependent on gas flow rate and stirring speed. The k_La obtained in this study is comparable those reported by Lancia et al. (1997), Uchida & Ariga (1985) and Uchida et al. (1978). The results reported in this section are compared with the value obtained through model fitting in Chapter 6, i.e. when considering the contribution of chemical reactions.

For better comparison of results from different apparatus, the operation that will give identical interfacial mass transfer and hydrodynamics must be calculated for respective apparatus, e.g. using the hydrodynamics and interfacial contact of a slurry droplet in the sprayer as a reference.

The commonly considered characteristics of a mechanically agitated reactor are hydrodynamic, heat and mass transfer. The typical hydrodynamic properties include flow patterns (velocity field and turbulence), power consumption in the presence of gas and solid particle suspension. The empirical equations recommended by Joshi et al. (1982) for flow patterns are dependent of stirrer blades (namely, disk turbine, pitched blade turbine and propeller).

For the power consumption in the presence of gas, the Hughmark equation Hughmark (1980) has been recommended. In the absence of gas, the Zweitering equation (Zwietering 1958) has been recommended for solid particle suspension, whereas in the presence of gas, the procedure given by Subbarao & Taneja (1979) had been recommended by Joshi et al. (1982).

In addition to the interphase mass transfer, the extend of mixing is also considered to be very important and is dependent on design variables, namely, impeller diameter, impeller clearance and impeller blade width. The equations for mixing times in the presence and in the absence of gas had been recommended by Joshi et al. (1982). For cases where both k_g and k_L are important and mass transfer is accompanied by chemical reaction (as in this study), the determination of the interfacial surface area becomes very important and should be evaluated experimentally separately or combined with k_g and/or k_L.

5.5 Chapter 5 Summary

Depending on the pH of the solution, the absorption of SO_2 from flue gas is controlled by the gas-side film resistance or liquid-side film resistance or both films, e.g., gas film resistance dominated SO_2 absorption into high pH solutions whereas both the gas-side film and liquid-side film resistances were important during SO_2 absorption into water (intermediate pH) and liquid-side film resistance dominated the absorption into low pH solution.

- Experiments were conducted to measure the absorption of SO_2 into aqueous solutions over a wide range of pH values ($0 \leq$ pH ≥ 12.4).
- The experimental results of SO_2 absorption into aqueous solution of high pH (NaOH solution) were employed to evaluate $k_g a$. The results for absorption into low pH (HCl solution) were used to evaluate $k_L a$.
- Two methods of evaluating the gas-liquid mass transfer constants were compared, namely, commonly used gradient method (from a plot of absorption rate vs driving force) and regression method (fitting a model to experimental results).
- Experiments of absorption of SO_2 into water were also performed. The results thereof were employed to test the validity of the determined mass transfer constants.

Chapter 6 Integrated model of SO_2 absorption into limestone slurry

The aim of this study is to develop an integrated model for SO_2 absorption into limestone slurry consisting of four sub-models, namely, absorption of SO_2; desorption of CO_2; dissolution of limestone and crystallization of calcium sulphite hemihydrate. The model requires information obtained in Chapters 2 through 5. The model also requires the development of numerical algorithm to solve a set of differential and algebraic equations, and the output also needs to be experimentally validated. The secondary objective is to compare the results with published work done by other workers. Laboratory experiments were also conducted under varied experimental conditions, namely, solids concentration, gas concentration and temperature. Model predictions were compared with experimental transient data for the concentrations of SO_2 in the bulk gas (head-space), pH of the bulk slurry and concentrations of $CaCO_3$ and $CaSO_3 0.5H_2O$ in the bulk slurry.

6.1 Introduction

SO_2 pollution are deleterious to mankind's health and to the environment. There are numerous sources of SO_2 emissions, with the major ones being electricity production plants (e.g. coal- and oil-fired), paper-pulp production and so forth. Ways of abatement of SO_2 emission are discussed in Chapter 1, Sub-section 1.1.2, where it is evident that SO_2 absorption in suspensions or solutions dominates.

For suspensions based technologies, wet scrubbers (e.g. open spray towers , packed towers, double-loop towers and so forth) dominates (Takeshita & Soud 1993). (Kiil et al. 1998) reported that the most used and researched WFGD is the counter-current spray tower.

A number of simulations studies on WFGD had been given in literature e.g. Kallinikos et al. (2010),Neveux et al. (2014),Zeng et al. (2007),Olausson et al. (1993)

and others. The most common inputs into those models are flow rates and concentrations. The models can be of any nature e.g. empirical, fundamental and so forth.

A plethora of reports (experimental and theoretical) on SO_2 into limestone slurries in an agitated vessels are blazoned in literature e.g. in Uchida & Ariga (1985), Uchida et al. (1978), Uchida & Wen (1977), Uchida et al. (1975), Uchida & Wen (1973), Sada et al. (1983), Sada et al. (1982), Sada, Kumazawa & Hashizume (1981), Sada et al. (1980), Sada et al. (1979), Sada et al. (1977) and so forth.

Theoretical interpretation of gas absorption into slurries comprising of reactive fine particles are complex, particularly when the slurry contain micro-particles. The pioneering theoretical study on this subject was performed by Ramachandran & Sharma (1969) with the attentiveness in meagrely soluble reactive fine particles. The same authors proposed two rate equations that were based on whether the dissolution of solid particles in the liquid film is significant or not.Uchida et al. (1978) amended the equations of Ramachandran on the basis of experimental observance that limestone dissolution in the liquid film augments SO_2 absorption.

Studies that provide models that integrate the rate limiting steps of the absorption of SO_2 into limestone in stirred tank reactors (semi-batch and batch processes) are scarce in literature. The aim of this chapter is to develop an integrated model for SO_2 absorption into limestone slurry in an agitated vessel while considering the rate of SO_2 absorption, limestone dissolution, CO_2 desorption and $CaSO_30.5H_2O$ crystallization. The specific objectives include experimental validation of the respective sub-models (SO_2 absorption, limestone dissolution, CO_2 desorption and $CaSO_30.5H_2O$ crystallization) and then testing the validity of the model under various experimental conditions, specifically , temperature,limestone loadings and SO_2 concentration.

The novelty in this chapter involves transient evaluation of SO_2 absorption process (through modelling and experimentation in a stirred tank reactor operated with continuous gas flow and a batch slurry) over long period (>50 hr), so as to enable the process transition from high pH regime, through intermediate regime, to low pH regime. The development and validation of an integrated model for the above-mentioned process is also considered to be novel.

6.2 Experimental

6.2.1 Materials

Details of the limestone that was used in this study (origin, motivation for selection and preparation) are given in Chapter 3,Sub-Section 3.1.1. Specifications and suppliers of other materials used (e.g simulated flue gas) are given in Chapters 4

(Sub-section 4.2.1) and 5 (Sub-section 5.2.1).

6.2.2 Apparatus

Details of the reactor used are in Chapter 4, Sub-section 4.2.2. Details of methods of its use as well as the required accessories included in Chapter 5 (Sub-section 5.2.2), with the exception being that, in this chapter, simulated flue gas is passed over 1500 cm^3 slurry with a flat interface. The absorption of SO_2 (from simulated flue gas) into limestone slurry is determined by measuring the concentration of SO_2 in the effluent flue gas using the gas analyser (X-STREAM GP Compact 1/2 19" Rack-mount & Portable Gas Analyser), supplied by Rand Instruments (South Africa). Metrohm 691 pH meter and a unitrode with Pt 1000 (supplied by Metrohm South Africa) were employed for pH measurement. Methods for determining transient concentrations of $CaCO_3$ and $CaSO_3 0.5H_2O$ are given in Sub-section 6.2.3.

6.2.3 Methods

Details of characterization techniques used to analyse limestone (chemical, mineral and structural analyses) and the results thereof are reported in Chapter 3. The procedure and operating conditions of Chapter 5 are applicable in this chapter. Slurry samples were withdrawn at pre-determined time intervals. The samples were sieved, and both the aliquot and solids were subjected various analysis, namely, the aliquot was analysed using the inductively coupled plasma optical emission spectrometer (ICP Expert II, Agilent Technologies 720 ICP-OES) and the relative phase amounts (weight %) in the solids was estimated using the Rietveld method (Autoquan program) measurements by XRD based on the effect of the crystalline structure of minerals on X-rays.

6.3 Integrated model

Following the approach employed by Kiil et al. (1998) on modelling the pilot plant, a model for a batch process in an agitated vessel is developed in this study, and is considered to be comprised of the following sub-models:

i SO_2 Absorption,

ii Dissolution of limestone,

iii CO_2 desorption, and

iv Crystallization of hannebachite.

The electrolytic thermodynamics has an impact on chemical absorption of SO_2 into limestone slurry, however as the activity coefficient approach 1, ideal conditions can be assumed. For SO_2-water system, the activity coefficients reported by Abdulsattar et al. (1977) for SO_2, CO_2, H^+, HSO_3^-, HCO_3^- and SO_3^{2-} at 25°C are 0.98, 1.13, 0.795, 0.56, 0.543 and 0.104, respectively.

WFGD solution is a complex mixture with numerous ions and saturated salts in equilibrium with solid, despite that, workers such as Desch et al. (2006), Kiil et al. (1998), Zhong et al. (2008) and so forth, assumed ideal solutions. Some workers, e.g.Neveux & Le Moullec (2011) considered non-ideal conditions and reported a desulphurization efficiency difference of approximately 13% between an ideal solution model (activity coefficient equal to unity) and the Debye-Hückel solution model.

Solutions in laboratory scale stirred tank reactors are less complex than those in industrial scale, and despite the advantages of extrapolability and accuracy of non-ideality, workers such as Lancia et al. (1997), Uchida & Ariga (1985), Uchida et al. (1978) and so forth, assumed ideal solutions. Some workers, e.g. Bravo et al. (2002) considered non-ideal conditions. For simplicity, ideal solution is assumed in this study and the following species were considered : SO_2(g), SO_2(aq), HSO_3^-, SO_3^{2-},CO_2(g), CO_2(aq), HCO_3^-, CO_3^{2-}, H^+, OH^-, $CaCO_3$, $CaSO_3 0.5H_2O$ and Ca^{2+}.

The developed model is still open for improvements, e.g., the model is still to incorporate design and operational empirical relations for it to be applicable on other systems and geometries, improvements for the model to cater for both ideal solutions and non-ideal solutions, detailed hydrodynamics and so forth.

6.3.1 Chemical Reaction Mechanism

The reaction mechanism of SO_2 chemical absorption into limestone slurry has been given by various workers, namely, Nannen et al. (1974), Rochelle & King (1977), Takashina et al. (2001),Uchida & Ariga (1985), Uchida et al. (1978) and others.

Among the many reactions involved, the major reactions and processes include SO_2 diffusion in the film and subsequent chemical reactions, and limestone dissolution. The main reaction steps are:

Diffusion of SO_2 through the gas film

SO_2 hydration:

$$SO_2(g) \leftrightharpoons SO_2(aq) \tag{R6.1}$$

SO_2 reaction:

$$SO_2(aq) + H_2O(l) \rightleftharpoons H_2SO_3(aq) \quad \text{(R6.2)}$$

H_2SO_3 dissociation:

$$H_2SO_3(aq) \rightleftharpoons H^+ + HSO_3^- \quad \text{(R6.3)}$$

HSO_3^- dissociation:

$$HSO_3^- \rightleftharpoons H^+ + SO_3^{2-} \quad \text{(R6.4)}$$

Limestone hydration:

$$CaCO_3(s) \longrightarrow CaCO_3(aq) \quad \text{(R6.5)}$$

$CaCO_3$(aq) dissociation:

$$CaCO_3(aq) \rightleftharpoons Ca^{2+} + CO_3^{2-} \quad \text{(R6.6)}$$

CO_3^{2-} protonation:

$$H^+ + CO_3^{2-}(aq) \rightleftharpoons HCO_3^- \quad \text{(R6.7)}$$

HCO_3^- protonation:

$$H^+ + HCO_3^- \rightleftharpoons H_2CO_3(aq) \quad \text{(R6.8)}$$

CO_2(g) desorption

$$H_2CO_3(aq) \rightleftharpoons CO_2(g) + H_2O(l) \quad \text{(R6.9)}$$

Diffusion of dissolved chemical species in liquid film

Chemical reaction of diffused species:

$$SO_2(aq) + HCO_3^- \rightleftharpoons HSO_3^- + CO_2(g)$$

(R6.10)

Chemical reaction of diffused species:

$$SO_2\,(aq) + SO_3^{2-} + H_2O\,(l) \leftrightharpoons 2\,HSO_3^-$$

(R6.11)

Chemical reaction of diffused species:

$$CO_3^{2-} + HSO_3^- \leftrightharpoons HCO_3^- + SO_3^{2-}$$

(R6.12)

Chemical reaction of diffused species:

$$Ca^{2+} + SO_3^{2-} + 0.5\,H_2O\,(l) \leftrightharpoons CaSO_3 0.5\,H_2O(s)$$

(R6.13)

SO_2 diffuses through the gas-liquid film and react with water according to reaction R6.1 and R6.2. When the concentration of SO_2 is low,in the order of ppm, as it is the case in this study, R6.1 and R6.2 are important Uchida et al. (1978), because resistance to diffusion is considered to be significant. The produced H_2SO_3 subsequently dissociates to produce HSO_3^-, according to R6.3, which also dissociates subsequently (R6.4), to produce SO_3^{2-}.

In parallel to reactions R6.1 through R6.4, hydrated $CaCO_3$ dissociates according to R6.6. The solubility and dissolution of $CaCO_3$ are strongly affected by the species available in the bulk slurry (e.g sulphites,carbonates and protons) and the partial pressure of CO_2 in the overhead (Uchida et al. 1978). The produced CO_3^{2-} is protonated to produce HCO_3^-, which is subsequently protonated to H_2CO_3.

Thereafter, CO_2 gas is desorbed according to R6.9. Chemical reactions R6.7 and R6.8 had been reported to enhance the dissolution of $CaCO_3$ (Barton & Vatanatham 1976, Uchida & Ariga 1985). The available species in the liquid film and bulk reacts according to R6.10 to R6.12. $CaSO_3$ produced by the reaction of Ca^{2-} with $SO_{3^{2-}}$ combines with 0.5 H_2 moles to form hannebachite according to R6.13. The overall reaction is considered to take place according to R6.14 (Uchida et al. 1978).

Overall reaction :

$$CaCO_3(s) + SO_2\,(g) + H_2O\,(l) \longrightarrow CaSO_3 0.5\,H_2O(s) + CO_2\,(g)$$

(R6.14)

Reactions R6.2, R6.3, R6.10 and R6.11 have been reported to be fast by Chang & Rochelle (1981) and Liu & Xiao (2006). Chemical reactions R6.4, R6.7 and R6.8 are based on proton transfer, and had been reported to be even faster than reaction R6.2, and are therefore considered to be instantaneous (Liu & Xiao 2006). Conse-

quently, instantaneous equilibrium is assumed for reactions (R6.3), (R6.4), (R6.5), (R6.8), (R6.9), (R6.11) and (R6.12) throughout the liquid film. Chemical reaction R6.4 have low dissociation constant, and is thus negligible at low pH. Hannebachite (produced according to reaction R6.14) has low solubility, and will thus precipitate (Uchida et al. 1978).

6.3.2 Sub-model I: SO_2 Absorption

Following the discussion in Chapter 5, Section 5.3, absorption of SO_2 into a slurry is considered to be controlled by both gas and liquid films. In this study, SO_2 is absorbed into a slurry in a stirred tank reactor (batch) over a long period (>50 hour), such that the pH changes from high (e.g pH of 8.13 for slurry with initial limestone loading of 0.5 wt %) to low pH (e.g pH of 2.62 for slurry with initial limestone loading of 0.5 wt %). As the pH decreases, the SO_2 absorption resistance in the two-film is considered to shift from gas-side controlled to liquid-side controlled. However, both resistances are considered, and following the two film theory (Whitman 1924) (presented in Sub-section 5.3.1), the rate of SO_2 absorption can be given by Equation 6.1

$$N_{SO_2} = \frac{P_{bulkgas} - H_{SO_2} c_{SO_2,bulkslurry}}{\frac{1}{k_g a} + \frac{H_{SO_2}}{k_L a}} \tag{6.1}$$

Chemical reactions increase the rate of SO_2 absorption.The contribution of such chemical reactions is quantified by the ratio of the rate with chemical reactions to the rate without chemical reactions, known as the enhancement factor (E). Various enhancement factor expressions are available in literature (Brogren & Karlsson 1997*c*, Chang & Rochelle 1982*b*, Dou et al. 2009, Kallinikos et al. 2010, Kiil et al. 1998, Neveux & Le Moullec 2011, Pasiuk-Bronikowska & Rudziński 1991, Uchida & Ariga 1985), and they depend on the chemical reactions considered. When the diffusion of SO_2(g) and the dissociation of SO_2(aq)and HSO_3^- (chemical reactions R6.1 - R6.4) are considered, the enhancement factor can be given by Equation 6.2 (Neveux & Le Moullec 2011)

$$E = 1 + \frac{D_{HSO_3^-}}{D_{SO_2}} \frac{(C_{HSO_3^-,interphase} - C_{HSO_3^-,bulkslurry})}{(C_{SO_2,interphase} - C_{SO_2,bulkslurry})} + \frac{D_{SO_3^{2-}}}{D_{SO_2}} \frac{(C_{SO_3^{2-},interphase} - C_{SO_3^{2-},bulkslurry})}{(C_{SO_2,interphase} - C_{SO_2,bulkslurry})} \tag{6.2}$$

The concentrations of SO_2, HSO_3^- and SO_3^{2-} at both the gas-liquid interphase and in the bulk slurry are evaluated from the definition of total sulphite,(S_{total}), as given in Equation 6.3 equalling the sum of SO_2, HSO_3^- and SO_3^{2-}.

$$S_{total} = SO_2 + HSO_3^- + SO_3^{2-} \tag{6.3}$$

Equation 6.3 is first expressed in terms of the desired species, $H_3O^+$and equilibrium constants, then rearranged to make the desired species the subject of the formula. For details, the reader is referred to Pasiuk-Bronikowska & Rudziński (1991).

The equilibrium relationships at the gas-liquid interphase can be given by Equations 6.4 through 6.8.

$$C_{OH^-,interphase} = \frac{K_W}{C_{H^+,interphase}} \tag{6.4}$$

$$C_{SO_2,interphase} = H_{SO_2} \cdot SO_{2,bulkgas} \cdot R \cdot T \tag{6.5}$$

$$C_{HSO_3^-,interphase} = \frac{K_{SO_2} \cdot H_{SO_2} \cdot SO_{2,bulkgas} \cdot R \cdot T}{C_{H^+,interphase}} \tag{6.6}$$

$$C_{SO_3^{2-},interphase} = \frac{K_{HSO_3^-} \cdot K_{SO_2} \cdot H_{SO_2} \cdot SO_{2,bulkgas} \cdot R \cdot T}{(C_{H^+,interphase})^2} \tag{6.7}$$

Electroneutrality at the gasliquid interphase can be given by Equation 6.8

$$\begin{aligned} C_{H^+,interphase} + 2 \cdot C_{Ca^{2+},interphase} = {} & C_{HSO_3^-,interphase} + 2 \cdot C_{SO_3^{2-},interphase} \\ & + C_{HCO_3^-,interphase} + 2 \cdot C_{CO_3^{2-},interphase} + C_{OH^-,interphase} \end{aligned} \tag{6.8}$$

The equilibrium relationships in bulk slurry can be given by Equations 6.9 through 6.13.

$$C_{OH^-,slurry} = \frac{K_W}{C_{H^+,slurry}} \tag{6.9}$$

$$C_{SO_2,slurry} = \frac{S_{total} \cdot C_{H^+,slurry}^2}{C_{H^+,slurry}^2 + K_{SO_2} \cdot C_{H^+,slurry} + K_{SO_2} \cdot K_{HSO_3^-}} \tag{6.10}$$

$$C_{HSO_3^-,slurry} = \frac{S_{total} \cdot K_{SO_2} \cdot C_{H^+,slurry}}{C^2_{H^+,slurry} + K_{SO_2} \cdot C_{H^+,slurry} + K_{SO_2} \cdot K_{HSO_3^-}} \tag{6.11}$$

$$C_{SO_3^{2-},slurry} = \frac{S_{total} \cdot K_{SO_2} \cdot K_{HSO_3^-}}{C^2_{H^+,slurry} + K_{SO_2} \cdot C_{H^+,slurry} + K_{SO_2} \cdot K_{HSO_3^-}} \tag{6.12}$$

Electroneutrality in the bulk slurry can be given by Equation 6.13

$$C_{H^+,slurry} + 2 \cdot C_{Ca^{2+}} = C_{HSO_3^-,slurry} + 2 \cdot C_{SO_3^{2-},slurry} + C_{HCO_3^-,slurry} + 2 \cdot C_{CO_3^{2-},slurry} + C_{OH^-,slurry} \tag{6.13}$$

The equilibrium constants for chemical reactions R6.3 and R6.4, K_{CO_2} and $K_{HCO_3^-}$, respectively, are taken from literature (Brewer 1982).

The second method of evaluating the enhancement factor is based on considering the dissolution of limestone (chemical reaction R6.6). This approach was applied by Dou et al. (2009) and Kallinikos et al. (2010), the latter gave an equation that is based on the two-film model for instantaneous chemical reaction (Equation 6.14) Levenspiel (1999)

$$E = 1 + \frac{D_{Ca^{2+}} \cdot C_{Ca^{2+}}}{D_{SO_2} \cdot S_{total}} \tag{6.14}$$

where $D_{Ca^{2+}}$ and D_{SO_2} are the diffusivities of Ca^{2+} and SO_2, respectively, and were taken from literature (Boudreau 1997). In this study, both approaches were tested, and the former method was observed to give better results.

6.3.3 Sub-model II: Limestone dissolution during SO_2 absorption

The limestone dissolution sub-model consisting of both the mass transfer step in the liquid phase and the chemical reaction step at the solid-liquid interface was employed in this study. When the inhibition by SO_3^{2-} ions is negligible (CSO_3^{2-} less than 1 mol/m^3) (Weng 2016), the overall rate of limestone dissolution has been given by Equation 6.15 (Carletti et al. 2015b)

$$R_{CaCO_3} = -k_{tot} \cdot SA \cdot C_{H^+} \cdot (1 - \frac{K_{ad} \cdot C_{H^+}}{1 + K_{ad} \cdot C_{H^+}}) \tag{6.15}$$

The rate of production of calcium ions can be given by

$$R_{Ca^{2+}} = k_{tot} \cdot SA \cdot C_{H^+} \cdot (1 - \frac{K_{ad} \cdot C_{H^+}}{1 + K_{ad} \cdot C_{H^+}}) \tag{6.16}$$

where k_{tot} is the overall coefficient,consisting of k_l and k_r. The total rate can be given by the reciprocal addition of resistances of according to Equation 4.12, and thus, the overall rate of dissolution can be given by Equation 4.16 (see Chapter 4). Following the discussion in Chapter 4, Section 4.7, the dissolution process is dominated by mass transfer, however the significance of chemical reactions increases with the increase in concentration of SO_3^{2-} ions.

K_{ad} (in m^3mol^{-1}) is the adsorption constant. SA is the surface area given by

$$SA = SSA_{BET} \cdot MW_{CaCO_3} \cdot c_{CaCO_3} \tag{6.17}$$

where SSA_{BET} (in m^2/g) is the specific surface area of limestone particles evaluated using the BET theory. MW_{CaCO_3} and c_{CaCO_3} are the molar mass and concentration of $CaCO_3$, respectively.

6.3.4 Sub-model III: CO_2 desorption

The two-film theory discussed in Chapter 5, Section 5.3 and applied in this chapter's Section 6.3.2, is applicable during CO_2 desorption. The main difference is that the liquid film resistance is considered to be the only resistance that affect the desorption of CO_2 (Gómez et al. 2007, Kallinikos et al. 2010), and the rate equation (Equation 6.1) is reduced to Equation 6.18

$$R_{CO_2} = k_{L,CO_2} \cdot E_{CO_2} \cdot a_i \cdot (\frac{P_{CO_2}}{H_{CO_2}} - C_{CO_2,bulkslurry}) \tag{6.18}$$

The enhancement factor theory given in Section 6.3.2 is applicable, however, chemical reaction R6.9 is considered to be slow, and thus, the enhancement factor for CO_2 desorption is approaches 1 (Kiil et al. 1998). For cases where the exact value of the enhancement factor for CO_2 desorption (E_{CO_2}) is crucial, Equation 6.19 is used.

$$E = 1 + \frac{D_{HCO_3^-}}{D_{CO_2}} \frac{(C_{HCO_3^-,interphase} - C_{HCO_3^-,bulkslurry})}{(C_{CO_2,interphase} - C_{CO_2,bulkslurry})} + \frac{D_{CO_3^{2-}}}{D_{CO_2}} \frac{(C_{CO_3^{2-},interphase} - C_{CO_3^{2-},bulkslurry})}{(C_{CO_2,interphase} - C_{CO_2,bulkslurry})} \tag{6.19}$$

As was done in Sub-section 6.3.2, the concentrations of CO_2, HCO_3^- and CO_3^{2-} at both the gas-liquid interphase and in the bulk slurry were evaluated from the definition of total carbonates,(C_{total}), as given in Equation 6.20 equalling the sum of CO_2, HCO_3^- and CO_3^{2-}.

$$C_{total} = CO_2 + HCO_3^- + CO_3^{2-} \tag{6.20}$$

Equation 6.20 is first expressed in terms of the desired species, H_3O^+ and equilibrium constants, then rearranged to make the desired species the subject of the formula. For details, the reader is referred to Pasiuk-Bronikowska & Rudziński (1991).

The equilibrium relationships at the gas-liquid interphase can be given by Equations 6.21 through 6.24.

$$C_{OH^-,interphase} = \frac{K_W}{C_{H^+,interphase}} \tag{6.21}$$

$$C_{CO_2,interphase} = H_{CO_2} \cdot CO_{2,bulkgas} \cdot R \cdot T \tag{6.22}$$

$$C_{HCO_3^-,interphase} = \frac{K_{CO_2} \cdot H_{CO_2} \cdot CO_{2,bulkgas} \cdot R \cdot T}{C_{H^+,interphase}} \tag{6.23}$$

$$C_{CO_3^{2-},interphase} = \frac{K_{HCO_3^-} \cdot K_{CO_2} \cdot H_{CO_2} \cdot CO_{2,bulkgas} \cdot R \cdot T}{(C_{H^+,interphase})^2} \tag{6.24}$$

The equilibrium relationships in bulk slurry can be given by Equations 6.25 through 6.28.

$$C_{OH^-,slurry} = \frac{K_W}{C_{H^+,slurry}} \tag{6.25}$$

$$C_{CO_2,slurry} = \frac{C_{total} \cdot C^2_{H^+,slurry}}{C^2_{H^+,slurry} + K_{CO_2} \cdot C_{H^+,slurry} + K_{CO_2} \cdot K_{HCO_3^-}} \tag{6.26}$$

$$C_{HCO_3^-,slurry} = \frac{C_{total} \cdot K_{CO_2} \cdot C_{H^+,slurry}}{C^2_{H^+,slurry} + K_{CO_2} \cdot C_{H^+,slurry} + K_{CO_2} \cdot K_{HCO_3^-}} \tag{6.27}$$

$$C_{CO_3^{2-},slurry} = \frac{C_{total} \cdot K_{CO_2} \cdot K_{HCO_3^-}}{C^2_{H^+,slurry} + K_{CO_2} \cdot C_{H^+,slurry} + K_{CO_2} \cdot K_{HCO_3^-}} \tag{6.28}$$

The equilibrium constants for chemical reactions R6.8 and R6.7, K_{CO_2} and $K_{HCO_3^-}$, respectively, are taken from literature (Brewer 1982).

6.3.5 Sub-model IV: calcium sulphite crystallization

Tseng & Rochelle (1986*a*) and Tseng & Rochelle (1986*b*) reported that the crystallization rate of seed crystal agglomeration was second order relative to the supersaturation of calcium sulphite and inversely proportional to gypsum saturation. The crystallization rate is normalized by the BET surface area of solids, and is given Equation 6.29 (Kallinikos et al. 2010, Olausson et al. 1993)

$$R_{CaSO_3} = 0.162 \cdot e^{\frac{-5153}{T}} \cdot (RS_{CaSO_3} - 1)^n \cdot \frac{BET_{CaSO_3}}{RS_{CaSO_3}} \tag{6.29}$$

where

$$RS_{CaSO_3} = \frac{c_{Ca^{2+}} \cdot c_{SO_3^{2-}}}{K_{sp,CaSO_3}} \tag{6.30}$$

The same authors considered the BET_{CaSO_3} surface area of slurry to be 10 $m^2 g^{-1}$ and the gypsum saturation was taken to be 0.025 when no sulphate was added to the reactor.

6.3.6 Mass Balance

The reactor used in this study is a well-mixed reactor. It consisted of two compartments, namely, the overhead compartment and the bulk slurry compartment. The general transient mass balance equations (Equations 6.31 through 6.37) were developed based on chemical reactions R5.1 through R5.14 and sub-models (SO_2 absorption, limestone dissolution, CO_2 desorption and $CaSO_3 0.5H_2O$ crystallization)

SO_2 in gas phase:

$$\frac{dC_{SO_2}}{dt} = \frac{1}{V_{Headspace}} \cdot (F \cdot C_{SO_2,inlet} - F \cdot C_{SO_2,bulkgas}) - \frac{V_{bulkslurry}}{V_{Headspace}} \cdot N_{SO_2} \tag{6.31}$$

CO_2 in gas phase:

$$\frac{dC_{CO_2}}{dt} = \frac{1}{V_{Headspace}} \cdot (F \cdot C_{CO_2,inlet} - F \cdot C_{CO_2,bulkgas}) - \frac{V_{bulkslurry}}{V_{Headspace}} \cdot N_{CO_2} \tag{6.32}$$

Total sulphur balance:

$$\frac{dC_{S_{total}}}{dt} = N_{SO_2} - R_{CaSO_3} \tag{6.33}$$

Total carbon balance:

$$\frac{dC_{C_{total}}}{dt} = R_{CaCO_3} - N_{CO_2} \tag{6.34}$$

Total calcium balance:

$$\frac{dC_{Ca^{2+}_{total}}}{dt} = R_{CaCO_3} - R_{CaSO_3} \tag{6.35}$$

Limestone dissolution:

$$\frac{dC_{CaCO_3}}{dt} = R_{CaCO_3} \tag{6.36}$$

Product crystallization:

$$\frac{dC_{CaSO_3 \cdot 0.5H_2O}}{dt} = R_{CaSO_3 \cdot 0.5H_2O} \tag{6.37}$$

Some of the physical and chemical constants used in this study were measured in the laboratory and some were taken from various literature sources. The

mass transfer coefficients (gas-side, liquid and limestone dissolution mass transfer) were measured in the laboratory, details are presented in Chapters 4 and 5. Liquid-phase diffusion coefficient were estimated according to correlations given in Boudreau (1997). The gas phase diffusion coefficients were evaluated from Reid et al. (1987). Henry's constant for SO_2 was evaluated according to the correlation given in Pasiuk-Bronikowska & Rudziński (1991) and the one for CO_2 was taken from Wilhelm et al. (1977). The solubility of limestone and calcium sulphite were taken from Kiil (1998).

6.3.7 DAEs Numerical Methods

An analytical solution to a system of ODEs (derived from a mass action law of the rate limiting steps of SO_2 absorption process) that are coupled with algebraic equations (derived from the electroneutrality state assumption) prove to be difficult to obtain. On those basis, numerical solution emerged to be an attractive alternative, necessitating the use of a MATLAB software package (MATLAB 2018).

The nature of the equations being solved, the range of parameters and variables involved, led to stiffness (i.e dynamic step size adjustment of the explicit Runge-Kutta solver, ODE45, are made unnecessarily small to achieve stability) of the solution. This necessitated the use of stiff solvers based on Rosenbrock methods or backward or forward differentiation formulae e.g ODE15s, ODE15i, Euler etc. In this study, Euler methods were used. A sample matlab code can be seen in Appendix C, Section C1.

6.4 Results and Discussion: Experimental Results

6.4.1 Absorption, reaction, dissolution and precipitation in limestone slurries

The effluent SO_2 concentration for the absorption of 0.3 and 0.2 % in volume are presented in Figure 6.1. The absorption of 0.3 % in volume of SO_2 takes place at a faster rate and saturation is reached over a shorter period.

It has been reported in literature that when SO_2 in flue gas is less than 2000 ppm, gas-side mass transfer resistance dominates. Corollarily, when SO_2 in the flue gas is greater than 2000 ppm, liquid-side mass transfer resistance becomes epochal (Bravo et al. 2002, Pasiuk-Bronikowska & Rudziński 1991). In this study, SO_2 concentrations of 2000 and 3000 ppm were used, insinuating that both $k_g a$ and $k_L a$ are epochal.

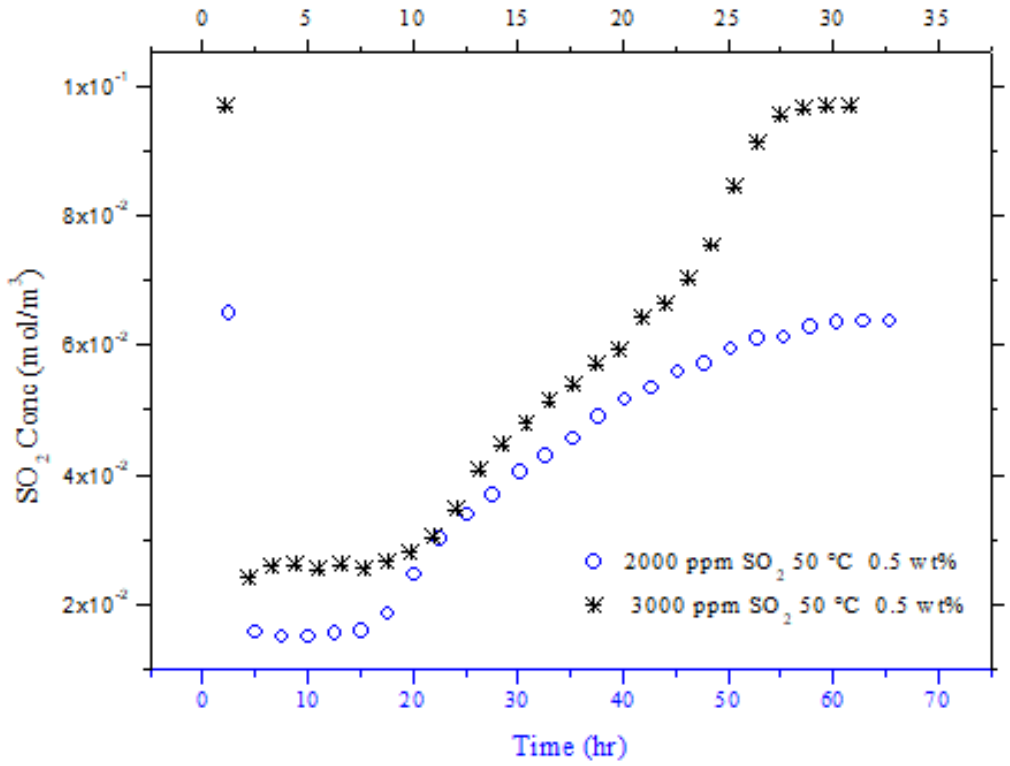

Figure 6.1: Concentration of effluent SO_2: Effect of inlet SO_2 concentration.

The results of effluent SO_2 concentration, when the limestone loading is varied, are given in Figure 6.2. The absorption rate of SO_2 had been observed to be directly proportional to the loading of limestone. This indicates that dissolution rate of $CaCO_3$ plays a prodigious role in the overall kinetics. Similar observations were reported by Bravo et al. (2002) and Uchida et al. (1978).

Shown in Figure 6.3 are the experimental results of limestone dissolution, calcium hemihydrate crystallization and pH. Consistent with the discussion in Chapter 4, as the pH decreases, the dissolution of limestone and the crystallization of calcium sulphite hemihydrate were observed to increase.

The pH was also reported to drop with the accruing concentration of total sulphite by Gleason & Rochelle (1987). The same authors reported that limestone dissolution was favoured at low pH.

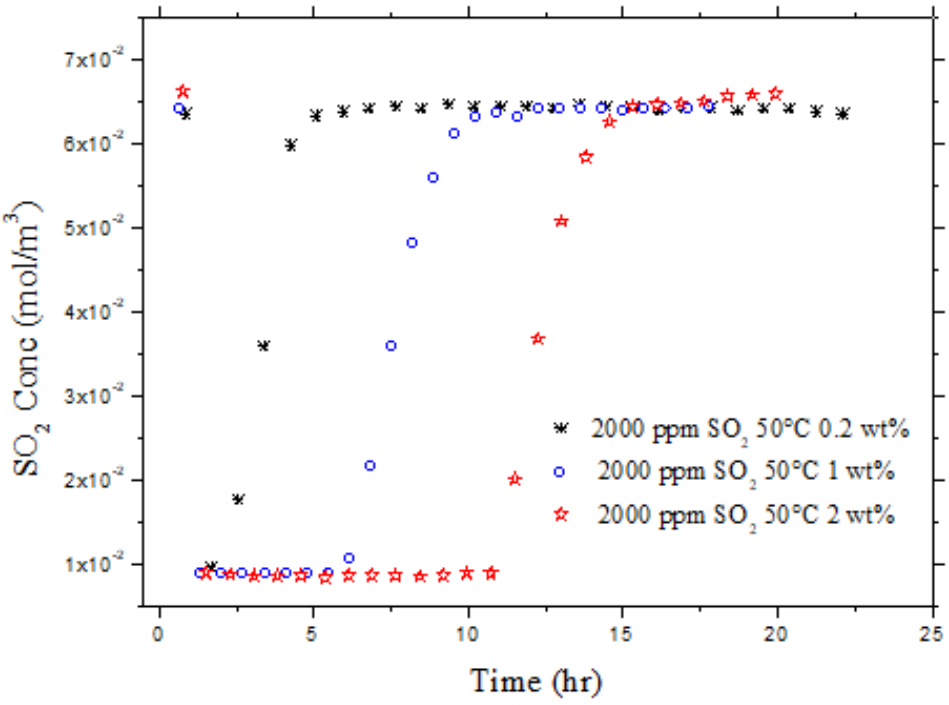

Figure 6.2: Concentration of effluent SO_2: Effect of limestone loading.

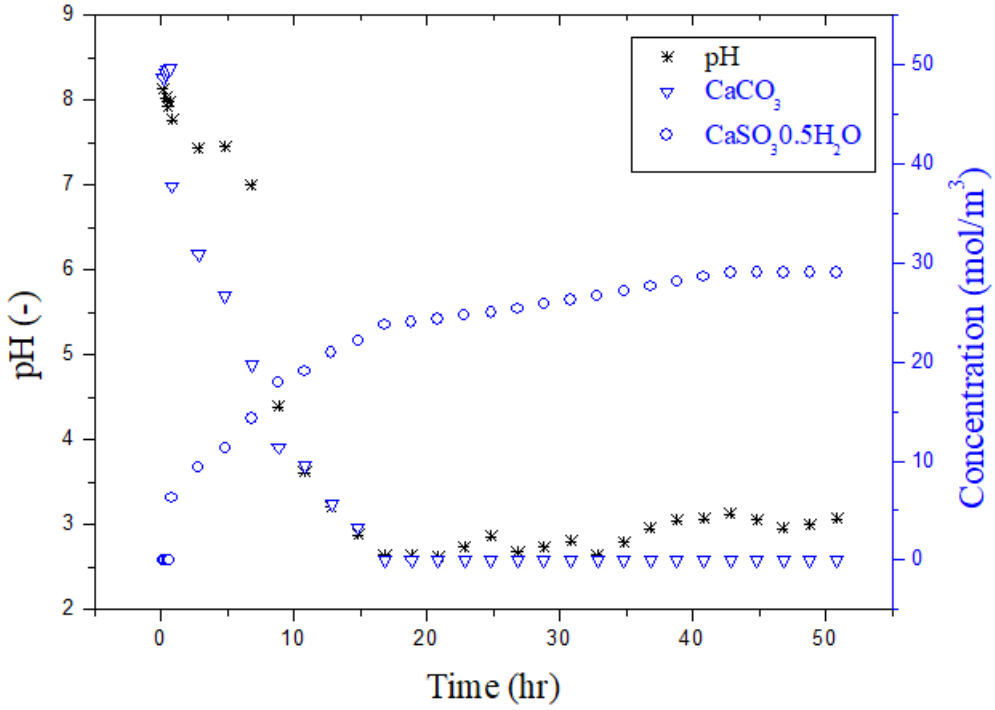

Figure 6.3: Effect of pH on dissolution and crystallization.

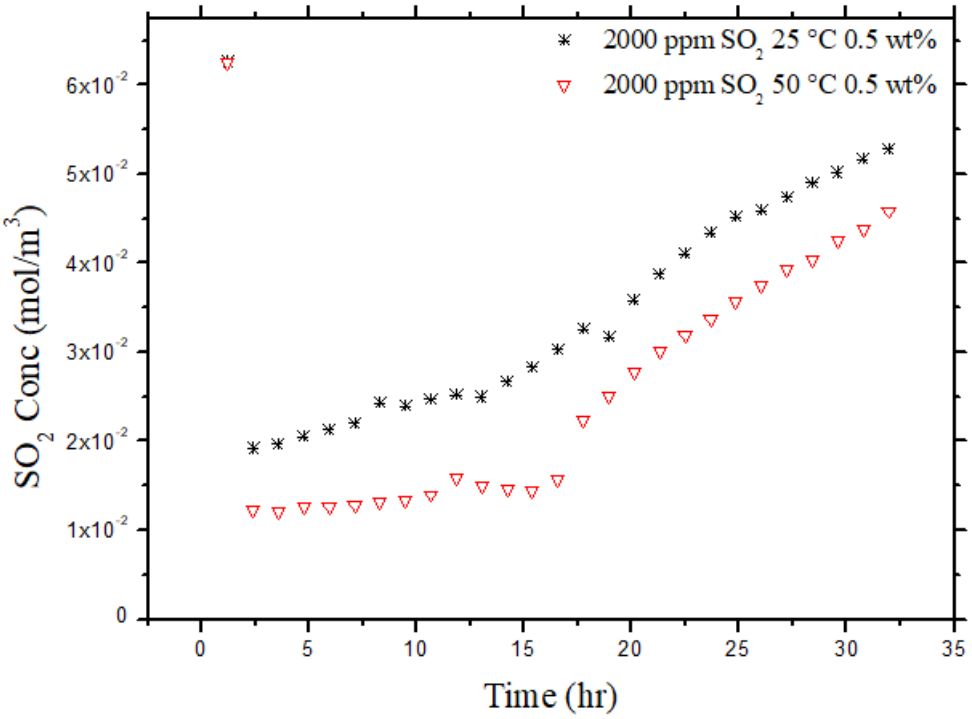

Figure 6.4: Concentration of effluent SO_2: Effect of temperature.

A comparison of effluent SO_2 concentration for experiments conducted at 25 °C and 50 °C is given in Figure 6.4. The SO_2 absorption rate had been observed to increase with the increasing temperature. In this study, as has been mentioned, the overall process is considered to be influenced by SO_2 absorption, limestone dissolution, CO_2 desorption and calcium sulphite hemihydrate crystallization. If any of the sub-processes are sensitive to temperature, the change in temperature will influence the overall process according to the proportional contribution of the respective sub-processes.

6.5 Results and Discussion: Modelling and comparison with experimental results

6.5.1 Absorption and reaction in aqueous solutions

The model, based on two film theory, developed to describe the absorption of SO_2 into aqueous solutions and presented in Section 6.3 had been used to generate the model results used in this section. Most of the parameters used were taken from literature, however some were experimentally determined. The details of the parameters can be seen in Appendix C, Section C6. The experimental results were generated as per method presented in Section 6.2.

The comparison of experimentally determined effluent SO_2 concentrations and those calculated by the model are shown Figures 6.5 and 6.6, and was satisfactory.To commensurate experimental and theoretical model results, the cognition of experimental set-up and conditions as well as model input parameters is epochal.

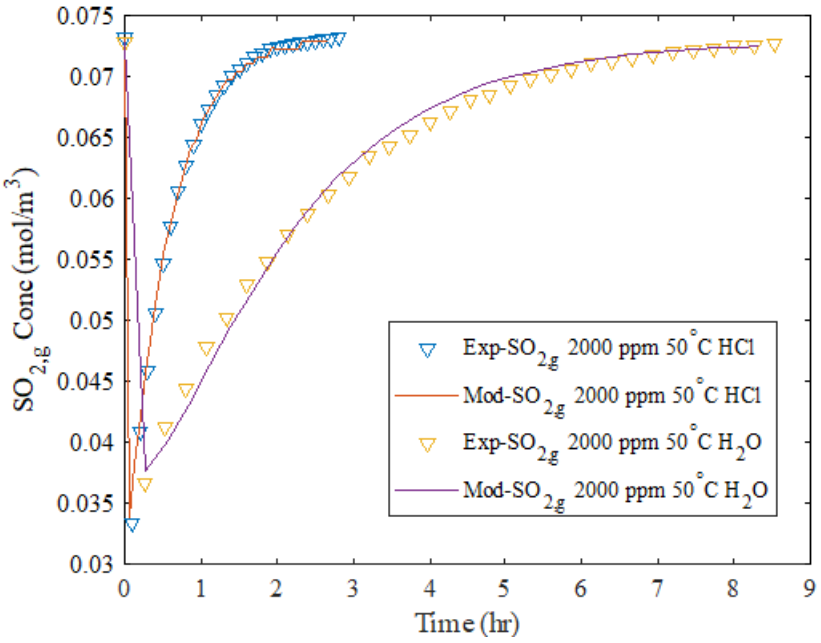

Figure 6.5: Comparison of model and experimental effluent SO_2 concentration results : SO_2 absorption into in aqueous solutions.

SO_2 absorption is dependent on mass transfer, k_g and k_L^o, the concentration of SO_2 in the gas and the chemical composition of the slurry. Based on arguments presented earlier in Section 5.4.1 above, the absorption into HCl solution controlled by liquid-side mas transfer resistance, the absorption into NaOH solution is controlled by gas-side mass transfer resistance and both resistances are imported for the absorption into water, with the dominance dependent on the pH.

For SO_2 absorption into aqueous solution, the transient variation of significant variables, determined according to procedure given in Section 6.6, are presented in Figures 6.7 through 6.9, such parameters are enhancement factor, SO_2 absorption rate and percentage SO_2 absorption, respectively.

The theory behind the enhancement factor for absorption of SO_2 into NaOH solution and water is given in Chapter 5, Sub-section 5.3.2. Equation 5.17 was employed to evaluate enhancement of SO_2 absorption into NaOH solution, and Equation 5.40, the respective results can be seen in Figure 6.7. The durable high enhancement factor for SO_2 absorption into NaOH solution can be attributed to instantaneous depletion of SO_2 in high pH NaOH solution.

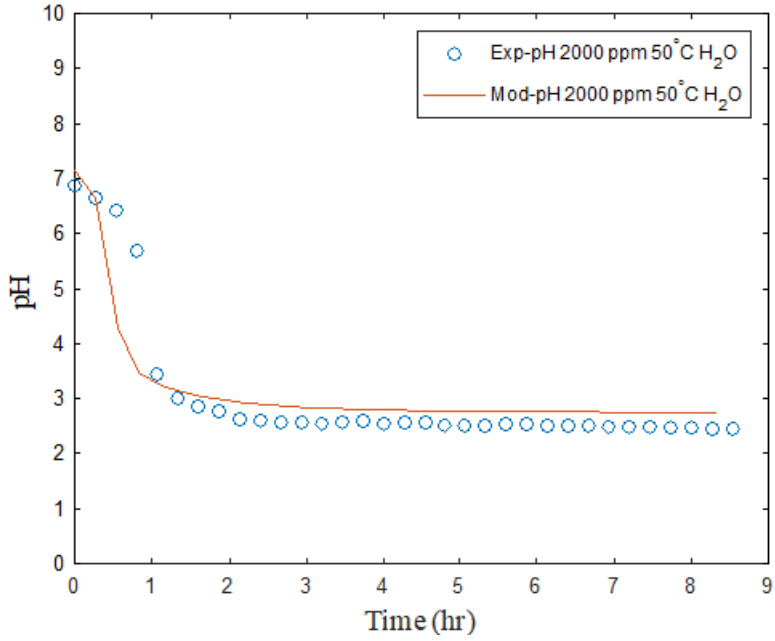

Figure 6.6: Comparison of model and experimental pH results : pH during SO_2 absorption into water.

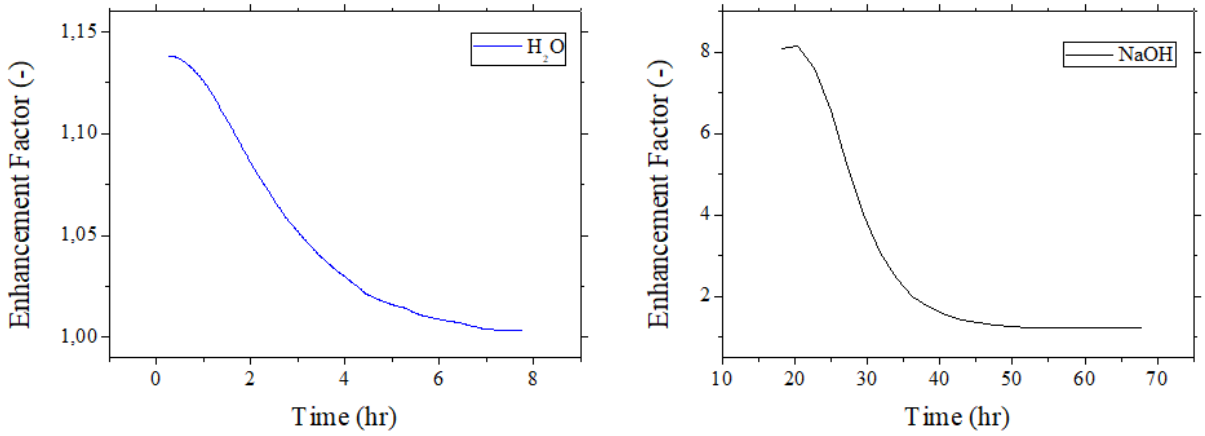

(a) Water (b) NaOH Solution

Figure 6.7: Enhancement factor for SO_2 absorption into aqueous solutions.

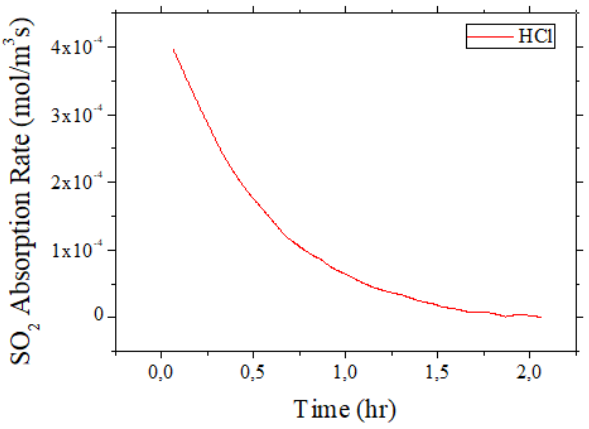

(a) HCl Solution

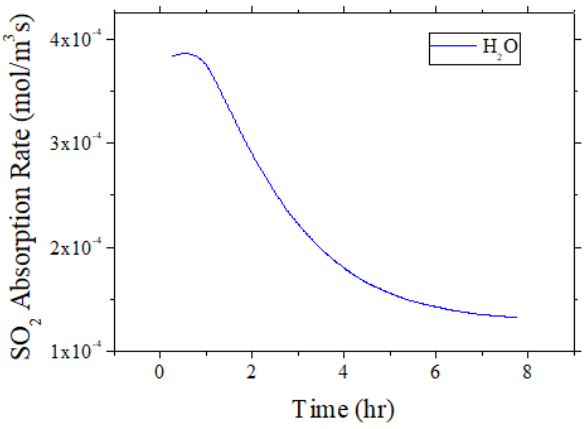

(b) Water

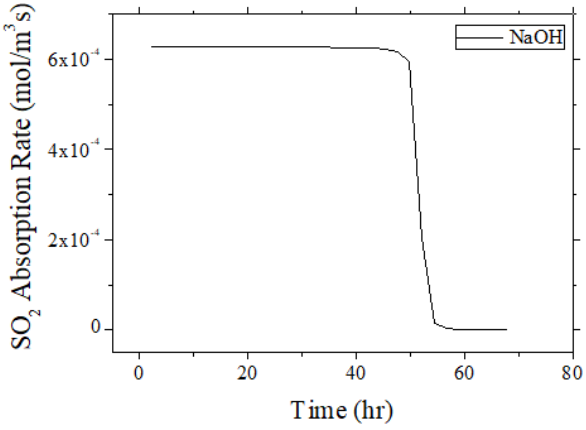

(c) NaOH Solution

Figure 6.8: SO_2 absorption rate into aqueous solutions.

Results recorded for the SO_2 absorption rate into aqueous solutions are given in Figure 6.8. The rates were observed to decrease steadily in the cases of HCl solution and deionized water. The rate of SO_2 absorption into NaOH solution was been observed to remain high (6.2 x 10^{-4} mol/m^3s) over a period of 49.9 hr. The arguments presented in Section 5.4.1, regarding the role of dissociation of SO_2 in solutions of varied initial pHs, are also applicable here (in this section). The absorption of SO_2 is considered to be gas-film controlled over an extended period ($\approx$ 49 hours). This is attributed to the instantaneous depletion of SO_2 in high pH NaOH solution (Deshwal & Hyung Keun 2009, Lancia et al. 1997, Uchida et al. 1978).

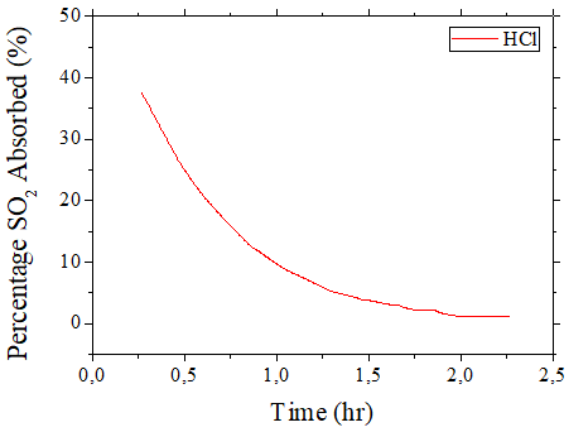

(a) HCl Solution

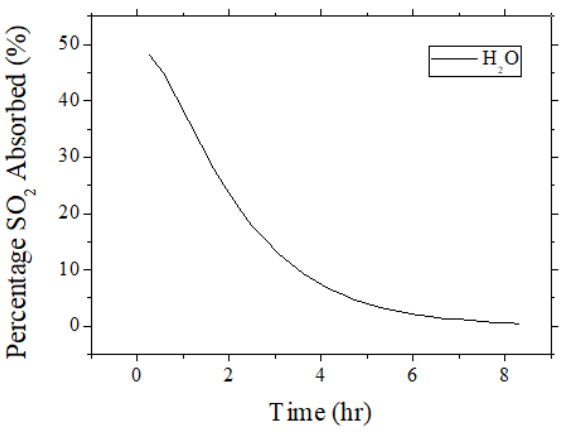

(b) Water

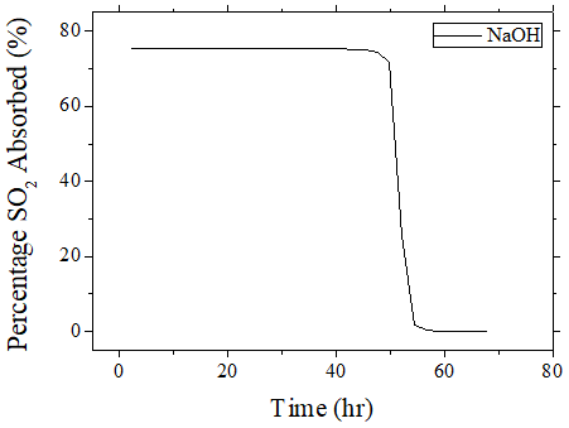

(c) NaOH Solution

Figure 6.9: Percentage SO_2 absorbed into aqueous solutions.

The low absorption rate of SO_2 into HCl is attributed to activity coefficients (physisorption) and possible formation of complex, SO_2Cl- (by chemisorption) on higher molarity solutions (3 and 5 M HCl) (Zimmermann et al. 2009). The same authors reported that the superposed chemical effects (controlled by low pH), were less apparent than the physical effects of increasing halides and proton concentrations.

Krissmann and co-workers (1997, 1999, 2000) measured and modelled the ternary system $HCl/SO_2/H_2O$ at 25 °C up to a HCl concentration of 1 mol/kg and a SO_2 partial pressure of 0.73 kPa using Pitzer's activity coefficient model. The measurement data indicate that at given SO_2 partial pressure the solubility of SO_2 decreases up to an HCl molality of about 0.5 mol/kg, and then moderately increases between 0.5 and 1.0 mol/kg solution. Explanation of the low absorption capacity (over time) of SO_2 into HCl solution was given in Section 5.4.1.

6.5.2 Absorption and reaction in limestone slurry

The model, based on two film theory, developed to describe the absorption of SO_2 into limestone slurry, dissolution of limestone, desorption of CO_2 and crystallization of calcium sulphite hemihydrate, and presented in Section 6.3, had been used to generate the model results used in this section. Most of the parameters used were taken from literature, however some were experimentally determined. The details of the parameters can be seen in Appendix C, Section C6. The experimental results were generated as per method presented in Section 6.2.

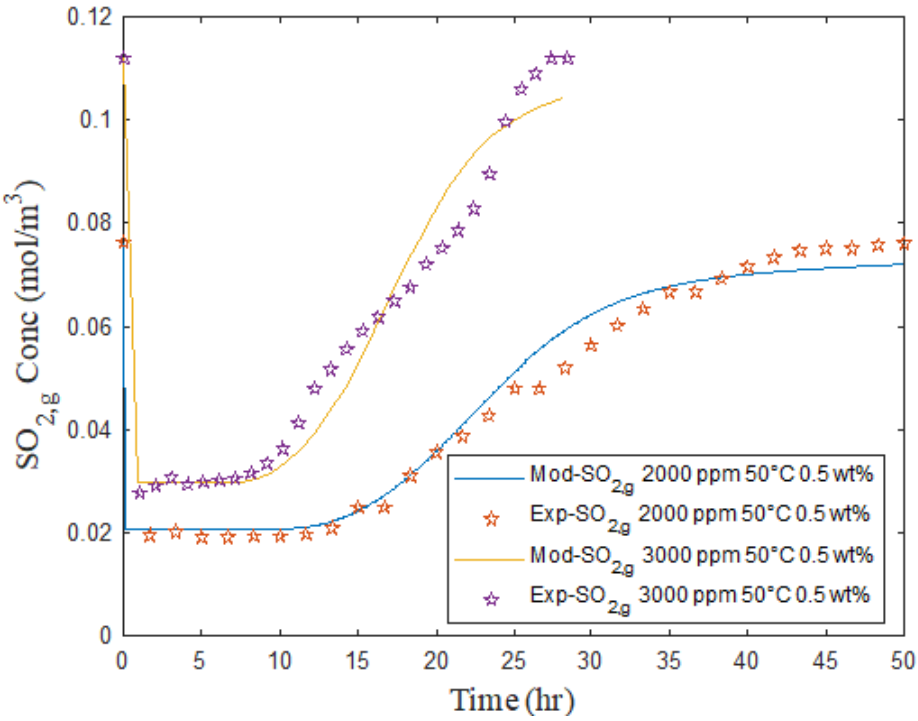

Figure 6.10: Comparison of model and experimental effluent SO_2 concentration results for SO_2 absorption into slurry: Effect of SO_2 concentration.

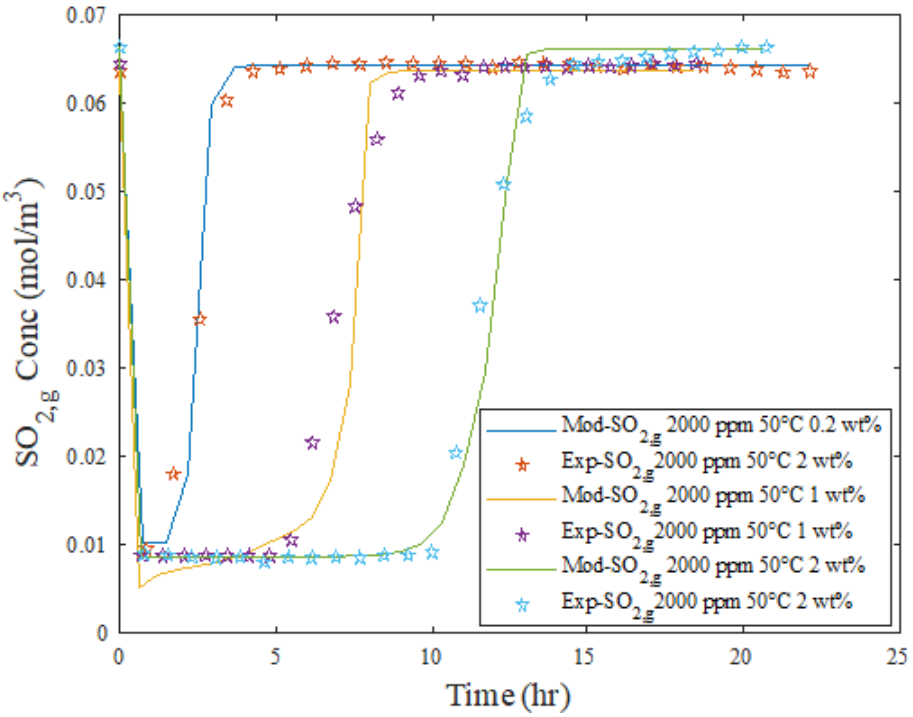

Figure 6.11: Comparison of model and experimental effluent SO_2 concentration results for SO_2 absorption into slurry: Effect of limestone loading.

Experimental and model effluent SO_2 concentration results for SO_2 absorption for varied inlet SO_2 concentration are given in Figure 6.10. As discussed in Subsection 6.4.1 , both $k_g a$ and $k_L a$ are significance, since the simulated flue gases used in this study comprises of 2000 and 3000 ppm. Nannen et al. (1974) reported that for low concentrations of SO_2 in power plant flue gas (less than 1000 ppm), the SO_2 absorption process approaches gas phase control.

The comparison between the experimental and model effluent SO_2 concentration results for varied limestone loading, are given in Figure 6.11. The discussion given in Section 6.4.1 are also applicable in this section, i.e. although the overall process is considered to be influenced by SO_2 absorption, limestone dissolution, CO_2 desorption and calcium sulphite hemihydrate crystallization, the sub-processes that are sensitive to temperature dominated the overall process.

Figures 6.12 compares the experimental and model effluent SO_2 concentration results for SO_2 absorption at 25 and 50 °C. The discussion presented in Section 6.4.1 is also valid in this section.

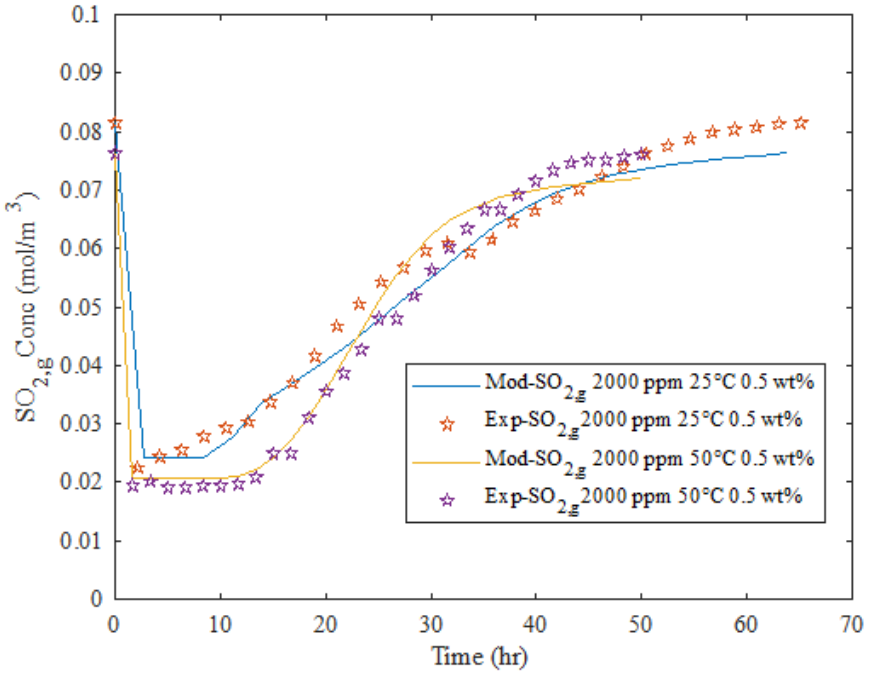

Figure 6.12: Comparison of model and experimental effluent SO_2 concentration results for SO_2 absorption into slurry: Effect of temperature.

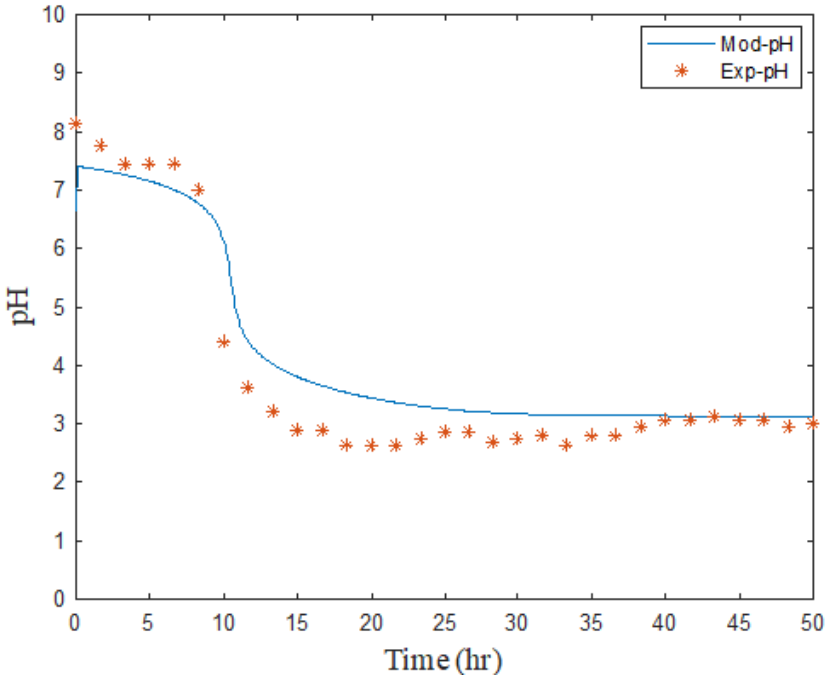

Figure 6.13: Comparison of model and experimental pH results for SO_2 absorption into a slurry.

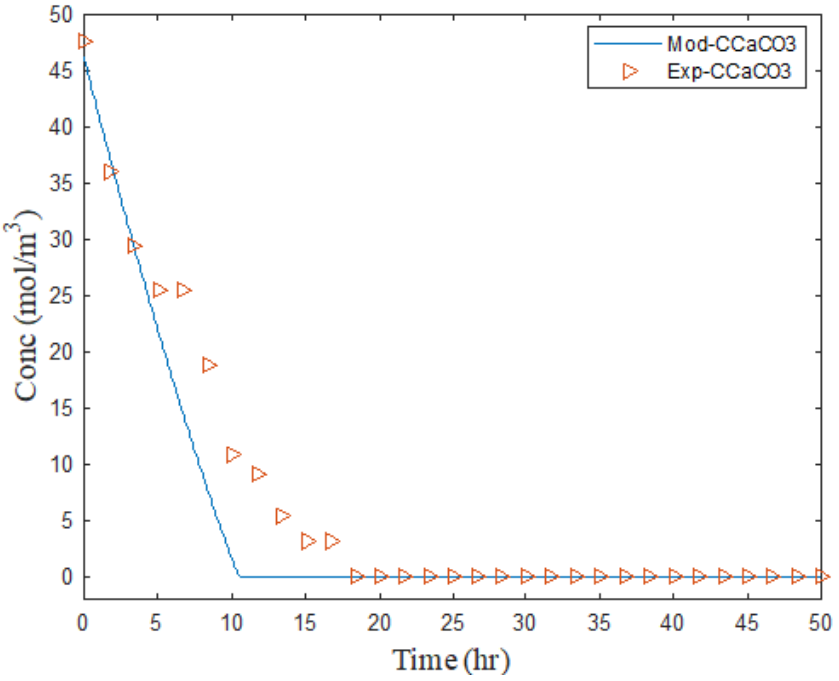

Figure 6.14: Comparison of model and experimental limestone dissolution results during SO_2 absorption into a slurry.

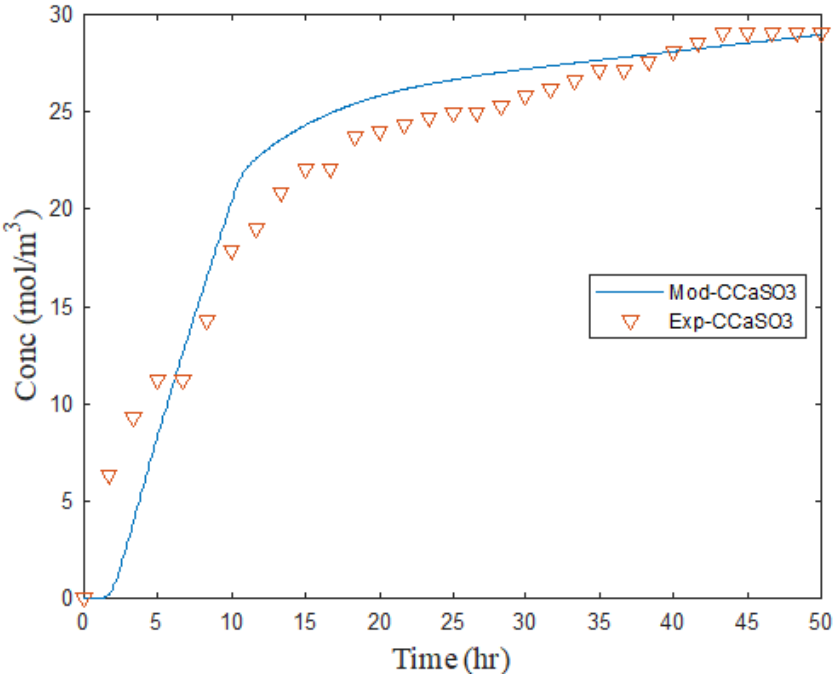

Figure 6.15: Comparison of model and experimental calcium sulphite hemihydrate crystallization results during SO_2 absorption into slurry.

Integrated model and experimental results

Figure 6.16 compares the integrated model and experimental results of SO_2 absorption, limestone dissolution, calcium sulphite hemihydrate and pH. Over the first 8.8 hours, high $CaCO_3$ (48.62 to 19.77 mol/m^3) concentration was observed to give high pH slurry, leading to high SO_2 absorption and low $CaSO_3 0.5H_2O$ crystallization.

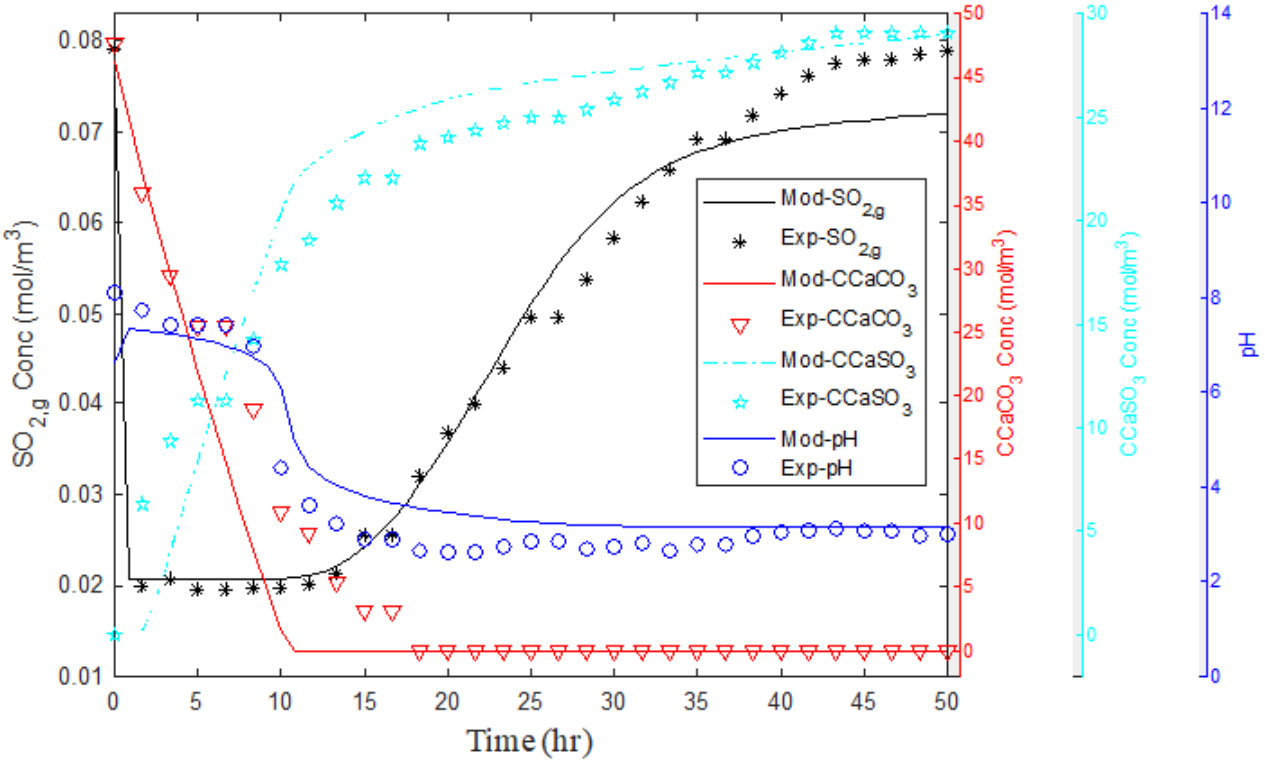

Figure 6.16: Integrated model and experimental results.

During this period, the rate of SO_2 absorption is considered to be influenced by SO_2 diffusion and dissociation, as well as other chemical reactions. Beyond this period, the concentration of $CaCO_3$ is less than 10 mol/m^3, and the SO_2 absorption is steadily slowing down, and the crystallization of $CaSO_3 0.5H_2O$ increases. These patterns concurs with the work reported by Kikkawa et al. (2002).

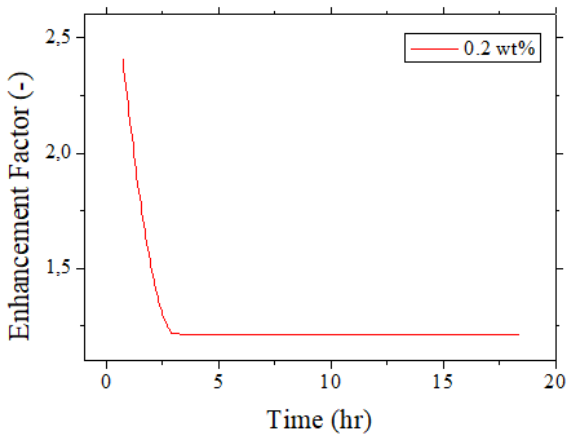

(a) 0.2 wt%

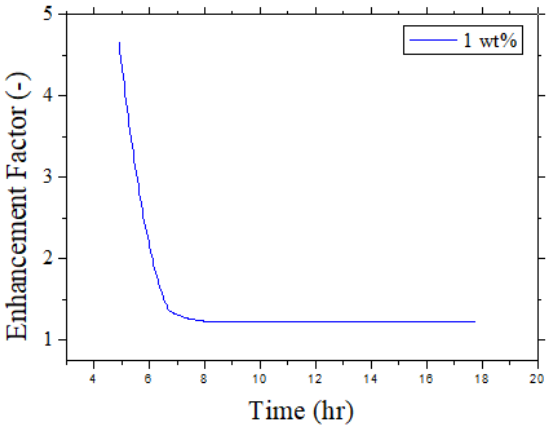

(b) 1 wt%

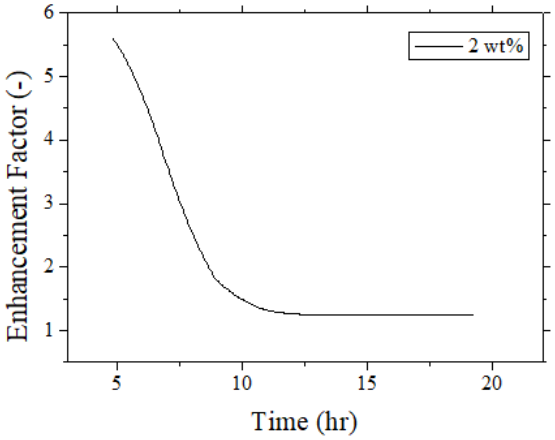

(c) 2 wt%

Figure 6.17: Enhancement factor for SO_2 absorption into limestone slurry.

For SO_2 absorption into slurries, the transient variation of significant variables, determined according to procedure given in Section 6.3, are presented in Figures 6.17 through 6.19, such parameters are enhancement factor, SO_2 absorption rate and percentage SO_2 absorption, respectively.

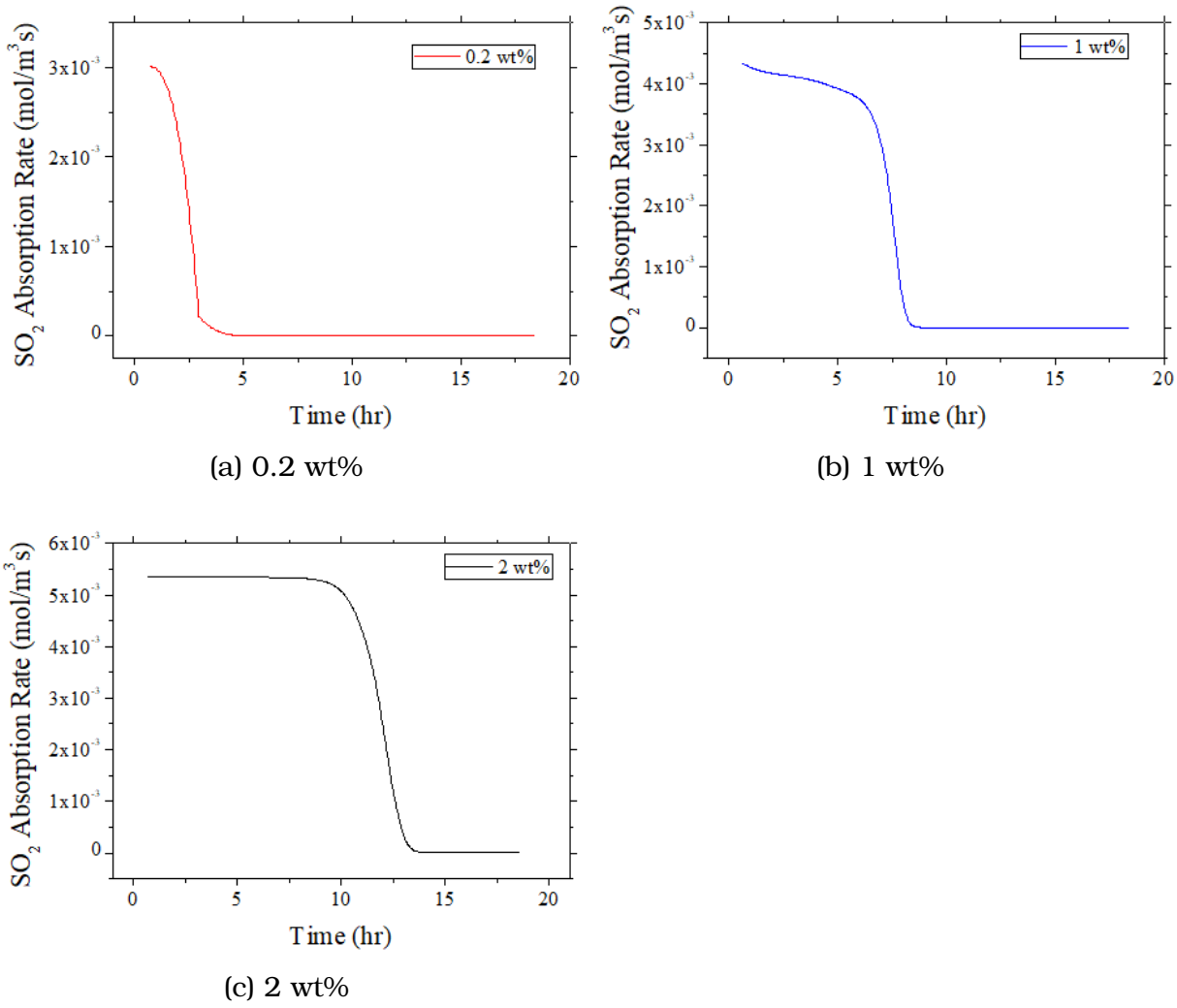

(a) 0.2 wt%

(b) 1 wt%

(c) 2 wt%

Figure 6.18: SO_2 absorption rate into limestone slurry.

The enhancement factors of SO_2 absorption into the different limestone-loading slurries are given in Figure 6.17, and increased with the loading. This results concurs with the observation reported by Uchida & Ariga (1985).

The enhancement factor is reliant on bulk slurry alkalinity , SO_2 concentration (in the bulk gas and bulk slurry) and the ratio between k_L and k_g. The enhancement factor has a high value when the alkalinity is high and the SO_2 concentration is low.

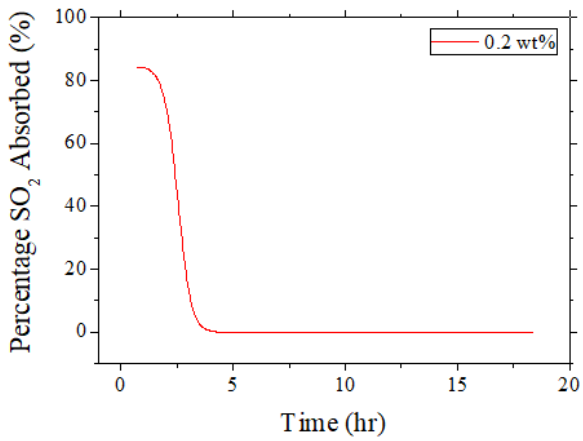

(a) 0.2 wt%

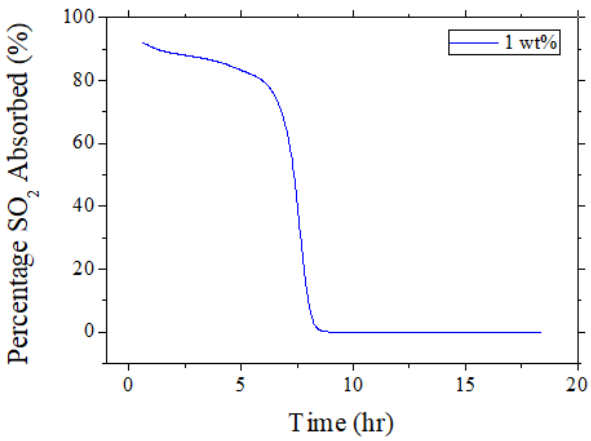

(b) 1 wt%

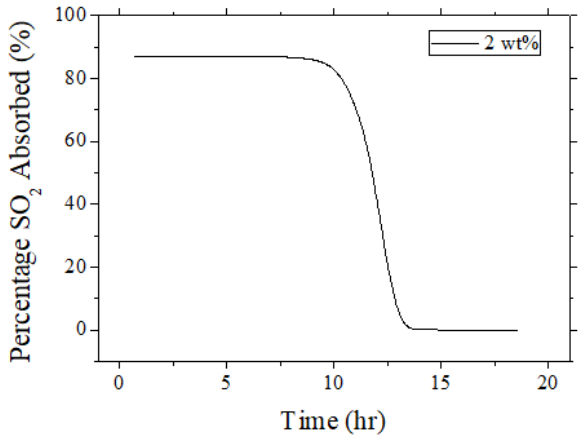

(c) 2 wt%

Figure 6.19: Percentage SO_2 absorbed into limestone slurry.

Figure 6.18 presents the rate SO_2 absorption into limestone slurries of varied loading, viz: 0.2, 1 and 2 wt%. The rates were observed to increase with $CaCO_3$ concentration. The discussion given in Section 6.4.1 are applicable in this section. The observation is in agreement with the work of Liu & Xiao (2006), who reported that SO_2 absorption rate is enhanced by the increase in $CaCO_3$ concentration.

6.6 Results and Discussion: Chemical Absorption Regimes

The coupling between SO_2 diffusing and its sub-sequent chemical reactions is generally termed chemical absorption. In this study, the regime in which in which SO_2 reacts instantaneously, and is depleted, is referred to as Regime I. However, in the

regime in which SO_2 reacts instantaneously, it can still accumulates in the liquid,this is referred to as Regime II. The remainder, which is the regime in which the accumulation of SO_2 is significant and increasing, is referred to as Regime III.

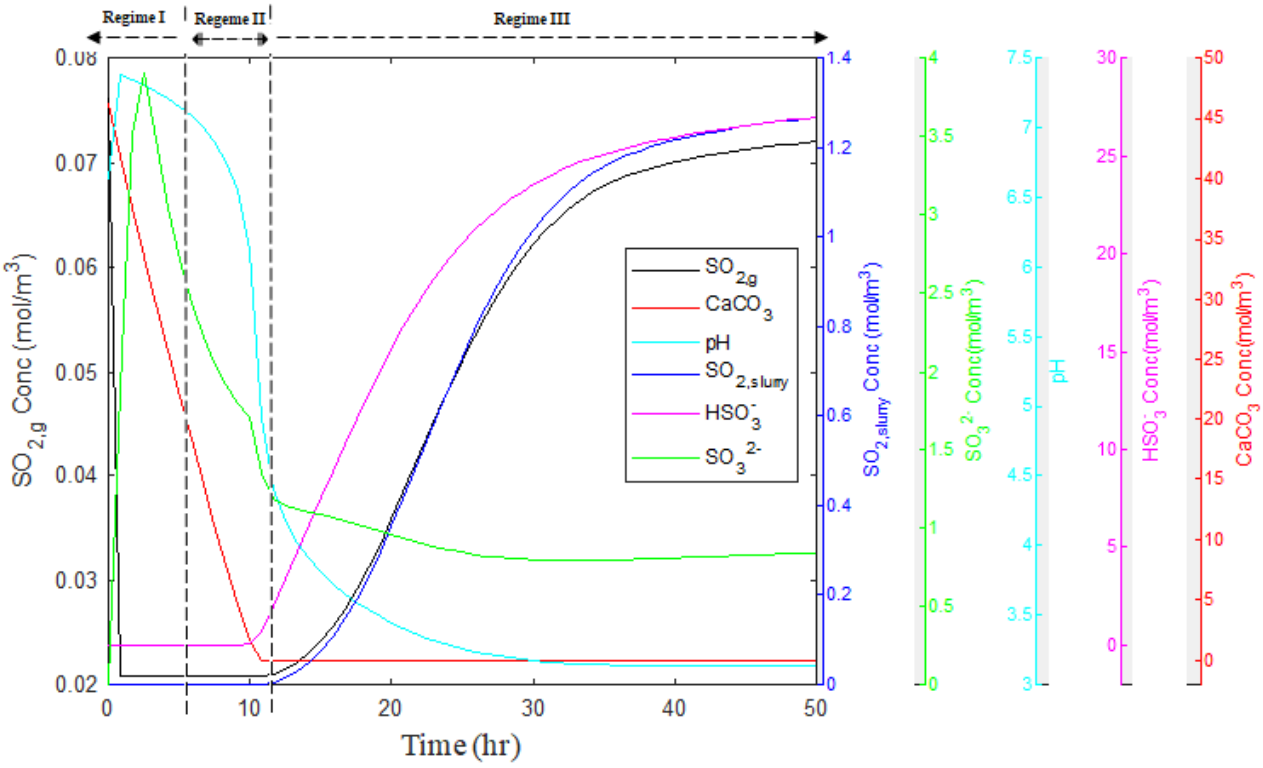

Figure 6.20: Identification of regimes.

Detailed regimes characteristics are given in Table 6.1 and discussed below. Figure 6.20 shows the demarcations of the regimes . The definitions of regimes given in literature are applicable to the allocation of the regime names assigned in this study, e.g. Regimes I & II in this study had been (combined) referred to as $'instataneousreactionregime'$ in the work of Lancia et al. (1994*b*) and Astarita et al. (1983).

As SO_2 is absorbed into limestone slurry over a long period ($\pm$ 50 hours),process is considered to move from Regime I, through Regime II, to Regime III. The objective of the work described in this section was to expand on part of the work done by Lancia et al. (1994*b*) and Astarita et al. (1983), with regard to the chemical absorption regimes when SO_2 is absorbed into limestone slurry.

The chemical reactions taking place during SO_2 absorption into limestone slurry (R6.1 to R6.14), and consequently the species present, are by and large considered to be dependent on the concentrations of H^+, SO_2 and $CaCO_3$ in the slurry,which

Table 6.1: Characteristics of SO_2 absorption regimes.

Regime	I	II	III
pH	Basic (pH $\geq$ 6.83 at 50 °C)	Intermediate (6.63 > pH > 3 at 50 °C)	Acidic (pH $\leq$ 3 at 50 °C)
Gas-side (gas-liquid mass transfer) resistance	Highly significant	Significant	Insignificant
Liquid-side (gas-liquid mass transfer) resistance	Insignificant	Significant	Highly significant
Dissociation of aqueous SO_2	Highly favoured	Favoured	Not favoured
Dissolution of limestone	Not favoured	Favoured	Highly favoured
HSO_3^- concentration	Insignificant	Significant	Highly significant
SO_3^{2-} concentration	Highly significant	Significant	Insignificant
SO_2slurry concentration	Insignificant	Significant	Highly significant
$CaCO_3$ concentration	Highly significant	Significant	Insignificant/absent

in turn, are influenced the diffusion SO_2 gas. It can therefore be assumed that, the regimes of the processes can be defined in terms of pH and SO_2 in the slurry. However, for completeness the roles of mass transfer and dissociations of species are included in the characterization of the regimes given in Table 6.1.

Table 6.1 shows that Regime I is controlled by gas resistance. This is attributed to the instantaneous dissociation of SO_2 in this regime due to the high pH. The dissolution of limestone is not favoured in this regime, although there is high concentration of of SO_3^{2-}. This is due low concentrations of $H_3O^+$for chemical reaction R6.7; R6.4 is favoured. In Regime II, both gas-side and liquid-side regimes are considered important. The dissociation of SO_2 and dissolution of limestone are also considered to be important. Regime III is a regime in which $CaCO_3$ is depleted (Figure 6.20) and the pH of the slurry is less or equal to 3. The dissociation of aqueous SO_2 is not favoured in this regime, due to the high concentration of H^+. A wide range of pH values (from $\pm$3.1 to $\pm$ 6) and different controlling resistance (e.g gas or liquid controlled) have been reported for full-scale wet FGD plants (Brogren & Karlsson 1997*c*, Neveux & Le Moullec 2011) and others, depending on the zone in the spray tower, hence necessitating the need to understand these regimes in the respective zones.

The chemical reactions that takes place in the gas-liquid film have been reported to be instantaneous by various authors e.g. Bravo et al. (2002), Chang & Rochelle (1981, 1985), Uchida et al. (1978) and so forth. This implies that the dimensionless parameter that compares the rate of reaction in a liquid film to the rate of mass transfer through the film (the Hatta number, Ha), is much bigger than 1. The classification given by Levenspiel (1999) are such that, instantaneous reactions and fast reactions will have a Hatta number greater than 2. Chemical reactions with intermediate rates will give Hatta numbers between 0.02 and 2, whereas slow reactions will give Hatta numbers less than 0.02. Consequently, as the interaction between chemical reaction and absorption, in this study, is taken into account with an enhancement factor

for instantaneous rates (Equations 6.19, 5.40,6.2, 5.17 and 6.14) since the Hatta is considered to be much greater than 1. This implies that SO_2 absorption is limited by physical mass transfer.

6.7 Summary

- An integrated model for SO_2 absorption into limestone slurry consisting of four sub-models, namely, absorption of SO_2; desorption of CO_2; dissolution of limestone and crystallization of calcium sulphite hemihydrate was developed and validated in this study.
- Experiments for validating the model were conducted using a laboratory scale stirred tank reactor when absorbing SO_2 gas (2000 and 3000 ppm, balance N_2) into limestone slurries. The reactor was operated in a continuous gas flow mode and batch mode for a slurry. The model was observed to satisfactory describe the SO_2 absorption process.
- The validity of the model over varied operating conditions was tested experimentally. The conditions considered are temperature, SO_2 and limestone concentrations. The model was observed to be applicable.
- The regimes of SO_2 absorption into limestone slurries were defined and characterised in this chapter. The definition and characterisation were based on the chemical absorption resistances involved, dissociation of aqueous SO_2, dissolution of limestone, the pH, the concentrations and participation of the species present e.g. aqueous SO_2, HSO_3^-, SO_3^{2-} and $CaCO_3$. Different regimes were considered to be present at different zones in the full scale wet FGD plants.

Chapter 7 Conclusions and Recommendations

7.1 Conclusions

1. The limestone used in this study was characterized for its mineral analysis(by QEMSCAN), chemical analysis (XRF) and physical structural analysis (for SSA, pore size distribution, PSD and helium skeletal density). Results of QEMSCAN concentration of $CaCO_3$ was used in modelling limestone dissolution (Chapter 4). Concentration of both $CaCO_3$ and $CaSO_3 \cdot 2H_2O$ that were used to validate the limestone dissolution and hannebachite sub-models of the integrated model (Chapter 6) were determined using XRD. The XRF results confirmed the distributions. The BET_{CaCO_3} surface area and pore volume used for limestone dissolution (in Chapters 4 and 6) were determined using the results from the Micromeritic ASAP 2010 presented in 3.1.5. The limestone density used during the determination of limestone dissolution mass transfer coefficient (Chapter 4), was determined using the Quantachrome Helium Pycnometer. The limestone particle size used during the determination of the limestone dissolution mass transfer coefficient (Chapter 4) was measured using the Malvern Mastersizer 3000.

2. The overall limestone dissolution rate constant(k_{tot}) was determined by evaluating solid-liquid k_l and k_r. The solid-liquid mass transfer coefficient was evaluated using the Frössling-type correlation of the Sherwood number. It was found to be dependent on the experimental operating conditions (solution pH, temperature and agitation) whereas the chemical reaction constant (k_r) was estimated from the slope of the linear plot of $\ln C_{H^+}$ vs t on dissolution conducted at stirring rates greater than triple the critical impeller speed($N>3N_{js}$). The total dissolution constant (k_{tot}) was estimated by the reciprocal addition of $1/(k_l)$ and $1/(k_r)$.The obtained k_{tot} is comparable with the k_{tot} regressed from the model fit-

ting. Limestone dissolution Ea in the present investigation is comparable with values published in literature. The obtained k_{tot} was used in the integrated mode in Chapter 6.

3. The gas-liquid mass transfer coefficients (for both gas-side and liquid-side) for SO_2 absorption from simulated flue gas in a stirred tank reactor were determined whilst employing solutions of various pHs (Chapter 5). NaOH solution was used to evaluate the $k_g a$, whereas the HCl solution was used to evaluate $k_L a$. The absorption of SO_2 into water was observed to be enhanced by chemical reactions. A mass balance model based on Two-film theory was observed to describe the rate of SO_2 absorption satisfactorily. The obtained values of both $k_g a$ and $k_L a$ were used in the integrated model in Chapter 6.

4. An integrated model for SO_2 absorption into limestone slurry consisting of four sub-models, namely, absorption of SO_2; desorption of CO_2; dissolution of limestone and crystallization of calcium sulphite hemihydrate was developed and validated in this study.Experiments for validating the model were conducted using a laboratory scale stirred tank reactor when absorbing SO_2 gas (2000 and 3000 ppm, balance N_2) into limestone slurries. The reactor was operated in a continuous gas flow mode and batch mode for slurry. The model satisfactory described the SO_2 absorption process. The validity of the model over various operating conditions was tested experimentally. The conditions considered are temperature, SO_2 and limestone concentrations. The model was observed to be applicable.

   The regimes of SO_2 absorption into limestone slurries were defined and characterised in this chapter. The definition and characterisation were based on chemical absorption resistances involved, dissociation of aqueous SO_2, dissolution of limestone, the solution pH, the concentrations and participation of the species present e.g. aqueous SO_2, HSO_3^-, SO_3^{2-} and $CaCO_3$. different regimes were considered to be present in different zones in the full scale wet FGD plants.

   An integrated model was developed and tested. Here a step-wise procedure was employed and it involved the evaluation of relevant processes, namely, absorption of SO_2; desorption of CO_2; dissolution of limestone and crystallization of calcium sulphite hemihydrate . Good agreement was obtained between the experimental results and the model which indicates the consistency and reliability of the modelling of the sub processes considered and the integrated model.

7.2 Contribution to Science

1. Development of an integrated model for the absorption of sulphur dioxide from a dilute flue gas (2000 and 3000 ppm) in a limestone slurry, comprising of SO_2 absorption with chemical reactions, dissolution of limestone, liberation of CO_2 and crystallization of calcium sulphite.(This model was successfully validated against results obtained from an experimental programme consisting of the unsteady state absorption of SO_2 in a laboratory scale semi-batch process). The methodology and concepts could be useful, with adaption for the modelling of FDG processes such as the WFGD process incorporating complex chemistry in moving droplets (space variation).

2. The development of a successful numerical code for the solution of the model equations consisting time dependant non- linear differential equations and ordinary equation describing all the mechanisms involved, for successfully solving a complex integrated absorption process.

3. The successful use of an integrated model (including a slurry phase) and a conventional simplified model (gas phase, with gas/liquid interface), and the two-film theory for mass transfer model, to confirm the validity of a mass transfer model for the dissolution of limestone.

4. Demonstration of the interacting effect (competing opposite effects) of the absorption of sulphur dioxide , the dissolution of the limestone and the crystallization of the calcium sulphite on the hydrogen concentration (pH), and of the analysis of the different regimes.

7.3 Recommendations

On conclusion of this study, I recommend that the following points/issues be considered in future studies

1. The concept and quantification of the relative interactions between the mass transfer with chemical reactions of SO_2, dissolution kinetics of limestone and kinetics of crystallization of products should be expanded. This would involve examining the influence of the dissolution kinetics of different quality limestones and parameters affecting the mass transfer rates.

2. The current model should be expanded to include the following:

    - The effect of carbon dioxide introduced with the sulphur dioxide on the overall performance such as the dissolution of the limestone.

- The oxidation of sulphite ions formed from the sulphur dioxide and the subsequent crystallization rate of calcium sulphate instead of calcium sulphite that occurs in the absence of oxygen.

3. Comprehensive modelling of industrial scale WFDG processes should be undertaken, to incorporate the complex chemistry of SO_2 and CO_2 dissociation, and the presence and dissolution of limestone and crystallization of products. These processes could include the use of wet wall columns and spray columns (WFGD) with emphasizes on the determination of the importance of detailed chemical effects in the liquid phases relative to the hydrodynamic behaviour of the gas and liquid phases.

4. An investigation towards evaluating the role of hydrodynamics on the kinetics of limestone dissolution and calcium sulphite in the sprayer zone of a typical WFGD tower. The use of computational fluid dynamics is strongly recommended in this regard.

5. A study towards understanding and evaluating any oxidation of SO32- and calcium sulphite (regardless of the magnitude) of the recycled slurry droplets in the sprayer zone of a typical WFGD tower. The oxygen could be from the remainder oxygen inherited from the reaction tank before recycling and/or from the flue gas.

References

Abdulsattar, A. H., Sridhar, S. & Bromley, L. A. (1977), 'Thermodynamics of the sulfur dioxide-seawater system', *AIChE Journal* **23**(1), 62–68.

Agarwal, R. S. & Rochelle, G. T. (1993), Chemistry of limestone slurry scrubbing, *in* 'S02 Control Symposium'.

Agnello, V. N. (2005), 'Dolomites and limestones south africa: South africa', *REPORT R49/2005 , Department of minerals resources, South Africa* .

Ahlbeck, J., Engman, T., Felten, S. & Vihma, M. (1995), 'Measuring the reactivity of limestone for wet flue-gas desulfurization', *Chemical Engineering Science* **50**(7), 1081 – 1089.
URL: http://www.sciencedirect.com/science/article/pii/0009250994004827

Al-Enezi, G., Ettouney, El-Dessouky, H. & Fawzi, N. (2001), 'Solubility of sulfur dioxide in seawater', *Industrial & Engineering Chemistry Research* **40**(5), 1434–1441.

Alkattan, M., Oelkers, E. H., Dandurand, J.-L. & Schott, J. (1998), 'An experimental study of calcite and limestone dissolution rates as a function of pH from -1 to 3 and temperature from 25 to 80°c', *Chemical Geology* **151**(1-4), 199–214.

Amrhein, C., Jurinak, J. J. & Moore, W. M. (1985), 'Kinetics of calcite dissolution as affected by carbon dioxide partial pressure1', *Soil Science Society of America Journal* **49**(6), 1393.

Arif, A. (2016), The simulation of an industrial wet flue gas desulfurization absorber, Phdthesis, north west university, south africa.

Astarita, G., Bisio, A. & Savage, D. W. (1983), *Gas treating with chemical solvents*, New York : John Wiley. "A Wiley Interscience publication.".

Aunela-Tapola, L., Hatanpää, E., Hoffren, H., Laitinen, T., Larjava, K., Rasila, P. & Tolvanen, M. (1998), 'A study of trace element behaviour in two modern coal-fired power plants', *Fuel Processing Technology* **55**(1), 13–34.

Aydoğan, S., Erdemoğlu, M., Uçar, G. & Aras, A. (2007), 'Kinetics of galena dissolution in nitric acid solutions with hydrogen peroxide', *Hydrometallurgy* **88**(1-4), 52–57.

Baig, S. & Yousaf, M. (2017), 'Coal fired power plants: Emission problems and controlling techniques', *Journal of Earth Science & Climatic Change* **08**(07).

Barton, P. & Vatanatham, T. (1976), 'Kinetics of limestone neutralization of acid waters', *Environ. Sci. Technol.* **10**(3), 262–266.

Bäckström, H. L. J. (1927), 'THE CHAIN-REACTION THEORY OF NEGATIVE CATALYSIS1', *Journal of the American Chemical Society* **49**(6), 1460–1472.

Beilke, S. & Lamb, D. (1975), 'Remarks on the rate of formation of bisulfite ions in aqueous solution', *AIChE Journal* **21**(2), 402–404.

Berner, R. A. & Morse, J. W. (1974), 'Dissolution kinetics of calcium carbonate in sea water Iv , theory of calcite dissolution', *American Journal of Science* **274**(2), 108–134.

Bjerle, I. & Rochelle, G. T. (1984), 'Limestone dissolution from a plane surface', *Chem. Eng. Sci.* **39**(1), 183–185.

Blasio, C. D., Carletti, C., Salonen, J. & Björklund-Sänkiaho, M. (2018), 'Ultrasonic power to enhance limestone dissolution in the wet flue gas desulfurization process. modeling and results from stepwise titration experiments', *ChemEngineering* **2**(4), 53.

Boudreau, B. P. (1997), *Diagenetic modelsandtheir implementation. Modelling transportandreactions in aquatic sediments*, Vol. 171.

Brantley, S. L., Kubicki, J. D. & White, A. F., eds (2008), *Kinetics of Water-Rock Interaction*, Springer New York.

Bravo, R. V., Camacho, R. F., Moya, V. M. & Garcia, L. A. I. (2002), 'Desulphurization of SO 2 –n 2 mixtures by limestone slurries', *Chem. Eng. Sci.* **57**(11), 2047–2058.

Brewer, L. (1982), Thermodynamic values for desulfurization processes, *in* 'ACS Symposium Series', AMERICAN CHEMICAL SOCIETY, pp. 1–39.

Brogren, C. & Karlsson, H. T. (1997*a*), 'The impact of the electrical potential gradient on limestone dissolution under wet flue gas desulfurization conditions', *Chemical Engineering Science* **52**(18), 3101–3106.

Brogren, C. & Karlsson, H. T. (1997*b*), 'A model for prediction of limestone dissolution in wet flue gas desulfurization applications', *Industrial & Engineering Chemistry Research* **36**(9), 3889–3897.

Brogren, C. & Karlsson, H. T. (1997*c*), 'Modeling the absorption of SO2in a spray scrubber using the penetration theory', *Chemical Engineering Science* **52**(18), 3085–3099.

Brown, S. R., De Vault, R. F. & Williams, P. J. (2010), 'Determination of Wet FGD Limestone Reactivity', *Electric Power 2010* **2010**, BR–1835.
URL: https://www.scribd.com/document/138093764/FGD-system-by-Babcock

Buhmann, D. & Dreybrodt, W. (1985), 'The kinetics of calcite dissolution and precipitation in geologically relevant situations of karst areas', *Chemical Geology* **53**(1-2), 109–124.

Busenberg, E. & Plummer, L. N. (1986), A comparative study of the dissolution-andcrystal growth kinetics of calciteandaragonite, *in* 'Studies in Diagenesis, U.S. Geological Survey Bulletin 1578', Vol. 1578, US Geol.Surv. Bull, pp. 139–168.
URL: http://www.scirp.org/(S(351jmbntvnsjt1aadkposzje))/reference/ReferencesPapers.aspx?ReferenceID=907718

Carlett, C., De Blasio, C., Grenman, H. & Westerlund, T. (2015a), 'On modeling the roles played by diffusiveandconvective transport in limestone dissolution for wet flue gas desulfurization', *Chemical Engineering Transactions* **43**(l), 2131–2136.

Carletti, C., Bjondahl, F., Blasio, C. D., Ahlbeck, J., Järvinen, L. & Westerlund, T. (2012), 'Modeling limestone reactivity and sizing the dissolution tank in wet flue gas desulfurization scrubbers', *Environmental Progress & Sustainable Energy* **32**(3), 663–672.

Carletti, C., Blasio, C. D., Miceli, M., Pirone, R. & Westerlund, T. (2017), 'Ultrasonic enhanced limestone dissolution: Experimental and mathematical modeling', *Chemical Engineering and Processing: Process Intensification* **118**, 26–36.

Carletti, C., Grenman, H., De Blasio, C., Makila, E., Salonen, J., Murzin, D. Y., Salmi, T. & Westerlund, T. (2015b), 'Revisiting the dissolution kinetics of limestone - experimental analysis and modeling', *J. Chem. Technol. Biotechnol.* **91**(5), 1517–1531.

Carmichael, G. R. & Peters, L. K. (1979), 'Some aspects of SO2 absorption by water-generalized treatment', *Atmospheric Environment (1967)* **13**(11), 1505–1513.

Chan, Pui, K. & Rochelle, G. T. (1982), Limestone dissolution, *in* 'ACS Symposium Series', AMERICAN CHEMICAL SOCIETY, pp. 75–97.

Chang, C. S. & Rochelle, G. T. (1981), 'SO2 absorption into aqueous solutions', *AIChE Journal* **27**(2), 292–298.

Chang, C.-S. & Rochelle, G. T. (1982*a*), 'Effect of organic acid additives on SO2 absorption into CaO/CaCO3 slurries', *AIChE Journal* **28**(2), 261–266.

Chang, C. S. & Rochelle, G. T. (1982*b*), 'Mass transfer enhanced by equilibrium reactions', *Industrial & Engineering Chemistry Fundamentals* **21**(4), 379–385.

Chang, C. S. & Rochelle, G. T. (1985), 'Sulfur dioxide absorption into sodium hydroxide and sodium sulfite aqueous solutions', *Ind. Eng. Chem. Fundam.* **24**(1), 7–11.

Chen, W.-H., Chen, Y.-Y. & Hung, C.-I. (2011), 'A simplified model of predicting SO2 absorption by single atmospheric raindrops with chemical dissociation and internal circulation', *Aerosol and Air Quality Research* **11**(7), 860–872.

Chen, W.-H., Chiu, T.-W., Hung, C.-I. & Lin, M.-R. (2009), 'Hysteresis and reaction characterization of methane catalytic partial oxidation on rhodium catalyst', *Journal of Power Sources* **194**(1), 467–477.

Chu, H., Chien, T.-W. & Twu, B.-W. (2003), *Water, Air, and Soil Pollution* **143**(1/4), 337–350.

Clarke, L. B. (1993), 'The fate of trace elements during coal combustion and gasification: an overview', *Fuel* **72**(6), 731–736.

Clarke, L. & Sloss, L. (1992), 'Trace elements – emissions from coal combustion and gasification, ieacr/49'.

Córdoba, P. (2015), 'Status of Flue Gas Desulphurisation (FGD) systems from coal-fired power plants: Overview of the physic-chemical control processes of wet limestone FGDs', *Fuel* **144**, 274–286.

Coto, B., Martos, C., Peña, J., Rodríguez, R. & Pastor, G. (2012), 'Effects in the solubility of CaCO3: experimental studyandmodel description', *Fluid Phase Equilib.* **324**, 1–7.

Dagaonkar, M. V., Beenackers, A. A. & Pangarkar, V. G. (2001), 'Enhancement of gas–liquid mass transfer by small reactive particles at realistically high mass transfer coefficients: absorption of sulfur dioxide into aqueous slurries of ca(OH)2andmg(OH)2 particles', *Chemical Engineering Journal* **81**(1-3), 203–212.

Danckwerts, P. V. (1955), 'Gas absorption accompanied by chemical reaction', *AIChE Journal* **1**(4), 456–463.

DeBlasio, C., Makila, E. & Westerlund, T. (2012), 'Use of carbonate rocks for flue gas desulfurization: Reactive dissolution of limestone particles', *Applied Energy* **90**(1), 175–181.

Desch, W., Horn, K. & Propst, G. (2006), 'Computation of equilibria in models of flue gas washer plants', *Computers & Chemical Engineering* **30**(6-7), 1169–1177.

Deshwal, B. R. & Hyung Keun, L. (2009), 'Mass transfer in the absorption of SO2and NOxusing aqueous euchlorine scrubbing solution', *Journal of Environmental Sciences* **21**(2), 155–161.
URL: http://dx.doi.org/10.1016/S1001-0742(08)62244-5

Dou, B., Pan, W., Jin, Q., Wang, W. & Li, Y. (2009), 'Prediction of SO2 removal efficiency for wet flue gas desulfurization', *Energy Conversion and Management* **50**(10), 2547–2553.

Dragan, S. & Ozunu, A. (2012), 'Characterization of calcium carbonates used in wet flue gas desulphurization processes', *Open Chemistry* **10**(5).

Eden, B. D. & Luckas, M. (1998), 'A heatandmass transfer model for the simulation of flue gas treatment according to the wet limestone process', *FuelandEnergy Abstracts* **39**(5), 392.

EIA (2017), International energy outlook independent statics and analysis, techreport DOE/EIA-0484, US Energy Information.

Eriksen, T. E. (1969), 'Diffusion studies in aqueous solutions of sulfur dioxide', *Chemical Engineering Science* **24**(2), 273–278.

Falk, M. & Giguère, P. A. (1958), 'ON THE NATURE OF SULPHUROUS ACID', *Canadian Journal of Chemistry* **36**(7), 1121–1125.

Fellner, P. & Khandl, V. (1999), 'Characterization of limestone reactivity for absorption of s0 2 from fume gases', *Chem. Papers* **53**, 238 – 241.

Frandsen, J. B., Kiil, S. & Johnsson, J. E. (2001), 'Optimisation of a wet FGD pilot plant using fine limestoneandorganic acids', *Chem. Eng. Sci.* **56**(10), 3275–3287.

Fusi, L., Monti, A. & Primicerio, M. (2012), 'Determining calcium carbonate neutralization kinetics from experimental laboratory data', *J. Math. Chem.* **50**(9), 2492–2511.

Fusi, L., Primicerio, M. & Monti, A. (2015), 'A model for calcium carbonate neutralization in the presence of armoring', *Applied Mathematical Modelling* **39**(1), 348–362.

Gage, C. (1989), 'Limestone dissolution in modeling of slurry scrubbing for flue-gas desulfurization', *PhD Thesis, Texas Univ., Austin, TX (USA)* .

Gage, C. L. & Rochelle, G. T. (1992), 'Limestone dissolution in flue gas scrubbing: Effect of sulfite', *Journal of the Air & Waste Management Association* **42**(7), 926–935.
URL: https://doi.org/10.1080/10473289.1992.10467043

Gao, X., Huo, W., Luo, Z.-y. & Cen, K.-f. (2008), 'Cfd simulation with enhancement factor of sulfur dioxide absorption in the spray scrubber', *Journal of Zhejiang University-SCIENCE A* **9**(11), 1601–1613.
URL: https://doi.org/10.1631/jzus.A0820507

Garg, A., Kapshe, M., Shukla, P. & Ghosh, D. (2002), 'Large point source (LPS) emissions from india: regional and sectoral analysis', *Atmospheric Environment* **36**(2), 213–224.

Gerard, P., Segantini, G. & Vanderschuren, J. (1996), 'Modeling of dilute sulfur dioxide absorption into calcium sulfite slurries', *Chemical Engineering Science* **51**(12), 3349–3358.

Gerbec, M., Stergaršek, A. & Kocjančič, R. (1995), 'Simulation model of wet flue gas desulphurization plant', *Computers and Chemical Engineering* **19**(SUPPL. 1), 283–286.

Gibert, O., de Pablo, J., Cortina, J. L. & Ayora, C. (2003), 'Evaluation of municipal compost/limestone/iron mixtures as filling material for permeable reactive barriers forin-situ acid mine drainage treatment', *J. Chem. Technol. Biotechnol.* **78**(5), 489–496.

Gleason, C. & Rochelle, G. (1987), 'Dissolution and crystallization of calcium sulfite platelets', *Conference: American Institute of Chemical Engineers spring national meeting, Houston, TX, USA, 29 Mar 1987; Other Information: Technical Paper 77B* .

Gledhill, D. K. & Morse, J. W. (2006), 'Calcite dissolution kinetics in na–ca–mg–cl brines', *Geochimica et Cosmochimica Acta* **70**(23), 5802–5813.

Goldberg, R. & Parker, V. (1985), 'Thermodynamics of solution of SO2(g) in water and of aqueous sulfur dioxide solutions', *Journal of Research of the National Bureau of Standards* **90**(5), 341.

Gómez, A., Fueyo, N. & Tomás, A. (2007), 'Detailed modelling of a flue-gas desulfurisation plant', *Computers & Chemical Engineering* **31**(11), 1419–1431.

Gunn, J. (2003), *Encyclopedia of Caves and Karst Science*, Routledge.
URL: https://www.amazon.com/Encyclopedia-Caves-Karst-Science-John/dp/

1579583997?SubscriptionId=AKIAIOBINVZYXZQZ2U3A&tag=chimbori05-20&linkCode=xm2&camp=2025&creative=165953&creativeASIN=1579583997

Haripersad, N. & Swart, P. (2014), 'Rsa sorbant status and application to electricity generation'.

Harriott, P. (1962), 'A random eddy modification of the penetration theory', *Chemical Engineering Science* **17**(3), 149 – 154.
URL: http://www.sciencedirect.com/science/article/pii/0009250962800268

Higbie, R. (1935), 'The rate of absorption of a pure gas into a still liquid during short periods of exposure', *Trans. Am. Inst. Chem. Eng.* **31**, 365–377.
URL: https://ci.nii.ac.jp/naid/10024192494/en/

Hikita, H., Asai, S. & Nose, H. (1978), 'Absorption of sulfur dioxide into water', *AIChE Journal* **24**(1), 147–149.

Hikita, H., Asai, S. & Tsuji, T. (1977), 'Absorption of sulfur dioxide into aqueous sodium hydroxideandsodium sulfite solutions', *AIChE Journal* **23**(4), 538–544.

Horváth, G. & Kawazoe, K. (1983), 'Method for the calculation of effective pore size distribution in molecular sieve carbon.', *Journal of Chemical Engineering of Japan* **16**(6), 470–475.

Hughmark, G. A. (1980), 'HeatandMass Transfer for Spherical Particles in a Fluid Field', *Industrial and Engineering Chemistry Fundamentals* **19**(2), 198–201.

Huminicki, D. M. & Rimstidt, J. D. (2008), 'Neutralization of sulfuric acid solutions by calcite dissolution and the application to anoxic limestone drain design', *Applied Geochemistry* **23**(2), 148–165.

Jamil, R., Ming, L. & Jamil, Irfanand Jamil, R. (2013), 'Application and development trend of flue gas desulfurization (fgd) process: A review', *International Journal of InnovationandApplied Studies* **4**(2), 286–297.

Jarvis, J. B., Meserol, F. B., Selm, T. J., Rochelle, G. T., Gage, C. L., Moser & R.E. (1988), Development of a predictive model for limestone dissolution in wet FGD systems. Presented at EPA/EPRI First Combined, *in* 'FGD and Dry SO2 Control Symposium', St. Louis Mo.

Joshi, J., Pandit, A. & Sharma, M. (1982), 'Mechanically agitated gas-liquid reactors', *Chemical Engineering Science* **37**(6), 813 – 844.
URL: http://www.sciencedirect.com/science/article/pii/0009250982801711

Kaesemann, R. & Fahlenkamp, H. (2002), 'The meaning of droplet-droplet interaction for the wet flue-gas cleaning process', *Chemical Engineering & Technology* **25**(7), 739.

Kallinikos, L. E., Farsari, E. I., Spartinos, D. N. & Papayannakos, N. G. (2010), 'Simulation of the operation of an industrial wet flue gas desulfurization system', *Fuel Processing Technology* **91**(12), 1794–1802.
URL: http://dx.doi.org/10.1016/j.fuproc.2010.07.020

Khan, M. A., Wasif, S. & Salama, S. B. (1978), 'Weak complexes of sulphur and selenium. part 5. halide-ion replacement in 1:1 complexes of sulphur dioxide, thionyl chloride, and sulphonyl choride with halide ions in acetonitrile and dimethyl sulphoxide', *Journal of the Chemical Society, Dalton Transactions* (8), 915.

Kiil, S. (1998), *Experimental and Theoretical Investigations of Wet Flue Gas Desulphurisation*, Tekst & Tryk A/S.

Kiil, S., Michelsen, M. L. & Dam-Johansen, K. (1998), 'Experimental Investigation and Modeling of a Wet Flue Gas Desulfurization Pilot Plant', *Industrial & Engineering Chemistry Research* **37**(7), 2792–2806.
URL: http://pubs.acs.org/doi/abs/10.1021/ie9709446

Kiil, S., Nygaard, H. & Johnsson, J. E. (2002), 'Simulation studies of the influence of HCl absorption on the performance of a wet flue gas desulphurisation pilot plant', *Chemical Engineering Science* **57**(3), 347–354.

Kikkawa, H., Nakamoto, T., Morishita, M. & Yamada, K. (2002), 'New wet FGD process using granular limestone', *Industrial & Engineering Chemistry Research* **41**(12), 3028–3036.

Koech, L., Rutto, H., Everson, R. & Neomagus, H. (2014), 'Semi-empirical model for limestone dissolution in adipic acid for wet flue gas desulfurization', *Chemical Engineering & Technology* **37**(11), 1919–1928.

Krissmann, J., Siddiqi, M. A. & Lucas, K. (1998), 'Thermodynamics of SO2 absorption in aqueous solutions', *Chemical Engineering & Technology* **21**(8), 641–644.

Krissmann, J., Siddiqi, M. & Lucas, K. (1997), 'Absorption of sulfur dioxide in dilute aqueous solutions of sulfuric and hydrochloric acid', *Fluid Phase Equilibria* **141**(1-2), 221–233.

Lancia, A., Musmarra, D. & Pepe, F. (1997), 'Modeling of SO2 Absorption into Limestone Suspensions', *IndustrialandEngineering Chemistry Research* **36**(1), 197–203.

URL: http://www.scopus.com/inward/record.url?eid=2-s2.0-0030909629{&}partnerID=tZOtx3y1

Lancia, A., Musmarra, D., Pepe, F. & Volpicelli, G. (1991), 'Concentration profiles in the diffusional film in the calcium carbonate dissolution process', *Chemical Engineering Science* **46**(10), 2507–2512.

Lancia, A., Musmarra, D., Pepe, F. & Volpicelli, G. (1994*a*), 'Characteristic times for limestone particle dissolution in the production of gypsum from the wet flue gas desulfurization process', *Environmental Science & Technology* **28**(6), 1031–1036.

Lancia, A., Musmarra, D., Pepe, F. & Volpicelli, G. (1994*b*), 'SO 2 absorption in a bubbling reactor using limestone suspensions', *Chemical Engineering Science* **49**(24), 4523–4532.

Lee, J.-Y., Khang, S.-J., Tseng, C.-H. & Keener, T. C. (2001), 'The effects of pulsed corona discharge on SO2 absorption into water', *Industrial & Engineering Chemistry Research* **40**(24), 5822–5830.

Levenspiel, O. (1999), *Chemical Reaction Engineering*, JohnWiley, NewYork, New York.

Lisnic, R. & Jinga, S. (2018), 'Study on current state and future trends of flue gas desulphurization tehnologies: A review', *Revista Romana de Materiale/ Romanian Journal of Materials* **48**, 83–90.

Liu, S.-Y. & Xiao, W.-D. (2006), 'Modeling and simulation of a bubbling SO2 absorber with granular limestone slurry and an organic acid additive', *Chemical Engineering & Technology* **29**(10), 1167–1173.

Lund, K., Fogler, H., McCune, C. & Ault, J. (1975), 'Acidization—II. the dissolution of calcite in hydrochloric acid', *Chemical Engineering Science* **30**(8), 825–835.

Lund, K., Fogler, H. S. & McCune, C. (1973), 'Acidization—i. the dissolution of dolomite in hydrochloric acid', *Chemical Engineering Science* **28**(3), 691 – IN1.
URL: http://www.sciencedirect.com/science/article/pii/0009250977800031

Lynn, S., Straatemeier, J. & Kramers, H. (1955), 'Absorption studies in the light of the penetration theory', *Chemical Engineering Science* **4**(2), 49–57.

MacInnis, I. N. & Brantley, S. L. (1992), 'The role of dislocations and surface morphology in calcite dissolution', *Geochimica et Cosmochimica Acta* **56**(3), 1113–1126.

Marocco, L. (2010), 'Modeling of the fluid dynamics and SO2 absorption in a gas–liquid reactor', *Chemical Engineering Journal* **162**(1), 217–226.

Marocco, L. & Inzoli, F. (2009), 'Multiphase euler–lagrange CFD simulation applied to wet flue gas desulphurisation technology', *International Journal of Multiphase Flow* **35**(2), 185–194.

MATLAB (2018), *Version 9.5.0.944444 (R2018b)*, The MathWorks Inc., Natick, Massachusetts.

Michalski, J. A. (1997), 'Aerodynamic characteristics of FGD spray towers', *Chemical Engineering & Technology* **20**(2), 108–117.

Micromeritics (2010), *Accelerated surface area and porosimetry system (ASAP 2020), Operator's manual v3.01*, Vol. 4, Micromeritics Instrument Corporation, Norcross, Georgia, US.

Morse, J. W. (1974), 'Dissolution kinetics of calcium carbonate in sea water: A new method for the study of carbonate reaction kinetics', *Am. J. Sci.* **274**(2), 97–107.

Morse, J. W. & Arvidson, R. S. (2002), 'The dissolution kinetics of major sedimentary carbonate minerals', *Earth Sci. Rev.* **58**(1-2), 51–84.

Murphy, W. M., Oelkers, E. H. & Lichtner, P. C. (1989), 'Surface reaction versus diffusion control of mineral dissolution and growth rates in geochemical processes', *Chemical Geology* **78**(3-4), 357–380.

Nannen, L. W., West, R. E. & Kreith, F. (1974), 'Removal of SO ₂ from Low Sulfur Coal Combustion Gases by Limestone Scrubbing', *Journal of the Air Pollution Control Association* **24**(1), 29–39.
URL: http://www.tandfonline.com/doi/abs/10.1080/00022470.1974.10469890

Nelder, J. A. & Mead, R. (1965), 'A simplex method for function minimization', *The Computer Journal* **7**(4), 308–313.

Neveux, T., Hagi, H. & Moullec, Y. L. (2014), 'Performance simulation of full-scale wet flue gas desulfurization for oxy-coal combustion', *Energy Procedia* **63**, 463–470.

Neveux, T. & Le Moullec, Y. (2011), 'Wet industrial flue gas desulfurization unit: Model development and validation on industrial data', *Industrial & Engineering Chemistry Research* **50**(12), 7579–7592.
URL: https://doi.org/10.1021/ie102239q@proofing

Nygaard, H. G., Kiil, S., Johnsson, J. E., Jensen, J. N., Hansen, J., Fogh, F. & Dam-Johansen, K. (2004), 'Full-scale measurements of SO2 gas phase concentrations and slurry compositions in a wet flue gas desulphurisation spray absorber', *Fuel* **83**(9), 1151–1164.

Olausson, S., Wallin, M. & Bjerle, I. (1993), 'A model for the absorption of sulphur dioxide into a limestone slurry', *The Chemical Engineering Journal* **51**(2), 99–108.

Ortiz, F. G. (2010), 'A simple realistic modeling of full-scale wet limestone FGD units', *The Chemical Engineering Journal* **165**(2), 426–439.

Pasiuk-Bronikowska, W. & Rudziński, K. (1991), 'Absorption of SO2 into aqueous systems', *Chemical Engineering Science* **46**(9), 2281–2291.

Pepe, F. (2001), 'Dissolution of finely ground limestone particles in acidic solutions', *IndustrialandEngineering Chemistry Research* **40**(23), 5378–5385.

Perales, A. L. V., Ollero, P., Ortiz, F. J. G. & B., F. V. (2008), 'Dynamic analysis and identification of a wet limestone flue gas desulfurization pilot plant', *Industrial & Engineering Chemistry Research* **47**(21), 8263–8272.

Plummer, L. N. & Busenberg, E. (1982), 'The solubilities of calcite, aragoniteandvaterite in CO2-H2O solutions between 0and90 °C and an evaluation of the aqueous model for the system CaCO3-CO2-H2O', *Geochim. Cosmochim. Acta* **6**(6), 1011–1040.

Plummer, L. N., Wigley, T. M. L. & Parkhurst, D. L. (1978), 'The kinetics of calcite dissolution in CO 2 -water systems at 5 degrees to 60 degrees cand0.0 to 1.0 atm CO 2', *Am. J. Sci.* **278**(2), 179–216.

Plummer, L. & Wigley, T. (1976), 'The dissolution of calcite in CO2-saturated solutions at 25°c and 1 atmosphere total pressure', *Geochimica et Cosmochimica Acta* **40**(2), 191–202.

Pretorius, I., Piketh, S., Burger, R. & Neomagus, H. (2015), 'A perspective on South African coal fired power station emissions', *Journal of Energy in Southern Africa* **26**, 27 – 40.
URL: http://www.scielo.org.za/scielo.php?script=sci_arttext&pid=S1021-447X2015000300004&nrm=iso

Quantachrome (2009), *Stereopycnometer operating manual (Part No.: 05006 Rev D SPY-D160-E).*

Ramachandran, P. & Sharma, M. (1969), 'Absorption with fast reaction in a slurry containing sparingly soluble fine particles', *Chem. Eng. Sci.* **24**(11), 1681–1686.

Rochelle, G. T. & King, C. J. (1977), 'The effect of additives on mass transfer in CaCO3 or CaO slurry scrubbing of SO2 from waste gases', *Industr.Engng Chem.Fundam.* **16**(1), 67–75.

Ross, K. (2012), Eskom air quality strategy, 32-1143, Technical report, Eskom.

Sada, E., Kumazawa, H. & Butt, M. (1977), 'Single gas absorption with reaction in a slurry containing fine particles', *Chem. Eng. Sci.* **32**(10), 1165–1170.

Sada, E., Kumazawa, H. & Butt, M. (1980), 'Absorption of sulfur dioxide into aqueous slurries of sparingly soluble fine particles', *Chem. Eng. Sci.* **35**(4), 771–777.

Sada, E., Kumazawa, H. & Butt, M. A. (1979), 'Single and simultaneous absorptions of lean SO2 and NO2 into aqueous slurries of Ca(OH)2 or Mg(OH)2 particles', *Journal of Chemical Engineering of Japan* **12**(2), 111–117.

Sada, E., Kumazawa, H. & Hashizume, I. (1981), 'Further consideration on chemical absorption mechanism by aqueous slurries of sparingly soluble fine particles', *Chemical Engineering Science* **36**(4), 639 – 642.
URL: http://www.sciencedirect.com/science/article/pii/0009250981850798

Sada, E., Kumazawa, H., Hashizume, I. & Nishimura, H. (1982), 'Absorption of dilute SO2 into aqueous slumes of CaSO3', *Chemical Engineering Science* **37**(9), 1432–1435.

Sada, E., Kumazawa, H. & Nishimura, H. (1983), 'Absorption of sulfur dioxide into aqueous double slurries containing limestoneandmagnesium hydroxide', *AIChE Journal* **29**(1), 60–65.

Sada, E., Kumazawa, H., Sawada, Y. & Hashizume, I. (1981), 'Kinetics of absorptions of lean sulfur dioxide into aqueous slurries of calcium carbonate and magnesium hydroxide', *Chemical Engineering Science* **36**(1), 149–155.

Saha, S., Sharma, B., Kumar, S., Sahu, G., Badhe, Y. & Kulkarni, S. T. (2007), 'Density measurements of coal samples by different probe gasesandtheir interrelation', *Fuel* **86**(10-11), 1594–1600.

Salama, A., Salama, S. B., Sobeir, M. & Wasif, S. (1971), 'Weak complexes of sulphur and selenium. part i. complex species of SO2, SOCl2, and SO2cl2 with chloride, bromide, and iodide ions', *Journal of the Chemical Society A: Inorganic, Physical, Theoretical* p. 1112.

Santoro L., C. P. & G., V. (1973), 'Attacco di calcare con soluzioni solforose', *Chim. Ind. (Milan)* **55**, 577 – 584.

Santoro, L., Volpicelli, G. & Caprio, V. (1987), 'Limestone neutralization of acid waters in the presence of surface precipitates', *Water Research* **21**(6), 641–647.

Schultes, M. (1998), 'Absorption of sulphur dioxide with sodium hydroxide solution in packed columns', *Chemical Engineering & Technology* **21**(2), 201–209.

Schutte, C. (2018), 'Value added utilisation possibilities of coal combustion products in south africa', *Masters Thesis, Noth West University, South Africa* .

Schwartz, S. & Freiberg, J. (1981), 'Mass-transport limitation to the rate of reaction of gases in liquid droplets: Application to oxidation of SO2 in aqueous solutions', *Atmospheric Environment (1967)* **15**(7), 1129–1144.

Sharma, A. K., Prasad, D. S. N., Acharya, S. & Sharma, R. (2012), 'Utility and application of FGD system (flue gas desulphurization) in chemical and environmental engineering', *International Journal of Chemical Engineering and Applications* pp. 129–135.

Shih, S. M., Lin, J. P. & Shiau, G. Y. (2000), 'Dissolution rates of limestones of different sources', *Journal of Hazardous Materials* **79**(1-2), 159–171.

Siagi, Z. & Mbarawa, M. (2009), 'Dissolution rate of south african calcium-based materials at constant pH', *J. Hazard. Mater.* **163**(2-3), 678–682.

Sjöberg, E. . L. & Rickard, D. T. (1984*a*), 'Calcite dissolution kinetics: Surface speciation and the origin of the variable pH dependence', *Chem. Geol.* **42**(1-4), 119–136.

Sjöberg, E. L. & Rickard, D. T. (1984*b*), 'Temperature dependence of calcite dissolution kinetics between 1and62°c at pH 2.7 to 8.4 in aqueous solutions', *Geochim. Cosmochim. Acta* **48**(3), 485–493.

Sjöberg, E. L. & Rickard, D. T. (1985), 'The effect of added dissolved calcium on calcite dissolution kinetics in aqueous solutions at 25°c', *Chem. Geol.* **49**(4), 405–413.

Sjöberg, E. & Rickard, D. (1983), 'The influence of experimental design on the rate of calcite dissolution', *Geochim. Cosmochim. Acta* **47**(12), 2281–2285.

Smith, S. J., van Aardenne, J., Klimont, Z., Andres, R. J., Volke, A. & Arias, S. D. (2011), 'Anthropogenic sulfur dioxide emissions: 1850–2005', *Atmospheric Chemistry and Physics* **11**(3), 1101–1116.

Soud, H. N. (2000), Developments in FGD. CCC/29, IEA Coal Research, *in* 'Developments in FGD. CCC/29, IEA Coal Research', London.

Souza, S. M. A. G. U., Santos, F. B. F., de Souza, A. A. U. & Barrero, F. V. (2010), 'Limestone dissolution in flue gas desulfurization-experimental and numerical study', *Journal of Chemical Technology & Biotechnology* **85**(9), 1208–1214.

Srivastava, R. K. & Jozewicz, W. (2001), 'Flue Gas Desulfurization : The State of the Art PAPER Flue Gas Desulfurization : The State of the Art', *Journal of the Air & Waste Management Association* **3289**(January), 1676–1688.

Stephen, C. L., Godana, P. R., Moganelwa, A., Van Heedren, C. S., Bore, J., Singh, Y., Patel, E. & Binkowski, S. (2014), Implementation of De-SOx technologies in an Eskom context, *in* 'First Eskom Power Plant Engineering Institute Student Conference Eskom Academy of Learning', Vol. 5.

Stromberg, A. M. (1992), Prospects for further development of spray-scrubbing., PhD thesis.

Subbarao, D. & Taneja, V. K. (1979), *"Three phase suspensions in agitated vessels," in Proceedings of the Third European Conference on Mixing: Held at the University of York, England, April 4th-6th, 1979*, BHRA Fluid Engineering.
URL: https://www.amazon.com/Proceedings-Third-European-Conference-Mixing/dp/0906085314?SubscriptionId=AKIAIOBINVZYXZQZ2U3A&tag=chimbori05-20&linkCode=xm2&camp=2025&creative=165953&creativeASIN=0906085314

Takashina, T., Honjo, S., Ukawa, N. & Oishi, T. (2001), 'Effect of limestone concentration and particle size on SO2 absorption in wet FGD process.', *J. Chem. Eng. Jpn.* **34**(6), 810–818.

Takeshita, M. & Soud, H. (1993), Fgd performanceandexperience on coal-fired plants, Technical report, IEA Coal Research, London (United Kingdom).

Tanaka, Y. (2010), 'Water dissociation reaction generated in an ion exchange membrane', *Journal of Membrane Science* **350**(1-2), 347–360.

Terraglio, F. P. & Manganelli, R. M. (1967), 'The absorption of atmospheric sulfur dioxide by water solutions', *Journal of the Air Pollution Control Association* **17**(6), 403–406.

Toprac, A. J. & Rochelle, G. T. (1982), 'Limestone dissolution in stack gas desulfurization. a mass-transfer model is shown to predict the the measured dissolution rates with less than 30% error', *Environ. Prog.* **1**(1), 52–58.

Tress, M. V., Loeppert, R. H. & Matis, J. H. (1985), 'A calcite dissolution model for the estimation of particle size distribution1', *Soil Science Society of America Journal* **49**(2), 302.

Tseng, C.-C. & Li, C.-J. (2018), 'Eulerian-eulerian numerical simulation for a flue gas desulfurization tower with perforated sieve trays', *International Journal of Heat and Mass Transfer* **116**, 329–345.

Tseng, P. C. & Rochelle, G. T. (1986*a*), 'Calcium sulfite hemihydrate: Crystal growth rate and crystal habit', *Environ. Prog.* **5**(1), 5–11.

Tseng, P. C. & Rochelle, G. T. (1986*b*), 'Dissolution rate of calcium sulfite hemihydrate in flue gas desulfurization processes', *Environmental Progress* **5**(1), 34–40.

Uchida, S. & Ariga, O. (1985), 'Absorption of sulfur dioxide into limestone slurry in a stirred tank', *The Canadian Journal of Chemical Engineering* **63**(5), 778–783.

Uchida, S., Koide, K. & Shindo, M. (1975), 'Gas absorption with fast reaction into a slurry containing fine particles', *Chem. Eng. Sci.* **30**(5-6), 644–646.

Uchida, S., Miyachi, M. & Ariga, O. (1981), 'Penetration model of gas absorption into slurry accompanied by an instantaneous irreversible chemical reaction', *The Canadian Journal of Chemical Engineering* **59**(4), 560–562.

Uchida, S., Moriguchi, H., Maejima, H., Koide, K. & Kageyama, S. (1978), 'Absorption of sulfur dioxide into limestone slurry in a stirred tank reactor', *Can. J. Chem. Eng.* **56**(6), 690–697.

Uchida, S. & Wen, C. (1977), 'Rate of gas absorption into a slurry accompanied by instantaneous reaction', *Chem. Eng. Sci.* **32**(11), 1277–1281.

Uchida, S. & Wen, C. Y. (1973), 'Gas Absorption by Alkaline Solutions in a Venturi Scrubber', *IndustrialandEngineering Chemistry Process DesignandDevelopment* **12**(4), 437–443.

Ukawa, N., Takashina, T., Shinoda, N. & Shimizu, T. (1993), 'Effects of particle size distribution on limestone dissolution in wet FGD process applications', *Environmental Progress* **12**(3), 238–242.

Van Alphen, C. (2009*a*), Calcium distribution in ash samples. Report RP FUEL/QS/08/16. Eskom Corporate Services Division, *in* 'ESKOM REPORTS', Eskom Corporate Services Division, VAN ALPHEN.

Van Alphen, C. (2009*b*), Calcium distribution in ash samples. report rp fuel/qs/09/39., Technical report, Eskom Corporate Services Division.

Vázquez, G., Antorrena, G., Chenlo, F. & Paleo, F. (1988), 'Absorption of SO2 by aqueous NaOH solutions in the presence of a surfactant', *Chemical Engineering & Technology - CET* **11**(1), 156–162.

Wallin, M. & Bjerle, I. (1989*a*), 'A mass transfer model for limestone dissolution from a rotating cylinder', *Chemical Engineering Science* **44**(1), 61–67.

Wallin, M. & Bjerle, I. (1989*b*), 'Rate models for limestone dissolution: A comparison', *Geochimica et Cosmochimica Acta* **53**(6), 1171–1176.

Wallin, M. & Bjerle, I. (1990), 'The use of the penetration model for the dissolution of limestone in the CO_2-water system', *Chemical Engineering Communications* **91**(1), 91–111.

Wang, Z., Peng, Y., Ren, X., Gui, S. & Zhang, G. (2015), 'Absorption of sulfur dioxide with sodium hydroxide solution in spray columns', *Industrial & Engineering Chemistry Research* **54**(35), 8670–8677.

Warych, J. & Szymanowski, M. (2001), 'Model of the wet limestone flue gas desulfurization process for cost optimization', *Industrial & Engineering Chemistry Research* **40**(12), 2597–2605.

Webb, P. A. (2001), *Volume and density determination for particle technologist. Micromeritics Instrument Corp., Norcross, Georgia, USA.*

Wedzicha, B. & Webb, P. (1996), 'Vapour pressure of SO2 above solutions of sulphur(IV) oxospecies: the effects of chloride ion and glycerol', *Food Chemistry* **55**(4), 337–341.

Weng, X. (2016), Effect of SO32- on wet flue gas desulfurization technology, *in* 'Proceedings of the 2016 6th International Conference on Machinery, Materials, Environment, BiotechnologyandComputer', Atlantis Press.

Whitman, W. (1924), 'The Two-Film Theory of Gas Absorption', *ChemicalandMetallurgical Engineering* **29**(4), 146–148.

Wilhelm, E., Battino, R. & Wilcock, R. J. (1977), 'Low-Pressure Solubility of Gases in Liquid Water', *Chemical Reviews* **77**(2), 219–262.

Wright, M. H. (2012), 'Nelder, mead, and the other simplex method', *Documenta Mathematica · Extra Volume ISMP* pp. 271–276.

Xiang, G., Rui-tang, G., Hong-lei, D., Zhong-yang, L. & Ke-fa, C. (2009), 'Dissolution rate of limestone for wet flue gas desulfurization in the presence of sulfite', *Journal of Hazardous Materials* **168**(2), 1059 – 1064.
URL: http://www.sciencedirect.com/science/article/pii/S0304389409003550

Xiao, Y., Li, C., Li, S., Zeng, G., Wen, Q., Guo, G. & Song, J. (2014), 'Optimal design of a wet-type desulphurization absorber by the numerical simulation method', *Chemical Engineering Research and Design* **92**(7), 1257–1266.

Yan, S. & Wu, G. (2017), 'SO2 emissions in china – their network and hierarchical structures', *Scientific Reports* **7**(1).

Yates, J. G. & Best, R. J. (1976), 'Kinetics of the reaction between sulfur dioxide, oxygen, and cupric oxide in a tubular, packed bed reactor', *Industrial & Engineering Chemistry Process Design and Development* **15**(2), 239–243.

Yoshida, F. & Miura, Y. (1963), 'Effective interfacial area in packed columns for absorption with chemical reaction', *AIChE Journal* **9**(3), 331–337.

Zeng, F., Yin, L. & Chen, L. (2007), Numerical simulation and optimized design of the wet flue gas desulphurization spray tower, *in* 'Challenges of Power Engineering and Environment', Springer Berlin Heidelberg, pp. 783–787.

Zhao, J., Jin, B. & Zhong, Z. (2007), 'The degree of desulphurization of a limestone/gypsum wet FGD spray tower using response surface methodology', *Chemical Engineering & Technology* **30**(4), 517–522.

Zhong, Y., Gao, X., Huo, W., yang Luo, Z., jiang Ni, M. & fa Cen, K. (2008), 'A model for performance optimization of wet flue gas desulfurization systems of power plants', *Fuel Processing Technology* **89**(11), 1025–1032.

Zidar, M. (2000), 'Gas liquid equilibrium operational diagram graphical presentation of absorption of so2 in the naoh so2 h2o system taking place within a laboratory absorber', *Industrial & Engineering Chemistry Research* **39**(8), 3042–3050.
URL: https://doi.org/10.1021/ie990711+

Zimmermann, K., Pasel, C., Luckas, M. & Herbell, J.-D. (2009), 'Solubility of sulphur dioxide in aqueous electrolyte solutions at higher ionic strengths—chloride and bromide containing systems', *Fluid Phase Equilibria* **279**(2), 105–114.

Zwietering, T. (1958), 'Suspending of solid particles in liquid by agitators', *Chemical Engineering Science* **8**(3-4), 244–253.
URL: http://linkinghub.elsevier.com/retrieve/pii/0009250958850319

Appendices

Appendix A: Error Analysis

Experimental errors in this study were calculated using MATLAB2018b in-built commands, given in Equations A.1 through A.5. For experimental runs that were repeated three times, the mean was calculated according to Equation A.1

$$mu = mean(A, 2) \tag{A.1}$$

Appendix A.1:Error Analysis Results

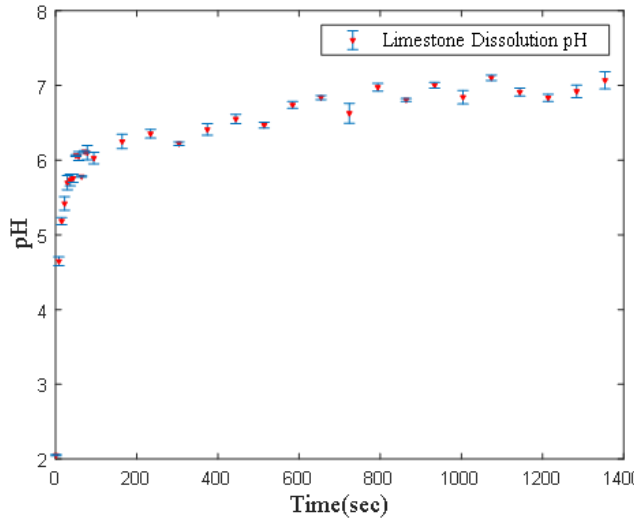

(a) pH of limestone dissolution

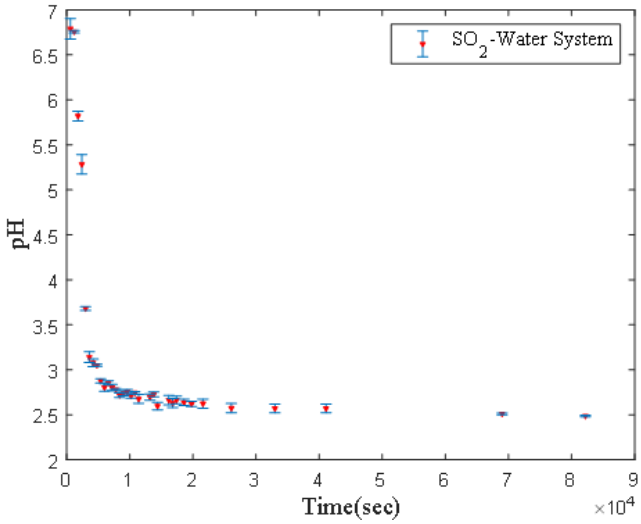

(b) pH in the SO_2 - Water system

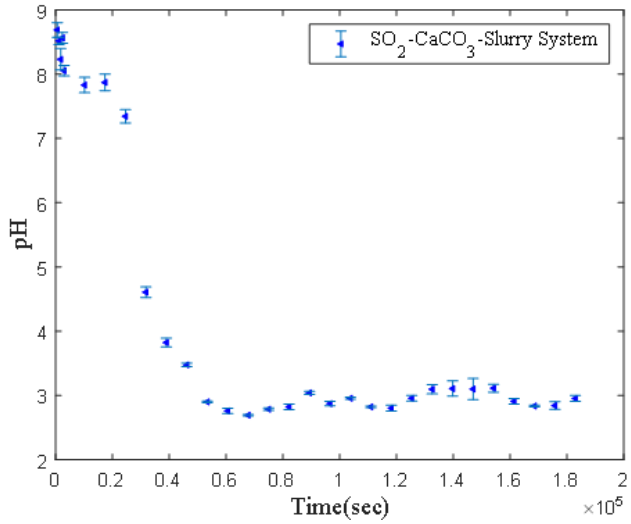

(c) pH in the SO_2 - slurry system

Figure A.1: Error Analysis Results: pH.

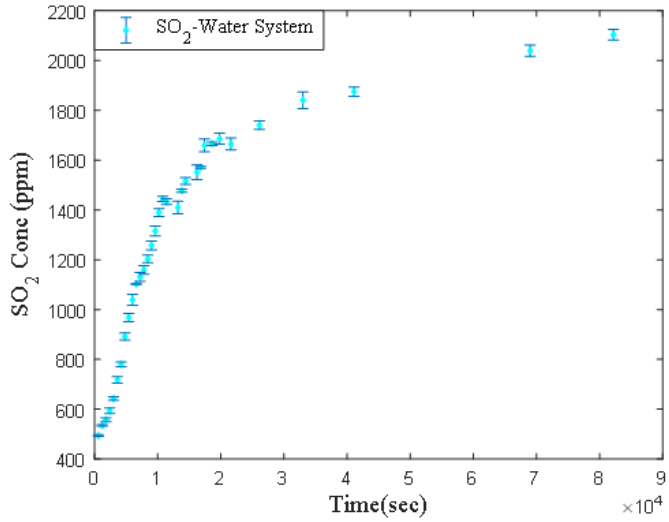

(a) Gas SO_2 concentration in the overhead space: water case

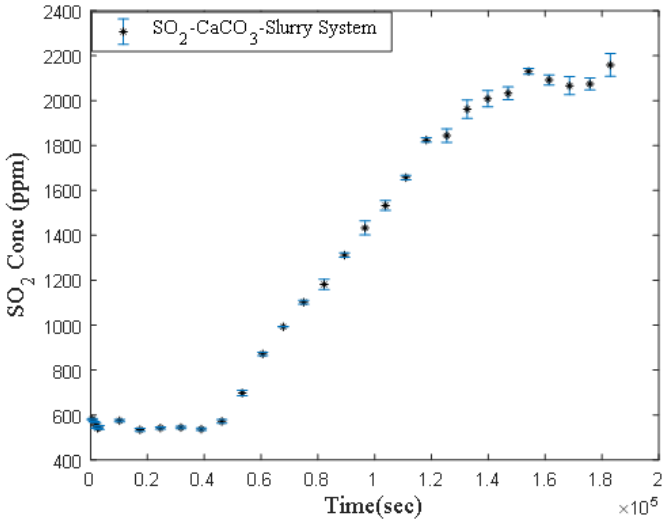

(b) Gas SO_2 concentration in the overhead space: slurry case

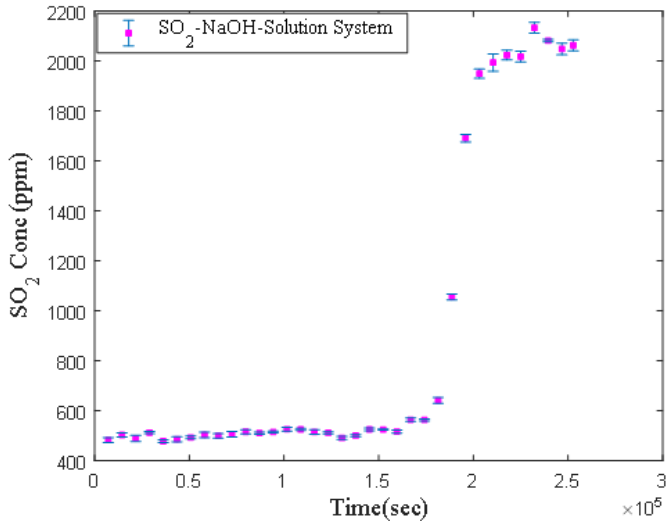

(c) Gas SO_2 concentration in the overhead space in the SO_2 - NaOH solution system

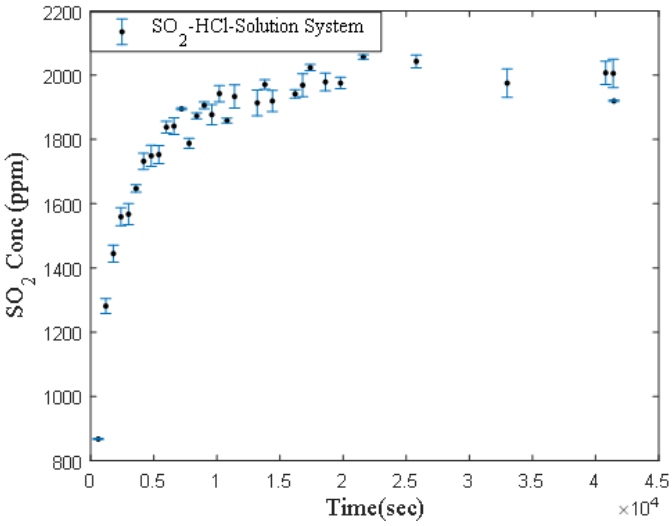

(d) Gas SO_2 concentration in the overhead space in the SO_2 - HCl solution system

Figure A.2: Error Analysis Results: SO_2.

The standard deviation is given by Equation A.2

$$s = std(A, 1, 2) \tag{A.2}$$

The variance was calculated using Equation A.3

$$sigma = var(A, 1, 2) \tag{A.3}$$

The standard error was thus given by Equation A.4

$$err = s/sqrt(3) \tag{A.4}$$

The fractional uncertainty was calculated using Equation A.5

$$FractionalUncertainty = EquipmentUncertainty./mu \tag{A.5}$$

MATLAB2018b errorbar plotting was also employed, the results for pH measurements are shown in Figure A.1, whereas Figure A.2 shows those for SO_2 measurements.

Appendix B:Limestone Dissolution

Appendix B.1:Sample Limestone Dissolution Matlab Code


```
function [] = LimestoneDissolutionKineticModel(k0)

% This code solves a system of 4 differential equations that describes the
% dissolution of limestone in a HCl solution.

%% The variables, x(1) ... x(4) are:
% x(1) : concentration of hydronium ions (mol/m3)
% x(2) : concentration of CaCO3 (mol/m3)
% x(3) : concentration of Ca2+ (mol/m3)
% x(4) : concentration of HCO3- (mol/m3)

%% The parameters k(1) ... k(4) are:
% k(1) : reaction rate constant (m/s)
% k(2) : adsorption constant (m3/mol)
% k(3) : BET specific surface area (m2/g)
% k(4) : mass transfer coefficient (m/s)

x0 = [x0(1); x0(2); x0(3); x0(4)];

k0 = [k0(1); k0(2); k0(3); k0(4)];

[t,x] = ode15s(@(t,x)myModel(t,x,k0),[t0 tf],x0);


figure
hold off
plot(t,x(:,1),'r--',t,x(:,2),'b',t,x(:,3),'c-.')
hold on;
xlabel('Time (sec)','FontSize',14,'FontName','Times New Roman')
ylabel('Concentration (mol/m^3)','FontSize',14,'FontName','Times New Roman')
legend('Mod-H^+', 'Mod-CaCO_3', 'Mod-Ca^2+', 'Location','best')


function dxdt = myModel(t,x,k)

    dxdt=zeros(4,1);
    dxdt(1)= (-2.85).*(1/((1/k(4))+(1/k(1))).*k(3).*x(2)*x(1).*(1-(k(2).*x(1))/(1+(k↙
(2).*x(1)))));
    dxdt(2)= -(1/((1/k(4))+(1/k(1))).*k(3).*x(2).*x(1).*(1-(k(2).*x(1))/(1+(k(2).*x↙
(1)))));
    dxdt(3)= (1/((1/k(4))+(1/k(1))).*k(3).*x(2).*x(1).*(1-(k(2).*x(1))/(1+(k(2).*x↙
(1)))));
    dxdt(4)= (1/((1/k(4))+(1/k(1))).*k(3).*x(2).*x(1).*(1-(k(2).*x(1))/(1+(k(2).*x↙
(1)))));

    dxdt = dxdt;

end

end
```

Appendix B.2:Sample Limestone Dissolution Parameter Fitting Matlab Code

```
function KineticParametersEstimation25degC

%Experimental Results

abscissa = [3.31
1.86
0.93325
0.32359
0.16982
0.10471
0.0631
0.04898
0.03631
0.02951
0.0257
0.02138
0.01738
0.01514
0.01349];

ordinatus = [1
2
3
4
5
6
7
8
9
10
11
12
13
14
15];

% Ordinatus is time
tspan = [min(ordinatus), max(ordinatus)];

% Initial values
y0 = 3.31;

% Parameter to guess
k0 = [10000;0.01;0.1];
% v0 = 2;
% ktot = 0.00845539301971187;


OptimisedEak_1andKad = fminsearch(@myObj, k0) % Optimization

% Nested minimization function
    function obj = myObj(k)
```

```
            Ea =k(1);
            k_1=k(2);
            Kad=k(3);
            sol = ode45(@limestonedissolution, tspan, y0, [], k);
            y_hat = deval(sol, ordinatus);      % Evaluate solution at
 given times
            obj = sum((y_hat' - abscissa).^2);    % Compute squared
 error
        end

% Plot with optimal parameter
[T,Y] = ode45(@limestonedissolution, tspan, y0, [],
 OptimisedEak_1andKad);


% Parameter Estimation
figure
plot(ordinatus, abscissa,'ko', 'DisplayName','Exp','MarkerFaceColor',
[0 0 1],...
    'MarkerSize',10,'Marker','pentagram','LineStyle','none','Color',[0
 0 1]);

hold on

plot(T,Y,'DisplayName','Mod','MarkerSize',2,'LineWidth',1,'Color',[1 0
 0]);
ylim([-0.2 4])
ylabel('Conc (mol/m^{3})','FontSize',14,'FontName','Times New Roman');
xlabel('Time (min)','FontSize',14,'FontName','Times New Roman');
lgd = legend('Exp','Mod');
title(lgd,['Ea = ' num2str(Ea) '    ' 'k_1 = ' num2str(k_1) '    Kad =
 ' num2str(Kad)])
end

function dy = limestonedissolution(t,y,k)

cs0=19.89;      % Initial concentration of CaCO3
MMs=100.0869;   % Molecular weight of CaCO3
stoic=2.85;     % Stoichimometric coefficient
kl=0.01224;  % Mass transfer coefficient
SSABET=10.5;   % Specific surface area BET
R=8.314;        % Universal gas constant
T=298.15;       % Modified temperature
Ea=k(1);        % Activation energy
k_1=k(2);       % Pre-expontial factor
Kad=k(3);       % Adsorption constant
k(4) = cs0*exp(-(y*MMs*SSABET*k(2)*kl*t)/((k(2) + kl*exp(k(1)/
(R*T)))*(y*k(3) + 1))); % CaCO3 concentration

dy(1) = -stoic*(1/((1/kl)+(1/(k(2)*exp(-k(1)/(R*T))))))*MMs*k(4)*y*(1-
(k(3)*y)/(1+k(3)*y));

end
```

Appendix B.3:Supplementary Fitting Results for Limestone Dissolution (Ea, k_1 and Kad)

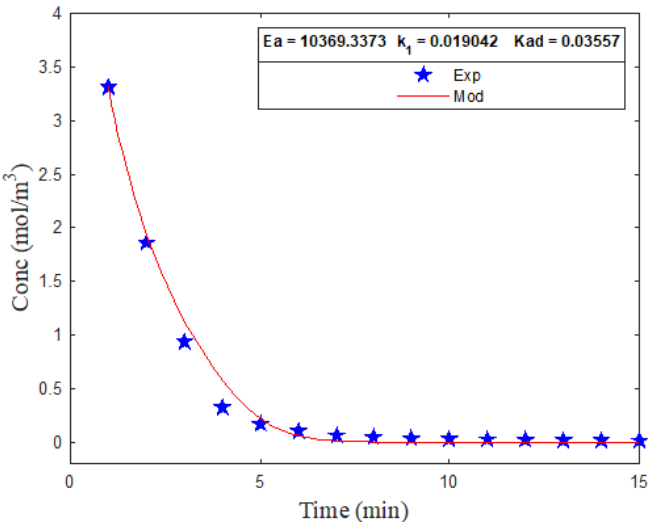

(a) 25 °

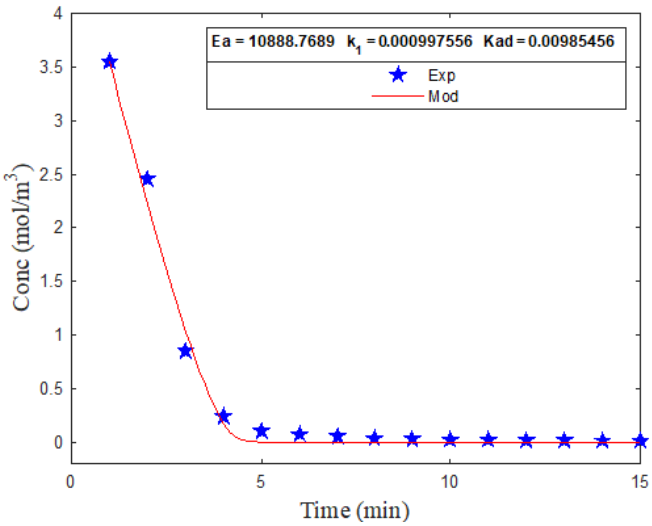

(b) 30 °

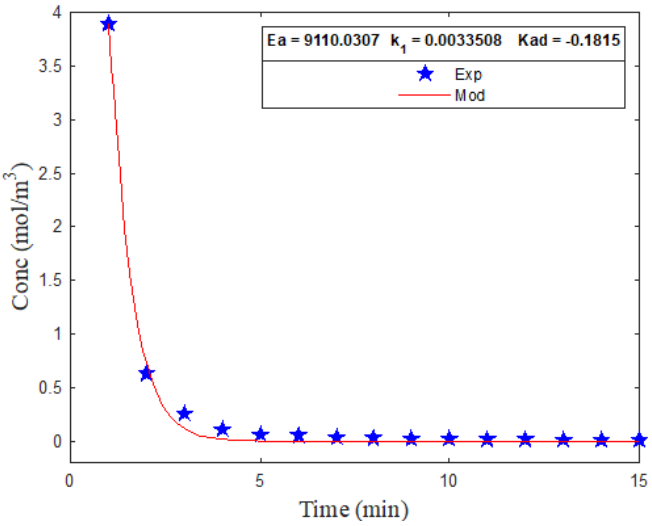

(c) 40 °

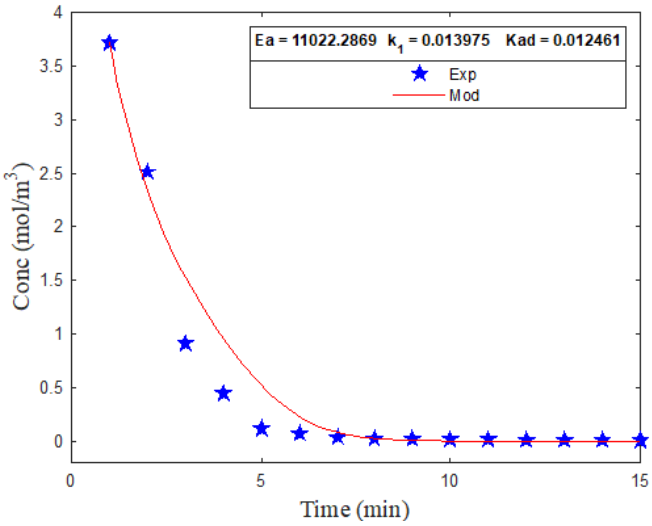

(d) 50 °

Figure B.1: Supplementary Limestone Dissolution Ea, k_1 and Kad Fitting Results.

Appendix C: Integrated Model

Appendix C1: Sample Matlab Code for Integrated Model

```
function Results = EulerMethodCaCO3Slurry(y,S)

% In this study, SO$_2$ is absorbed into limestone slurry in a stirred reactor.
% Simulated flue gas is operated in a continuous mode while limestone slurry is operated in a batch mode.
% Three rate determining mechanisms were considered.
% The mechanisms were expressed in terms of 7 ODEs and 2 algebraic equations.
% The equations are solved in this code.

global S_total C_total Ca_total CSO2_bulkslurry  CHSO3 CSO3 CCO2_bulkslurry CHCO3 CCO3 CCaCO3 CCaSO3 Trial CH ...
    nloop Delt t CH_trial CSO2_inter  CHSO3_inter  CSO3_inter CCO2_inter  CHCO3_inter CCO3_inter pHtrial pi pHInter

format shorte

%% Parameters

S.R     = 8.314;
S.HSO2  = 149;
S.HCO2  = 5.15e+3;
S.DCa2  = 1.39e-9;
S.DSO2  = 2.89e-9;
S.DCO2  = 3.53e-9;
S.KCO2  = 1.7e-3;
S.KHCO3  = 6.55e-8;
S.KSO2  = 6.24;
S.KHSO3 = 5.68e-5;
S.Kw  = 5.3E-8;
S.KSPCaSO3  = 3.1e-6;
S.BETCaSO3 = 10;
S.ktot = 8.825e-6;
S.BETCaCO3 = 12.54;
S.MWCaCO3 = 100.0869;
S.Kad = 0.0084;
S.rhoCaCO3 = 2703;
S.MWCaSO3 = 258.30;
S.rhoCaSO3 = 2540;
S.kCaSO3 = 2e-05;
S.P = 1.01E+05;
S.T = 323.15;
S.V_Headspace = 4.e-4;
S.F = 1.66667e-5;
S.y_so2 = 2e-3;
S.CSO2_in = 6.51332e-2;
S.y_co2 = 0.0;
S.CCO2_in = 0.0;
S.kga = 4e-5;
S.kLa = 8.4e-4;
S.kLa_CO2 = 9.598e-4;

%% Initial conditions and Relationships

pHtrial             = 7;
Ca_total            = 4.879E-02;
```

```
C_total             = 4.879E-02;
S_total             = 0.0;
CCaCO3              = 48.624- Ca_total;
CCaSO3              = 0;
fr                  = 1.;
SO2_g               =  fr * S.CSO2_in;
CO2_g               = S.CCO2_in;
CO2_g               = 0.2;
CCO2_inter          = CO2_g ;
pg                  = 200;
CSO2_inter          = pg/S.HSO2;
CH_trial            = 1.e-7;
pH1                 = 7.0;

pH                  = fzero(@(pH)HionpH(pH,S),pH1);

CH                  = 10^(3-pH);

CSO2_bulkslurry     = (S_total*CH^2)/(CH^2 + S.KSO2*CH + S.KSO2*S.KHSO3);

CHSO3               = (S_total*S.KSO2*CH)/(CH^2 + S.KSO2*CH + S.KSO2*S.KHSO3);

CSO3                = (S_total*S.KSO2*S.KHSO3)/(CH^2 + S.KSO2*CH + S.KSO2*S.KHSO3);

CCO2_bulkslurry     = (C_total*CH^2)/(CH^2 + S.KCO2*CH + S.KCO2*S.KHCO3);

CHCO3               = (C_total*S.KCO2*CH)/(CH^2 + S.KCO2*CH + S.KCO2*S.KHCO3);

CCO3                = (C_total*S.KCO2*S.KHCO3)/(CH^2 + S.KCO2*CH + S.KCO2*S.KHCO3);

pH2                 = 6.0;


pHInter             = fzero (@(pH)HionStar(pH,S),pH2);

CH                  = 10^(3-pH) ;

y0                  = [ SO2_g CO2_g  S_total C_total Ca_total CCaCO3 CCaSO3 ];
y0                  = y0';

Trial(1)            = (SO2_g * S.R *S.T ) / S.HSO2;
Trial(2)            = 1;
Trial(3)            = CH ;

%% Time
t0                  = 0.0;
Delt                = 1.0;
t                   = t0;
tmax                = 6100;
nloop               = tmax/Delt ;
nstep               = 30 ;
```

```
Results             = [ t  y0'    pH  pHInter];

%% Loop1


%figure;
%hold on


    for k               = 1:nstep
            y               = SO2_OdeDriver(y0,S);
            pH              = 3 - log10 (CH) ;
            tf              = t;
            Results         = [Results; tf y' pH pHInter];
            y0 =  y;
    end


%Results;



end

function ph =  HionpH (pH,S)
global S_total C_total Ca_total

CH =  10^(3-pH);

ph =  CH + 2  * Ca_total - ((S_total*S.KSO2*CH)/(CH^2 + S.KSO2*CH + S.KSO2*S.↙
KHSO3))...
 - 2*((S_total*S.KSO2*S.KHSO3)/(CH^2 + S.KSO2*CH + S.KSO2*S.KHSO3))...
 -((C_total*S.KCO2*CH)/(CH^2 + S.KCO2*CH + S.KCO2*S.KHCO3))...
 - 2*((C_total*S.KCO2*S.KHCO3)/(CH^2 + S.KCO2*CH + S.KCO2*S.KHCO3))- S.Kw /CH ;
end


function y = SO2_OdeDriver (y0,S)

global S_total C_total Ca_total CSO2_bulkslurry  CHSO3 CSO3 CCO2_bulkslurry CHCO3 CCO3↙
CCaCO3 CCaSO3 CH nloop Delt t CH_trial Tag pHInter

   for k = 1:nloop
        pH_trial            = 8.0;
        pH                  = fzero(@(pH)HionpH(pH,S),pH_trial);

        CH                  = 10^(3-pH);
        pH                  = 3 -log10 (CH) ;
        CSO2_bulkslurry     = (S_total*CH^2)/(CH^2 + S.KSO2*CH + S.KSO2*S.KHSO3);

        CHSO3               = (S_total*S.KSO2*CH)/(CH^2 + S.KSO2*CH + S.KSO2*S.KHSO3);

        CSO3                = (S_total*S.KSO2*S.KHSO3)/(CH^2 + S.KSO2*CH + S.KSO2*S.↙
KHSO3);
```

```
        CCO2_bulkslurry     = (C_total*CH^2)/(CH^2 + S.KCO2*CH + S.KCO2*S.KHCO3);

        CHCO3               = (C_total*S.KCO2*CH)/(CH^2 + S.KCO2*CH + S.KCO2*S.KHCO3);

        CCO3                = (C_total*S.KCO2*S.KHCO3)/(CH^2 + S.KCO2*CH + S.KCO2*S.↙
KHCO3);

        dydt                = odes (t, y0,S);

        y                   = y0 + dydt' * Delt;

        SO2_g               = y(1);
        CO2_g               = y(2);
        S_total             = y(3) ;
        C_total             = y(4) ;
        Ca_total            = y(5);
        CCaCO3              = y(6);
        CCaSO3              = y(7);
        y0                  = y ;
        t                   = t +Delt;
        CH_trial            = CH;

   end
end


function dcdt = odes (t,c,S)
global kCaSO3 CSO2_bulkslurry  CHSO3 CSO3 CCO2_bulkslurry CHCO3 CCO3 CCaCO3 CCaSO3 CH↙
S_total C_total Ca_total Trial CSO2_inter ...
    CHSO3_inter  CSO3_inter CCO2_inter  CHCO3_inter  CCO3_inter pHtrial pi pHInter pg

        S_total             = c(3) ;
        C_total             = c(4) ;
        Ca_total            = c(5) ;
        pH1                 = 7;
        pH                  = fzero (@(pH)HionpH(pH,S),pH1);
        CH                  = 10^(3-pH) ;

        CSO2_bulkslurry     = (S_total*CH^2)/(CH^2 + S.KSO2*CH + S.KSO2*S.KHSO3);

        CHSO3               = (S_total*S.KSO2*CH)/(CH^2 + S.KSO2*CH + S.KSO2*S.KHSO3);

        CSO3                = (S_total*S.KSO2*S.KHSO3)/(CH^2 + S.KSO2*CH + S.KSO2*S.↙
KHSO3);

        CCO2_bulkslurry     = (C_total*CH^2)/(CH^2 + S.KCO2*CH + S.KCO2*S.KHCO3);

        CHCO3               = (C_total*S.KCO2*CH)/(CH^2 + S.KCO2*CH + S.KCO2*S.KHCO3);

        CCO3                = (C_total*S.KCO2*S.KHCO3)/(CH^2 + S.KCO2*CH + S.KCO2*S.↙
KHCO3);

        CH;
        pH;
```

```
        p_exit              = c(1)*S.R*S.T ;
        pg                  = p_exit;

        Trial ;
        Tnew                = fsolve (@(Tr)NSub(Tr,S),Trial);

        pHInter             = 3-log10(Tnew(3) );
        pstar               = Tnew(1) * S.HSO2;
        NSO2                = S.kga *(pg-pstar) ;

        %Trial               = Tnew;

        dcdt(1)             = (1/S.V_Headspace) * (S.F * S.CSO2_in - S.F * c(1) ) -↙
NSO2  ;

        E_CO2               = 1;
         NCO2               = S.kLa_CO2*E_CO2*( c(2)*S.R*S.T/S.HCO2 - CCO2_bulkslurry);
        dcdt(2)             = (1/S.V_Headspace) * (S.F * S.CCO2_in - S.F * c(2)) - NCO2↙
;

        n                   = 3;
        sat                 = c(5)*CSO3/ S.KSPCaSO3   ;
        if ( sat < 1.0 )
            RCaSO3          = 0.0;
            else
             RCaSO3         = 1.0e-08 * ( sat -1)^n ;
        end

        RCaCO3              = S.ktot*S.BETCaCO3*S.MWCaCO3*CCaCO3*CH *(1 - (S.Kad*CH)/↙
(1+S.Kad*CH));

        dcdt(3)             = NSO2 -  RCaSO3;

        dcdt(4)             = NCO2 + RCaCO3;

        dcdt(5)             = RCaCO3 - RCaSO3;

        if ( c(6) < 1.0e-3 )
            c(6)            = 0.0;
            dcdt(6)         = 0.0;
            Time_c          = t ;
            Tag             = 1;
        else

            dcdt(6)         = - RCaCO3 ;
        end

        dcdt(7)             = RCaSO3;

end

function discrep = NSub (Tr,S)
   global S_total C_total Ca_total CSO2_bulkslurry  CHSO3 CSO3 CSO2_inter CHSO3_inter↙
CSO3_inter CCO2_inter  CHCO3_inter  CCO3_inter ...
```

```
        CCO2_bulkslurry CHCO3 CCO3 pg pHInter

         Tr;
         CSO2_inter      = Tr(1) ;
         pstar           = CSO2_inter * S.HSO2 ;
         SlTotal         = Tr(2) ;
         CH              = Tr(3) ;
         S_total         = CHSO3 + CSO3 + CSO2_bulkslurry ;
         CHSO3_inter     = S.KSO2*CSO2_inter  / CH ;
         CSO3_inter      = S.KHSO3  *CHSO3_inter  /CH;
         Ctotal          = CHCO3 + CCO3 ;
         CHCO3_inter     = Ctotal * ( 1+  S.KHCO3  / CH) ;
         CCO3_inter      = S.KHCO3  *CHCO3_inter  /CH ;
         S_total_inter   = CSO2_inter + CHSO3_inter +  CSO3_inter;
         df              = S_total_inter- S_total ;

         pstar;
         pg;
         Rate_gas        = S.kga * (pg-pstar) ;
         Rate_liq        = S.kLa * df;
         discrep(1)      = SlTotal - (CHSO3_inter + CSO3_inter) ;
         discrep(2)      = Rate_gas - Rate_liq ;
         mCH_cal         =  2*Ca_total -(CHSO3_inter + 2*CSO3_inter + CHCO3_inter + 2*↙
CCO3_inter +  S.Kw /CH ) ;
         discrep(3)      = CH + mCH_cal ;
end


function phl =  HionStar (pH,S)

 global S_total C_total Ca_total CSO2_bulkslurry  CHSO3 CSO3 CSO2_inter  CHSO3_inter↙
CSO3_inter CCO2_inter  CHCO3_inter ...
    CCO3_inter CCO2_bulkslurry CHCO3 CCO3 pg

    CH              =  10^(3-pH);
    CSO2_inter ;
    CHSO3_inter     = S.KSO2*CSO2_inter  / CH ;
    CSO3_inter      = S.KHSO3  *CHSO3_inter  /CH;
    Stotal          = CHSO3 + CSO3;
    Ctotal          = CHCO3 + CCO3 ;
    CHSO3_inter     = Stotal * (   1+  S.KHSO3 / CH) ;
    CSO3_inter      = S.KHSO3  * CHSO3_inter /CH;
    CHCO3_inter     = Ctotal * ( 1+  S.KHCO3 / CH);
    CCO3_inter      = S.KHCO3  *CHCO3_inter  /CH ;
    Ca              = Ca_total;
    phl             = CH + 2*Ca -(CHSO3_inter + 2*CSO3_inter + CHCO3_inter + 2*↙
CCO3_inter +  S.Kw /CH );

end
```

The typical supplementary results that are generated by the integrated model for aqueous solution cases are given in Tables C.1 and C.2. Those for limestone slurry cases are given in Tables C.3 and C.4.

Appendix C2: Supplementary results for SO_2 absorption into aqueous solutions

Table C.1: Concentration of SO_2, total sulphur and pH

Time (hr)	C $_{SO_2,bulkgas}$ (mol/m^3)	S_{total} (mol/m^3)	pH_{water}	$pH_{interface}$
0,00	0,073	0,00	7,15	5,14
0,28	0,038	0,43	6,65	3,34
0,56	0,040	0,81	4,28	3,12
0,83	0,043	1,16	3,47	3,00
1,11	0,046	1,48	3,24	2,91
1,39	0,049	1,76	3,11	2,85
1,67	0,052	2,01	3,03	2,81
1,94	0,055	2,22	2,97	2,77
2,22	0,058	2,40	2,92	2,75
2,50	0,060	2,56	2,89	2,73
2,78	0,062	2,69	2,86	2,71
3,06	0,063	2,81	2,84	2,70
3,33	0,065	2,91	2,83	2,69
3,61	0,066	2,99	2,81	2,68
3,89	0,067	3,06	2,80	2,67
4,17	0,068	3,12	2,79	2,66
4,44	0,069	3,17	2,79	2,66
4,72	0,069	3,21	2,78	2,65
5,00	0,070	3,25	2,77	2,65
5,28	0,070	3,28	2,77	2,65
5,56	0,071	3,30	2,77	2,64
5,83	0,071	3,32	2,76	2,64
6,11	0,071	3,34	2,76	2,64
6,39	0,072	3,36	2,76	2,64
6,67	0,072	3,37	2,76	2,64
6,94	0,072	3,38	2,76	2,64
7,22	0,072	3,39	2,76	2,64
7,50	0,072	3,40	2,75	2,63
7,78	0,072	3,40	2,75	2,63
8,06	0,072	3,41	2,75	2,63
8,33	0,072	3,41	2,75	2,63

Table C.2: Concentrations of SO_2, HSO_3^- and SO_3^{2-} at the gas-liquid interphase and in the water bulk

Time (hr)	$C_{SO_2,water}$ (mol/m^3)	$C_{SO_2,interphase}$ (mol/m^3)	$C_{HSO_3^-,water}$ (mol/m^3)	$C_{HSO_3^-,interphase}$ (mol/m^3)	$C_{SO_3^{2-},water}$ (mol/m^3)	$C_{SO_3^{2-},Interphase}$ (mol/m3)
0,28	0,00	0,04	0,34	0,45	8,65E-02	5,68E-05
0,56	0,01	0,11	0,80	0,76	8,59E-04	5,68E-05
0,83	0,07	0,20	1,09	1,01	1,83E-04	5,68E-05
1,11	0,15	0,30	1,32	1,23	1,31E-04	5,68E-05
1,39	0,24	0,39	1,52	1,40	1,12E-04	5,68E-05
1,67	0,32	0,49	1,69	1,56	1,02E-04	5,68E-05
1,94	0,39	0,57	1,82	1,68	9,65E-05	5,68E-05
2,22	0,46	0,64	1,94	1,79	9,26E-05	5,68E-05
2,50	0,52	0,70	2,03	1,87	8,99E-05	5,68E-05
2,78	0,58	0,76	2,11	1,95	8,80E-05	5,68E-05
3,06	0,63	0,81	2,18	2,01	8,65E-05	5,68E-05
3,33	0,67	0,85	2,24	2,06	8,54E-05	5,68E-05
3,61	0,70	0,89	2,29	2,11	8,45E-05	5,68E-05
3,89	0,73	0,92	2,33	2,15	8,38E-05	5,68E-05
4,17	0,76	0,95	2,36	2,18	8,33E-05	5,68E-05
4,44	0,78	0,97	2,39	2,20	8,28E-05	5,68E-05
4,72	0,80	0,99	2,41	2,22	8,25E-05	5,68E-05
5,00	0,82	1,01	2,43	2,24	8,22E-05	5,68E-05
5,28	0,83	1,02	2,45	2,26	8,19E-05	5,68E-05
5,56	0,84	1,03	2,46	2,27	8,17E-05	5,68E-05
5,83	0,85	1,04	2,47	2,28	8,15E-05	5,68E-05
6,11	0,86	1,05	2,48	2,29	8,14E-05	5,68E-05
6,39	0,87	1,06	2,49	2,30	8,13E-05	5,68E-05
6,67	0,87	1,06	2,50	2,30	8,12E-05	5,68E-05
6,94	0,88	1,07	2,50	2,31	8,11E-05	5,68E-05
7,22	0,88	1,07	2,51	2,31	8,10E-05	5,68E-05
7,50	0,89	1,08	2,51	2,32	8,10E-05	5,68E-05
7,78	0,89	1,08	2,51	2,32	8,09E-05	5,68E-05
8,06	0,89	1,08	2,52	2,32	8,09E-05	5,68E-05
8,33	0,89	1,08	2,52	2,33	8,09E-05	5,68E-05

Appendix C3: Sample sensitivity analysis results for SO_2 absorption into aqueous solutions

These sensitivities are most informative when the changes in parameter and outcomes are sufficiently small so as to be well approximated by infinitesimals and when parameters are sufficiently independent so that changes in outcomes due to each parameter may be examined separately. The 'one-factor-at-a-time' (OAT) approach was employed in this study. Samples of sensitivity analysis results are shown in Figures C.1 through C.6. The results can be used to determine the multiplication factors through which parameters in Table C.5 can be adjusted.

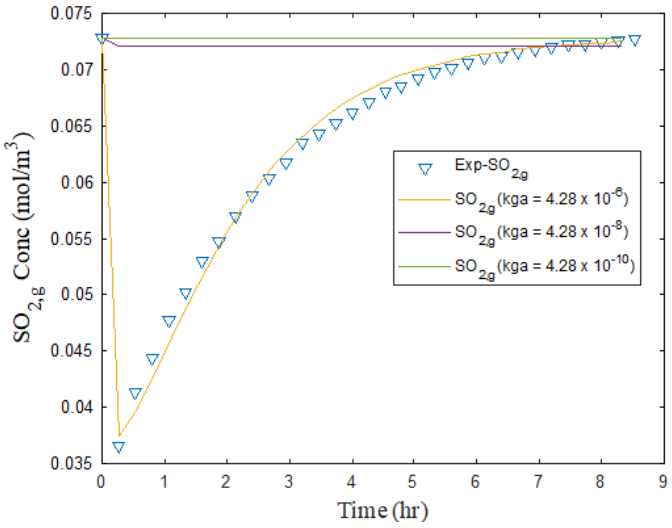

(a) SO_2 k_ga sensitivity: water case

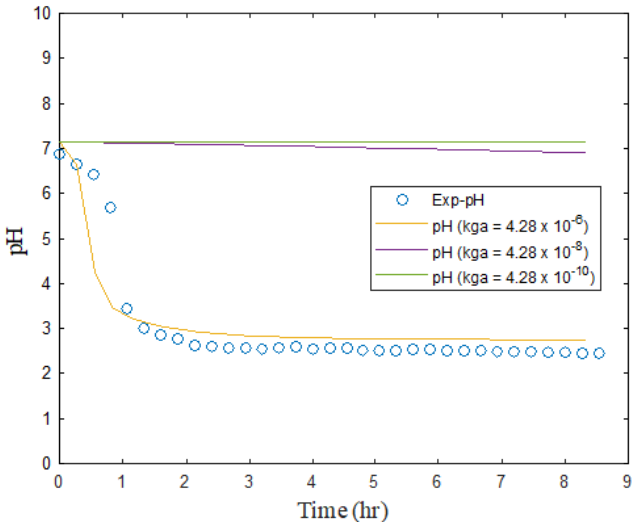

(b) pH k_ga sensitivity: water case

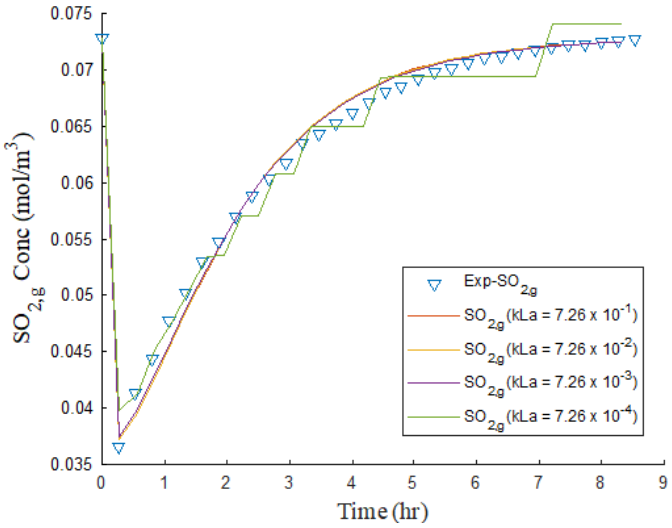

(c) SO_2 k_La sensitivity: water case

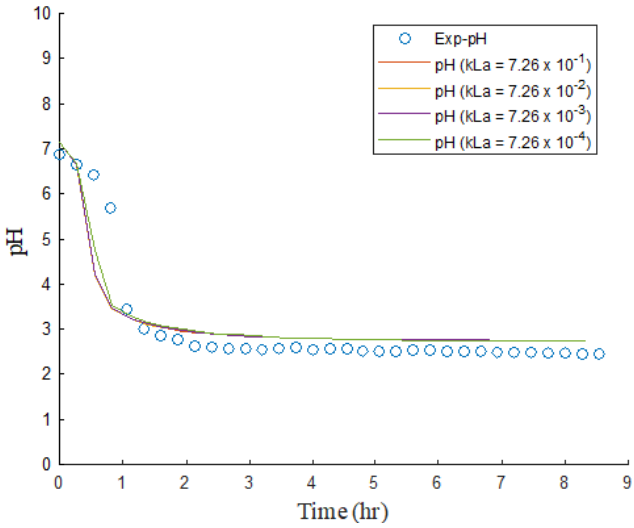

(d) pH k_La sensitivity: water case

Figure C.1: Sample k_ga and k_La sensitivity analysis in aqueous solution.

Appendix C4: Supplementary results for SO_2 absorption into limestone slurry

Table C.3: Concentrations of various in the species in the bulk gas and slurry

Time (hr) (hr)	$C_{SO_2,bulkgas}$ (mol/m^3) (mol/m^3)	$C_{CO_2,bulkgas}$ (mol/m^3) (mol/m^3)	S_{total} (mol/m^3)	C_{total} (mol/m^3)	Ca_{total} (mol/m^3)	C_{CaCO_3} (mol/m^3)	$C_{CaSO_3 \cdot 0.5H_2O}$ (mol/m^3)	pH_{slurry}	$pH_{interphase}$
0,00	7,61E-02	1,00E-23	0,00	0,00	0,00	46,19	0,00	6,64	6,64
0,83	2,08E-02	4,61E-07	1,89	4,38	4,38	41,81	0,00	7,38	6,65
1,67	2,08E-02	9,99E-07	3,53	8,54	8,34	37,65	0,21	7,34	6,71
2,50	2,08E-02	1,59E-06	3,91	12,62	10,94	33,58	1,67	7,30	6,70
3,33	2,08E-02	2,26E-06	3,48	16,59	12,66	29,60	3,94	7,26	6,67
4,17	2,08E-02	3,10E-06	3,05	20,48	14,27	25,72	6,21	7,21	6,64
5,00	2,08E-02	4,18E-06	2,71	24,26	15,87	21,93	8,39	7,15	6,59
5,83	2,08E-02	5,63E-06	2,45	27,94	17,44	18,25	10,50	7,08	6,52
6,67	2,08E-02	7,68E-06	2,23	31,51	18,95	14,68	12,56	7,00	6,45
7,50	2,08E-02	1,08E-05	2,07	34,97	20,41	11,22	14,57	6,90	6,35
8,33	2,08E-02	1,64E-05	1,93	38,32	21,77	7,87	16,55	6,76	6,21
9,17	2,08E-02	2,88E-05	1,82	41,54	23,04	4,65	18,50	6,55	5,99
10,00	2,08E-02	8,03E-05	1,75	44,58	24,18	1,61	20,41	6,13	5,56
10,83	2,08E-02	1,30E-03	2,07	46,17	24,25	9,89E-04	21,94	4,92	4,75
11,67	2,11E-02	4,16E-03	3,22	46,08	23,57	9,89E-04	22,62	4,41	4,32
12,50	2,15E-02	6,83E-03	4,54	45,89	23,06	9,89E-04	23,13	4,17	4,11
13,33	2,22E-02	9,27E-03	5,90	45,62	22,61	9,89E-04	23,58	4,02	3,96
14,17	2,31E-02	1,15E-02	7,28	45,27	22,22	9,89E-04	23,97	3,90	3,85
15,00	2,42E-02	1,36E-02	8,67	44,85	21,86	9,89E-04	24,33	3,80	3,76
15,83	2,56E-02	1,54E-02	10,06	44,36	21,54	9,89E-04	24,65	3,72	3,68
16,67	2,72E-02	1,71E-02	11,42	43,82	21,25	9,89E-04	24,94	3,65	3,62
17,50	2,91E-02	1,86E-02	12,76	43,22	20,99	9,89E-04	25,20	3,59	3,56
18,33	3,12E-02	1,99E-02	14,05	42,58	20,76	9,89E-04	25,43	3,53	3,51
19,17	3,34E-02	2,11E-02	15,30	41,89	20,55	9,89E-04	25,64	3,48	3,46
20,00	3,58E-02	2,20E-02	16,49	41,17	20,36	9,89E-04	25,83	3,44	3,42
20,83	3,83E-02	2,29E-02	17,62	40,42	20,19	9,89E-04	26,00	3,40	3,38
21,67	4,09E-02	2,35E-02	18,67	39,65	20,03	9,89E-04	26,16	3,36	3,35
22,50	4,35E-02	2,40E-02	19,66	38,85	19,89	9,89E-04	26,30	3,33	3,32
23,33	4,61E-02	2,44E-02	20,56	38,05	19,76	9,89E-04	26,43	3,30	3,29
24,17	4,86E-02	2,47E-02	21,40	37,23	19,64	9,89E-04	26,55	3,28	3,27
25,00	5,11E-02	2,49E-02	22,16	36,40	19,53	9,89E-04	26,66	3,25	3,25

Table C.4: Concentration of various species at the gasliquid interphase and the slurry bulk

Time (hr)	$C_{SO_2,slurry}$ (mol/m^3)	$C_{HSO_3^-,slurry}$ (mol/m^3)	$C_{SO_3^{2-},slurry}$ (mol/m^3)	$C_{CO_2,slurry}$ (mol/m^3)	$C_{HCO_3^-,slurry}$ (mol/m^3)	$C_{CO_3^{2-},slurry}$ (mol/m^3)	$C_{SO_2,interphase}$ (mol/m^3)	$C_{HSO_3^-,interphase}$ (mol/m^3)	$C_{SO_3^{2-},interphase}$ (mol/m^3)	$C_{CO_2,interphase}$ (mol/m^3)	$C_{HCO_3^-,interphase}$ (mol/m^3)	$C_{CO_3^{2-},interphase}$ (mol/m^3)
0,0	1,5E-30	1,0E-25	9,9E-24	4,4E-27	9,7E-24	2,8E-25	7,6E-02	1,0E-21	9,8E-20	1,0E-23	1,0E-23	2,9E-25
0,8	9,3E-09	3,5E-03	1,9E+00	3,1E-04	3,8E+00	5,9E-01	2,7E-07	1,9E-02	2,0E+00	1,0E-23	4,5E+00	1,3E-01
1,7	2,1E-08	7,0E-03	3,5E+00	6,7E-04	7,5E+00	1,1E+00	3,8E-07	3,1E-02	3,6E+00	1,0E-23	8,8E+00	3,0E-01
2,5	2,7E-08	8,6E-03	3,9E+00	1,1E-03	1,1E+01	1,5E+00	4,4E-07	3,5E-02	4,0E+00	1,0E-23	1,3E+01	4,3E-01
3,3	3,0E-08	8,4E-03	3,5E+00	1,6E-03	1,5E+01	1,8E+00	4,5E-07	3,3E-02	3,6E+00	1,0E-23	1,7E+01	5,3E-01
4,2	3,3E-08	8,3E-03	3,0E+00	2,3E-03	1,9E+01	2,0E+00	4,7E-07	3,2E-02	3,1E+00	1,0E-23	2,1E+01	5,9E-01
5,0	3,8E-08	8,4E-03	2,7E+00	3,1E-03	2,2E+01	2,1E+00	5,3E-07	3,2E-02	2,8E+00	1,0E-23	2,5E+01	6,3E-01
5,8	4,7E-08	8,9E-03	2,4E+00	4,2E-03	2,6E+01	2,1E+00	6,3E-07	3,3E-02	2,5E+00	1,0E-23	2,9E+01	6,3E-01
6,7	6,2E-08	9,8E-03	2,2E+00	5,8E-03	3,0E+01	1,9E+00	8,3E-07	3,6E-02	2,3E+00	1,0E-23	3,2E+01	5,9E-01
7,5	9,2E-08	1,1E-02	2,1E+00	8,3E-03	3,3E+01	1,7E+00	1,2E-06	4,2E-02	2,1E+00	1,0E-23	3,5E+01	5,2E-01
8,3	1,6E-07	1,5E-02	1,9E+00	1,3E-02	3,7E+01	1,4E+00	2,1E-06	5,4E-02	2,0E+00	1,0E-23	3,9E+01	4,1E-01
9,2	4,0E-07	2,2E-02	1,8E+00	2,2E-02	4,1E+01	9,5E-01	5,5E-06	8,4E-02	1,8E+00	1,0E-23	4,2E+01	2,7E-01
10,0	2,7E-06	5,6E-02	1,7E+00	6,5E-02	4,4E+01	3,9E-01	3,5E-05	2,0E-01	1,7E+00	1,0E-23	4,5E+01	1,1E-01
10,8	5,6E-04	7,2E-01	1,3E+00	1,1E+00	4,5E+01	2,4E-02	1,1E-03	9,5E-01	1,2E+00	1,0E-23	4,5E+01	1,7E-02
11,7	5,1E-03	2,0E+00	1,2E+00	3,3E+00	4,3E+01	7,2E-03	6,8E-03	2,2E+00	1,1E+00	1,0E-23	4,3E+01	5,9E-03
12,5	1,5E-02	3,4E+00	1,1E+00	5,4E+00	4,1E+01	4,0E-03	1,8E-02	3,6E+00	1,0E+00	1,0E-23	4,1E+01	3,4E-03
13,3	2,9E-02	4,7E+00	1,1E+00	7,3E+00	3,8E+01	2,6E-03	3,4E-02	4,9E+00	1,0E+00	1,0E-23	3,8E+01	2,3E-03
14,2	5,0E-02	6,1E+00	1,1E+00	9,0E+00	3,6E+01	1,9E-03	5,7E-02	6,3E+00	1,0E+00	1,0E-23	3,6E+01	1,7E-03
15,0	7,6E-02	7,5E+00	1,1E+00	1,1E+01	3,4E+01	1,4E-03	8,5E-02	7,7E+00	1,0E+00	1,0E-23	3,4E+01	1,3E-03
15,8	1,1E-01	8,9E+00	1,1E+00	1,2E+01	3,2E+01	1,1E-03	1,2E-01	9,0E+00	9,9E-01	1,0E-23	3,2E+01	1,0E-03
16,7	1,5E-01	1,0E+01	1,0E+00	1,3E+01	3,0E+01	8,9E-04	1,6E-01	1,0E+01	9,8E-01	1,0E-23	3,0E+01	8,3E-04
17,5	1,9E-01	1,2E+01	1,0E+00	1,5E+01	2,9E+01	7,3E-04	2,1E-01	1,2E+01	9,6E-01	1,0E-23	2,9E+01	6,8E-04
18,3	2,4E-01	1,3E+01	1,0E+00	1,6E+01	2,7E+01	6,1E-04	2,6E-01	1,3E+01	9,4E-01	1,0E-23	2,7E+01	5,7E-04
19,2	2,9E-01	1,4E+01	9,7E-01	1,6E+01	2,5E+01	5,1E-04	3,1E-01	1,4E+01	9,3E-01	1,0E-23	2,5E+01	4,8E-04
20,0	3,5E-01	1,5E+01	9,5E-01	1,7E+01	2,4E+01	4,3E-04	3,7E-01	1,5E+01	9,1E-01	1,0E-23	2,4E+01	4,1E-04
20,8	4,1E-01	1,6E+01	9,3E-01	1,8E+01	2,3E+01	3,7E-04	4,4E-01	1,6E+01	8,9E-01	1,0E-23	2,3E+01	3,6E-04
21,7	4,8E-01	1,7E+01	9,1E-01	1,8E+01	2,1E+01	3,2E-04	5,0E-01	1,7E+01	8,8E-01	1,0E-23	2,1E+01	3,1E-04
22,5	5,4E-01	1,8E+01	8,9E-01	1,9E+01	2,0E+01	2,8E-04	5,6E-01	1,8E+01	8,6E-01	1,0E-23	2,0E+01	2,8E-04
23,3	6,1E-01	1,9E+01	8,7E-01	1,9E+01	1,9E+01	2,5E-04	6,3E-01	1,9E+01	8,5E-01	1,0E-23	1,9E+01	2,5E-04
24,2	6,7E-01	2,0E+01	8,6E-01	1,9E+01	1,8E+01	2,3E-04	6,9E-01	2,0E+01	8,4E-01	1,0E-23	1,8E+01	2,2E-04
25,0	7,3E-01	2,1E+01	8,4E-01	1,9E+01	1,7E+01	2,0E-04	7,5E-01	2,1E+01	8,2E-01	1,0E-23	1,7E+01	2,0E-04

Appendix C5:Sample sensitivity analysis results for SO_2 absorption into limestone slurry

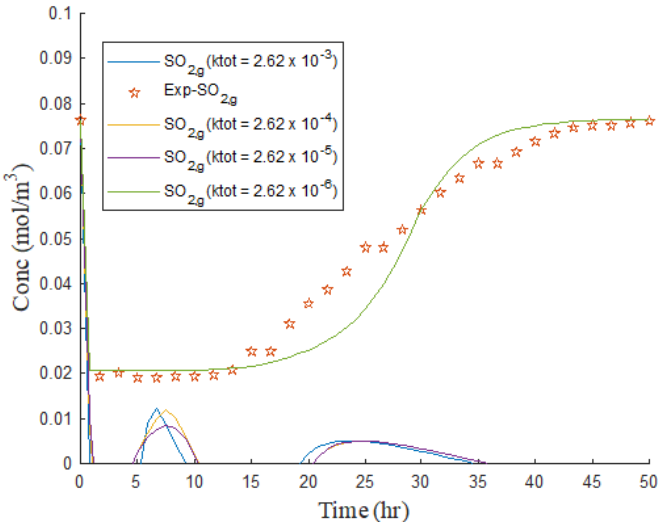

(a) SO_2 k_{tot} sensitivity analysis:slurry case

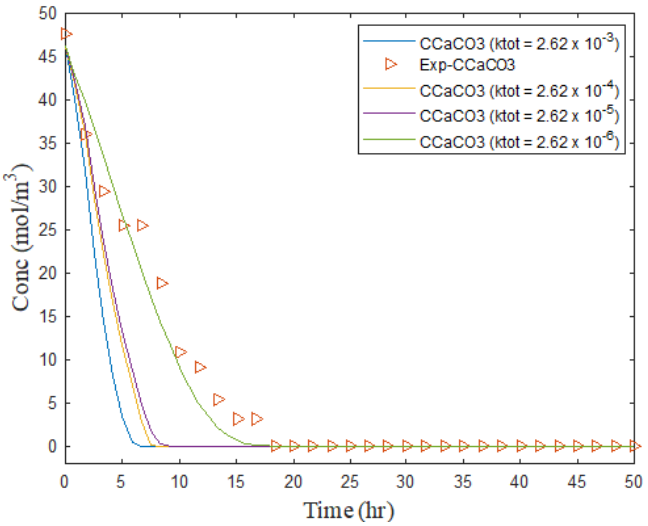

(b) $CaCO_3$ k_{tot} sensitivity analysis:slurry case

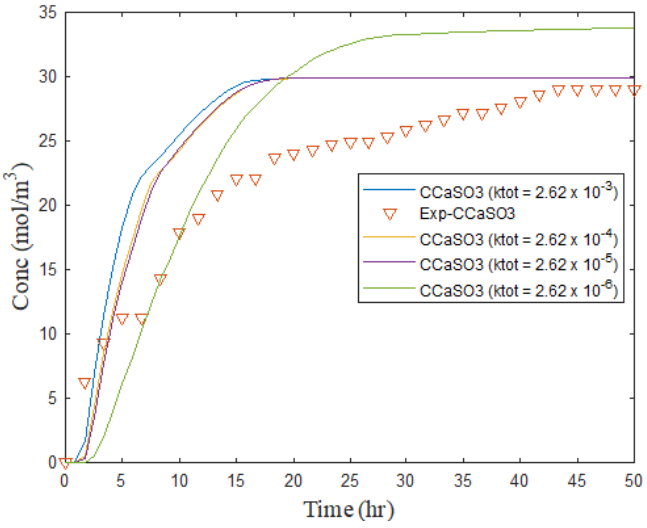

(c) $CaSO_3 0.5H_2O$ k_{tot} sensitivity analysis:slurry case

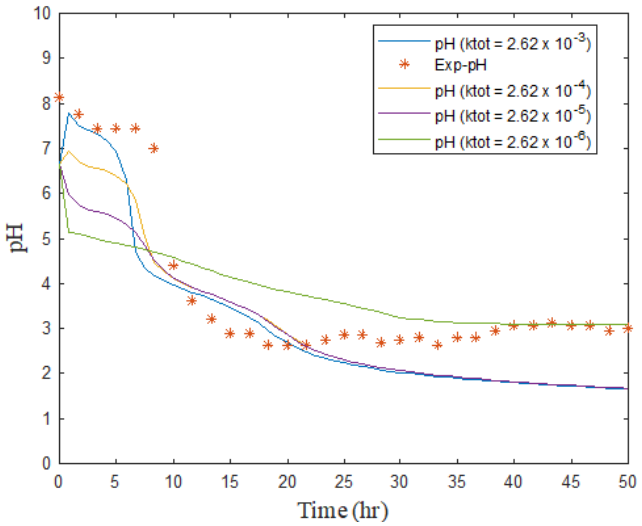

(d) pH k_{tot} sensitivity analysis: slurry case

Figure C.2: Sample k_{tot} sensitivity analysis: slurry case.

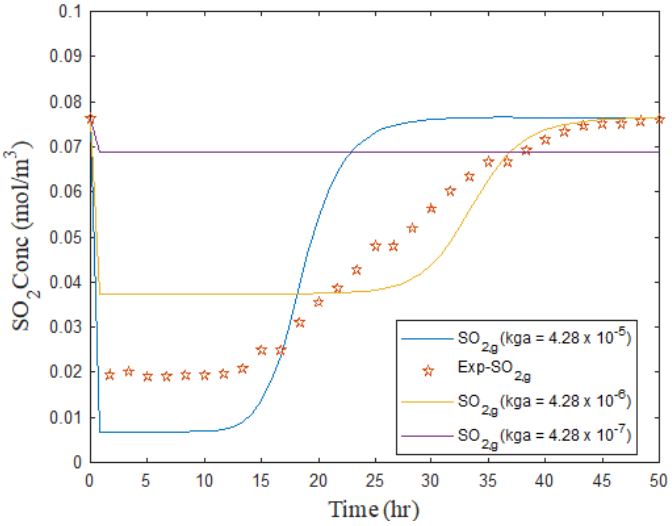

(a) SO_2 k_ga sensitivity analysis:slurry case

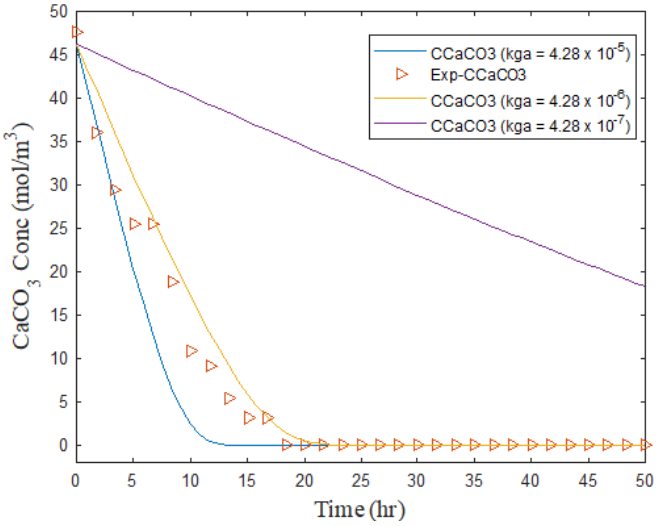

(b) $CaCO_3$ k_ga sensitivity analysis:slurry case

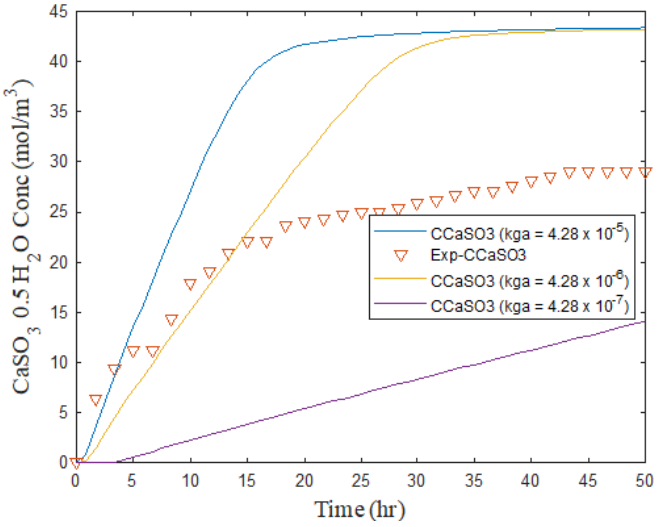

(c) $CaSO_3 0.5 H_2O$ k_ga sensitivity analysis:slurry case

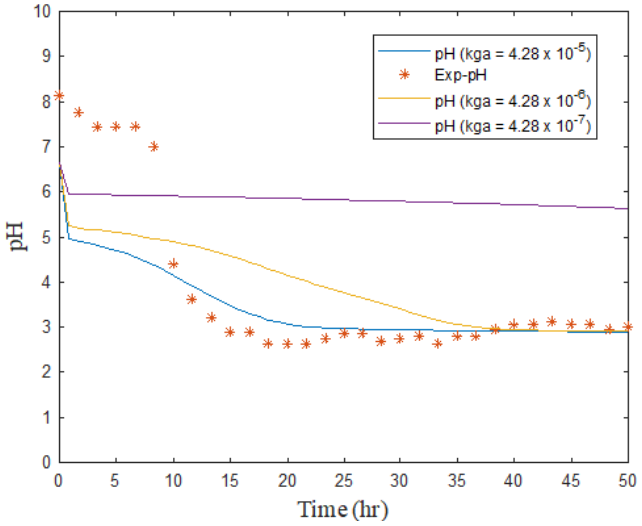

(d) pH k_ga sensitivity analysis: slurry case

Figure C.3: Sample k_ga sensitivity analysis: slurry case.

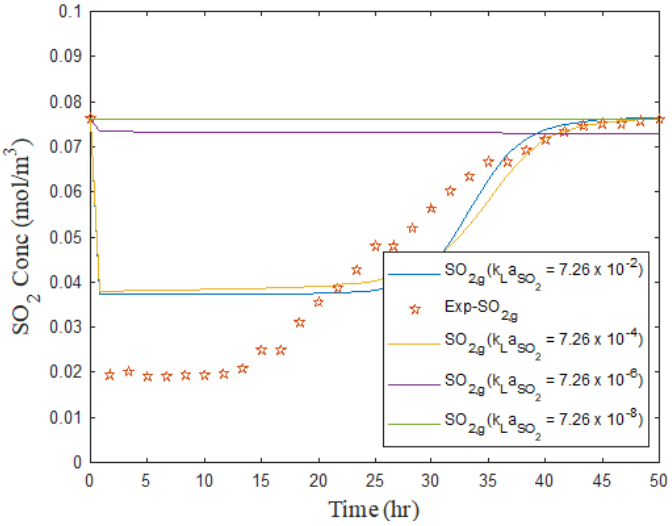

(a) SO_2 k_La sensitivity analysis:slurry case

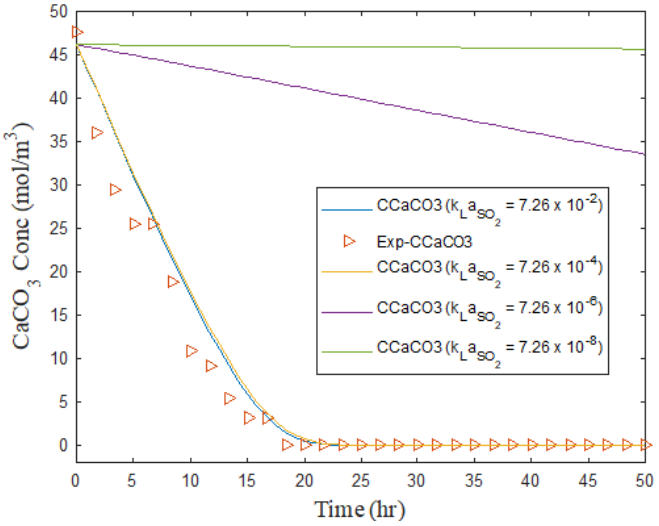

(b) $CaCO_3$ k_La sensitivity analysis:slurry case

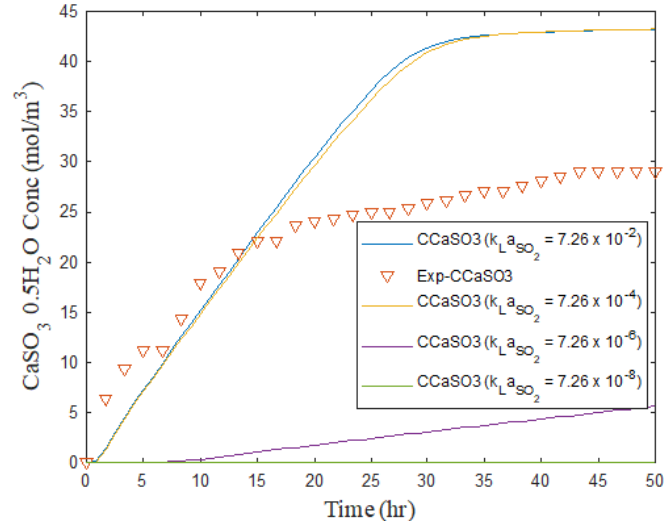

(c) $CaSO_30.5H_2O$ k_La sensitivity analysis:slurry case

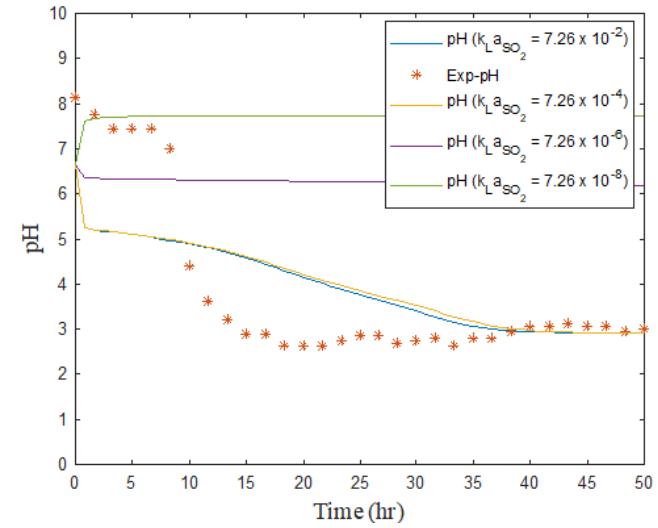

(d) pH k_La sensitivity analysis: slurry case

Figure C.4: Sample k_La sensitivity analysis: slurry case.

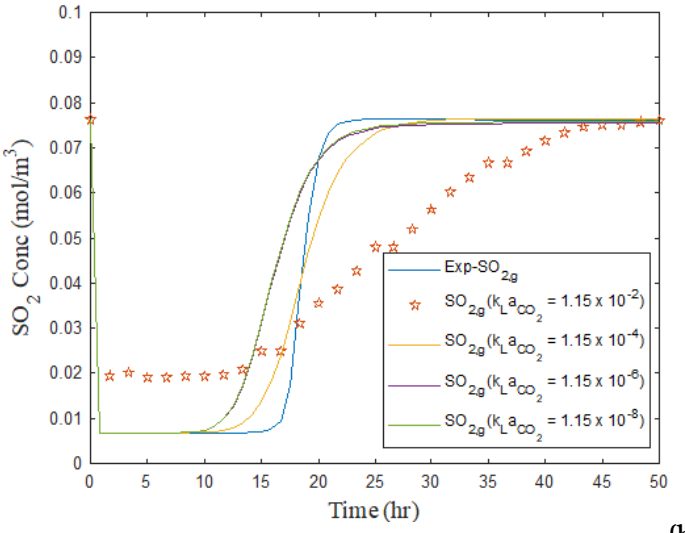

(a) SO_2 $k_La_{CO_2}$ sensitivity analysis:slurry case

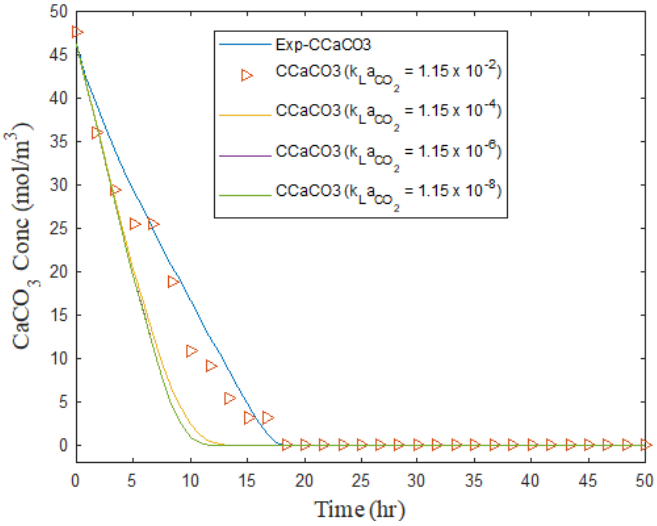

(b) $CaCO_3$ $k_La_{CO_2}$ sensitivity analysis:slurry case

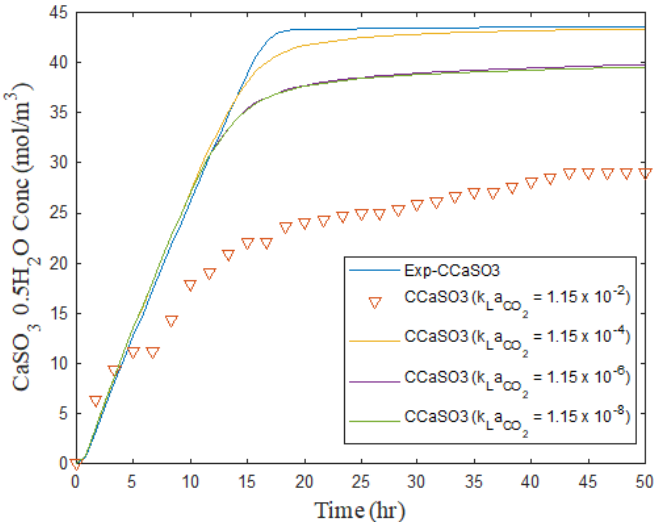

(c) $CaSO_3 0.5H_2O$ $k_La_{CO_2}$ sensitivity analysis:slurry case

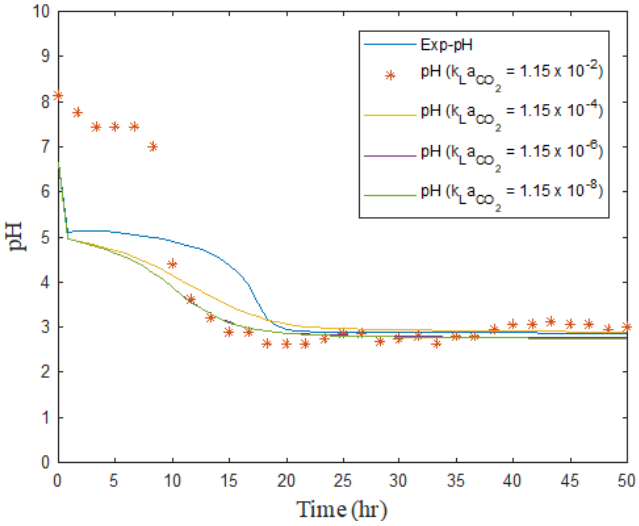

(d) pH $k_La_{CO_2}$ sensitivity analysis: slurry case

Figure C.5: Sample $k_La_{CO_2}$ sensitivity analysis: slurry case.

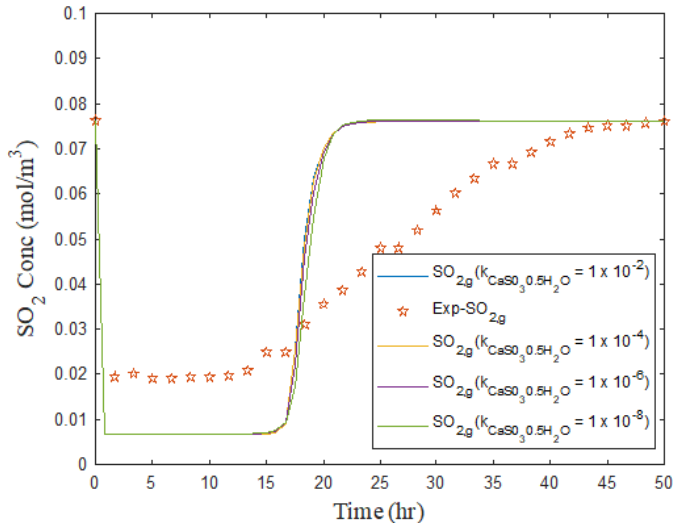

(a) SO_2 $k_{CaSO_30.5H_2O}$ sensitivity analysis:slurry case

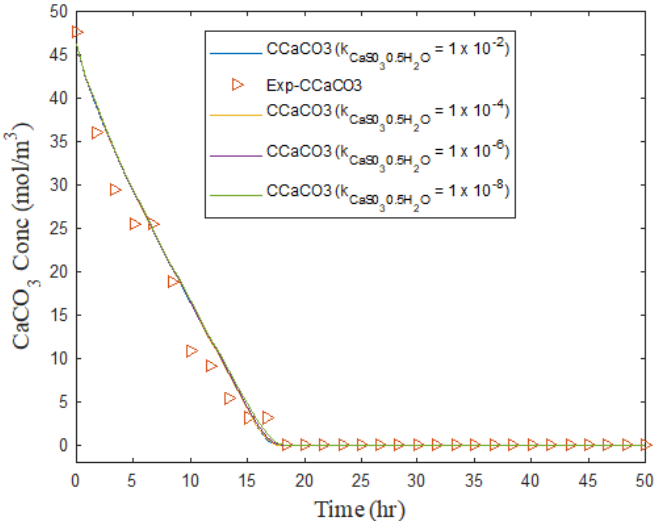

(b) $CaCO_3$ $k_{CaSO_30.5H_2O}$ sensitivity analysis:slurry case

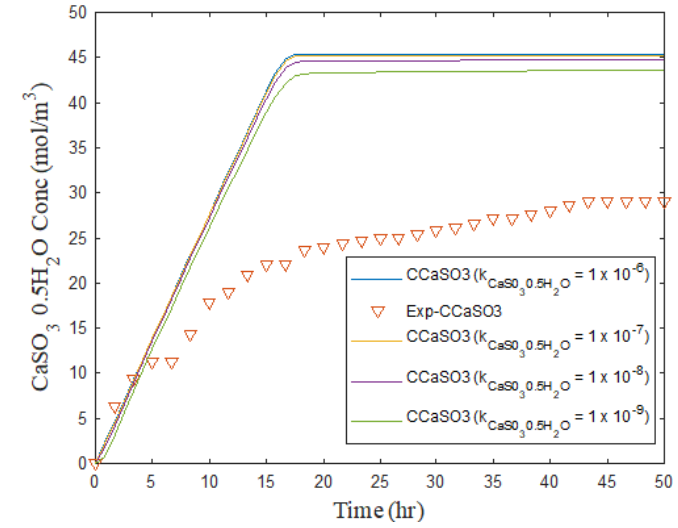

(c) $CaSO_30.5H_2O$ $k_{CaSO_30.5H_2O}$ sensitivity analysis:slurry case

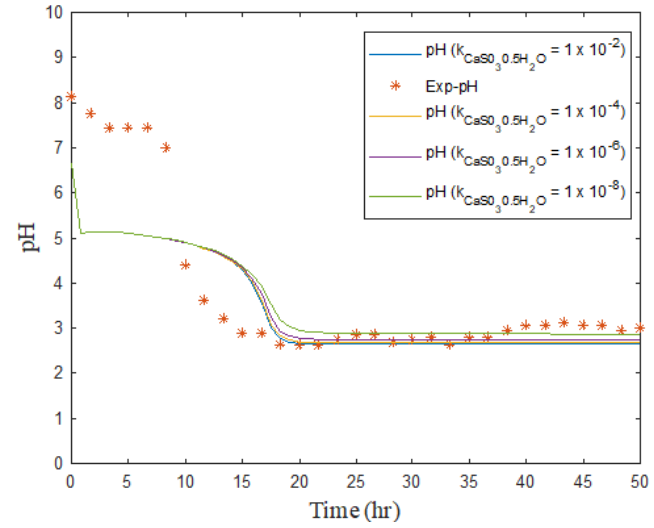

(d) pH $k_{CaSO_30.5H_2O}$ sensitivity analysis: slurry case

Figure C.6: Sample $k_{CaSO_30.5H_2O}$ sensitivity analysis: slurry case.

Appendix C6: Model input parameters and sensitivity adjustments

Table C.5: Comparison of experimental and fitted parameters

Experiment Name	Limestone (wt%)	Temp (°C)	SO_2 Conc (ppm)	Solun Conc (mol/dm^3)	Exp k_{tot} (m/s)	k_{tot} Sensitivity Factor	Exp $k_g a$ (mol/m^{3}sPa)	$k_g a$ Sensitivity Factor	Exp $k_L a$ (m/s)	$k_L a$ Sensitivity Factor	$k_{CaSO_3 0.5 H_2O}$ Literature (mol/m^{3}s)	$k_{CaSO_3 0.5 H_2O}$ Sensitivity Factor	k_{CO_2} Literature (m/s)	k_{CO_2} Sensitivity Factor
							Aqeueous solutions							
Water-2000ppm-25°C	0	25	2000	-	-	-	4,28E-04	1E-02	7,26E-02	-	-	-	-	-
Water-2000ppm-50°C	0	50	2000	-	-	-	4,28E-04	1E-02	7,26E-02	-	-	-	-	-
HCl-2000ppm-50°C	0	50	2000	1	-	-	-		7,26E-02		-	-	-	-
NaOH-2000ppm-50°C	0	50	2000	0.1	-	-	4,28E-04	3E-02	-	-	-	-	-	-
							Slurry							
Slurry-2000ppm-25°C-0.5wt%	0.5	25	2000	-	1,52E-05	3E01	4,28E-04	2.5E-02	7,26E-02	1E-01	1,17E-08	1	1,15E-04	1E-01
Slurry-2000ppm-50°C-0.5wt%	0.5	50	2000	-	2,62E-05	3E01	4,28E-04	2.5E-02	7,26E-02	1E-01	1,17E-08	1	1,15E-04	1E-01
Slurry-3000ppm-50°C-0.5wt%	0.5	50	3000	-	2,62E-05	3E01	4,28E-04	2.5E-02	7,26E-02	1E-01	1,17E-08	1	1,15E-04	1E-01
Slurry-2000ppm-50°C-0.2wt%	0.2	50	2000	-	2,62E-05	3E02	4,28E-04	2.5E-01	7,26E-02	1E-01	1,17E-08	1	1,15E-04	1
Slurry-2000ppm-50°C-1wt%	1	50	2000	-	2,62E-05	3E02	4,28E-04	7.5E-01	7,26E-02	1E-01	1,17E-08	1	1,15E-04	1E-01
Slurry-2000ppm-50°C-2wt%	2	50	2000	-	2,62E-05	3E01	4,28E-04	5.5E-01	7,26E-02	1E-01	1,17E-08	1	1,15E-04	1E-01